DOE/NASA/5906-79/1
NASA CR-159725
TRS 104



# EVALUATION OF FEASIBILITY OF PRESTRESSED CONCRETE FOR USE IN WIND TURBINE BLADES

Seymour Lieblein
Technical Report Services

D. S. Londahl, Donn B. Furlong,
and David J. Peery
Tuthill Pump Company of California

and
Mark E Dreier
Paragon Pacific, Inc.

September 1979

Prepared for
NATIONAL AERONAUTICS AND SPACE ADMINISTRATION
Lewis Research Center
Under Purchase Order C-25906

for
**U.S. DEPARTMENT OF ENERGY**
**Energy Technology**
**Distributed Solar Technology Division**

NOTICE

DOE/NASA/5906-79/1
NASA CR-159725
TRS 104

# EVALUATION OF FEASIBILITY OF PRESTRESSED CONCRETE FOR USE IN WIND TURBINE BLADES

Seymour Lieblein
Technical Report Services
Rocky River, Ohio

D. S. Londahl, Donn B. Furlong,
and David J. Peery
Tuthill Pump Company of California
San Rafael, California

and

Mark E. Dreier
Paragon Pacific, Inc.
El Segundo, California

Prepared for
National Aeronautics and Space Administration
Lewis Research Center
Cleveland, Ohio 44135
Under Purchase Order C-25906

for
U.S. DEPARTMENT OF ENERGY
Energy Technology
Distributed Solar Technology Division
Washington, D.C. 20545
Under Interagency Agreement EX-76-I-01-1028

## FOREWORD

The material in this report is based on a final report submitted by Tuthill Pump Company of California (formerely Hallikainan Associates) of San Rafael, California. The work was done under NASA Contracts NAS3-20596 and NAS3-20813 with the Lewis Research Center. The Lewis project manager was Thomas P. Cahill. Contractor project manager was Donn B. Furlong, project engineer was D. S. Londahl, and structural consultant was Dr. David J. Peery.

The first contract provided for a feasibility and cost study of prestressed concrete as a construction material for wind turbine blades. The second contract involved additional computer studies of blade hub and supporting tower loads as affected by the increase in blade weight with concrete. Also included in this second contract was some aerodynamic performance analysis and the fabrication of a 6-foot model blade section. The coupled dynamic analysis was conducted under subcontract with Paragon Pacific, Inc. of El Segundo, California. Results were reported by Mark E. Dreier.

The contractor final report was then evaluated, amplified, and revised. This final report work was done under NASA Order number C-25906 with Technical Report Services of Rocky River, Ohio, with Seymour Lieblein as project engineer. Also incorporated into this version were comments from in-house and other Government agency reviews.

CONTENTS

## SUMMARY

A preliminary evaluation was conducted of the feasibility of the use of prestressed concrete as a construction material for wind turbine rotor blades. The impetus for the consideration of concrete was the potential for achieving satisfactory blades at costs substantially less than for conventional aluminum blades. The study was keyed to the Department of Energy/NASA-LeRC experimental wind turbine (MOD-0) at Sandusky, Ohio. The evaluation was composed of three major elements: stress and cost analysis of a blade design suitable for the MOD-0 wind turbine; construction of a model blade section; and coupled dynamic analysis of the blade and tower interaction.

A baseline blade design was achieved that met the design requirements for the 125-foot diameter MOD-0 rotor. The blade configuration consisted of a prestressed concrete main section, fiberglass tip and trailing edges, and a steel hub tube. Aerodynamic analysis indicated the need for a sharp trailing edge and smooth surfaces with these blades. Calculated stresses provided adequate safety margins for fatigue life. Blade weight was calculated to be 4900 pounds, almost two and a half times the weight of a present aluminum blade. Limitations of the design approach and property data base for prestressed concrete blades were identified.

Fabrication drawings were made in sufficient detail to define construction procedures and estimate fabrication costs. For a production run of ten blades, the cost per blade was estimated to be $17,600. This compares to a cost of the order of $200,000 for each of the two MOD-0 aluminum blades. No fabrication problems were apparent. A 6-foot section of the baseline design (without bar prestressing) was satisfactorily cast to verify the fabrication approach with thin concrete walls.

A comprehensive coupled dynamic analysis of a concrete-bladed rotor on the MOD-0 tower showed increased cyclic loads on the tower due to the excessive weight and inertia of the blades. Hub yawing moments on the nacelle became excessive. The increased cyclic loads resulted from a reduction in damping ratio caused by the increased blade weight. The analysis explored the sensitivity of cyclic loads to concrete blade damping ratio and bending flapping frequency.

Several options were discussed to reduce the cyclic nacelle moments. The first involved reducing the flapping frequency of the concrete blade, which was originally required to be approximately the same as for the aluminum blades on the MOD-0 wind turbine (2.7/rev). According to a one-degree-of-freedom analysis, a reduction from 2.7 per revolution to around 2.2 per revolutions appeared adequate to give hub moments more in line with the present MOD-0 values. However, there may be advantages in a further reduction in flapping frequency to the 1.6 per revolution level. The second option was to install the rotor upstream of the tower so that excitation from the tower blockage wake is avoided. Further work items deemed necessary to strengthen the overall design system for concrete blades were identified.

## INTRODUCTION

Wind turbines utilize an energy source which is readily available, clean, free, and inexhaustible. However, the capital cost of present wind turbines constitutes a primary factor affecting the use of wind power. Wind turbine rotor blades must have efficient airfoil shapes and must resist many cycles of repeated dynamic loads, yet be built at low cost.

In view of the attractive potential of wind energy, the Federal Wind Energy Program was established under the direction of the Department of Energy (DOE) to accelerate the development, commercialization and utilization of reliable and economically viable wind energy systems (ref. 1). For large systems ($\geq$100 kW) with horizontal-axis wind turbine generators, the largest contributor to capital cost is the rotor blades. Accordingly, NASA's Lewis Research Center was given the project management responsibility for exploratory studies to determine the feasibility of several techniques for producing wind turbine blades at low cost (ref. 2). The materials used for these blades are not necessarily less costly than more commonly used structural materials. However, the fabrication techniques are designed to greatly reduce the labor and processes involved in producing the blades.

The fabrication concepts in the program to date are based on fiberglass, wood, cast urethane, and prestressed concrete. The results of the feasibility evaluation of cast reinforced urethane rotor blades are presented in reference 3. The present report contains an evaluation of the feasibility of prestressed concrete as a construction material for wind turbine blades. Prestressed reinforced concrete is one of the least expensive of structural materials, can be formed to accurate contours, and has long-established techniques for design and fabrication. Furthermore, it is noncorrosive and should, therefore, have very favorable maintenance characteristics.

The feasibility investigation of prestressed concrete contained three major parts. The first part involved preliminary design studies for a prestressed concrete blade suitable for the DOE/NASA 100-kW experimental wind turbine (ref. 4). This wind turbine, designated as MOD-0, is shown in figure 1. The rotor diameter is 125 feet, the design wind speed is 18 miles per hour ($V_W$ = 26.4 ft/sec), and the rotor speed is 40 revolutions per minute (tip speed, $V_T$ = 261.8 ft/sec).

The blade design effort involved trade-off studies resulting in a baseline design with detailed analysis of weight, strength, and cost. The second part covered the fabrication of a 6-foot length of blade with a typical cross-section of the baseline design. The purpose of the construction was to verify the casting of concrete to the configuration required by the blade.

The third part of the study dealt with the effect of the weight of the concrete blades on the MOD-0 hub and tower structures which were initially designed for lighter aluminum blades. Analyses of hub and shaft coupled dynamic loads including effects of support flexibility were conducted. Results of the three phases of this study form the basis of the feasibility evaluation reported herein.

## BLADE DESIGN

The items involved in the blade design part of the study include: aerodynamic considerations; design approach; blade description; blade loads and stresses; blade weight; and estimated cost. Symbols used in these sections and their appendixes are defined in appendix A.

### Aerodynamic Considerations

The two principal aerodynamic factors pertaining to concrete blade fabrication are the required surface finish and the trailing-edge thickness. Both of these factors can influence blade construction and, therefore, cost. These two factors also affect the available power output of the rotor blades because of their effects on blade section aerodynamic drag. Blade power losses are particularly sensitive to aerodynamic drag because of the aerodynamic design conditions dictated by the use of only two rotor blades to minimize rotor cost.

A simplified parametric analysis of the effects of blade surface roughness and trailing-edge thickness on power output is presented in appendix B based on isolated airfoil lift and drag data. Results of the analysis indicate that it is quite important for power output considerations, to provide blades with high values of lift-to-drag ratio; that is, with aerodynamically smooth surfaces and with sharp trailing edges. For example, at the design condition of the MOD-0 wind turbine, a smooth airfoil would produce an aerodynamic power loss of around 27 kW. The same airfoil shape with "standard" roughness has a loss of around 42 kW. For an airfoil with a blunt trailing edge, with a thickness of 3/4 inch, the power loss increases around 10 kW, and with a thickness of $1\frac{1}{4}$ inch, the loss increases around 20 kW. Since the useful power for MOD-0 is only 100 kW at design speed, the drag losses are very significant.

At wind speeds less than the design speed, the total energy varies as $V_w^3$. Thus, at 80 percent of design wind speed, only 51 percent as much kinetic energy is available in the undisturbed wind. However, the rotor blade drag loss decreases only 10 to 15 percent at lower wind speeds because the rotor has the same rotational speed in all winds. Thus, drag loss consumes an increasingly larger proportion of the rotor generated power as wind speed is reduced. At wind speeds above the design speed, some of the wind energy is intentionally wasted so that low drag is not so important.

Prestressed concrete for blades can approach the requirement for minimum surface roughness, since concrete can be cast and finished to a precise, smooth airfoil shape. Also, the concrete surface will not corrode, dent, or wrinkle in use. However, concrete cannot be cast to a thin sharp trailing edge. Thus, some other material (possibly in the form of an insert) must be used at the aft end of the blade to provide the sharp trailing edge required by aerodynamic considerations.

## Design Approach

The use of prestressed concrete for wind turbine rotor blades entails some unique features and requirements compared to those for conventional concrete structures such as bridges and buildings. In general, because of these unique features, it is necessary to deviate from conventional prestressed concrete design practice in order to achieve a blade that is practical for the intended application. The unique requirements for wind turbine blades are: (1) minimum weight; (2) very high fatigue resistance; and (3) geometry restrictions.

Weight. - In wind turbine blades, both the centrifugal tension forces and the gravity bending moments when the blades rotate to a horizontal position are proportional to the weight of the blades. Because of their dynamic nature, such dead-weight stresses in long slender beams are more important than dead-load stresses in other types of concrete structures. Furthermore, the design of the supporting tower is strongly affected by the weight of the rotor. Thus, overall wind turbine cost and structural considerations initially indicate blades with low weight.

For concrete rotor blades, reduced weight can be obtained by the use of a lightweight (low-density) concrete formulation, by a minimum volume for the concrete (i.e., thin walls, thin bar cover, etc.), and by an optimum relation between concrete and steel bars. A disadvantage of the use of lightweight concrete is that there is less information on its properties (e.g., fatigue resistance, creep, shrinkage, bond strength) than there is for normal-weight concrete. Also, the properties of lightweight concrete depend on the production method as well as on the raw materals used.

For wind turbine blades, the proportion between concrete and steel is evaluated for minimum overall weight rather than for minimum cost of steel plus concrete, as in conventional practice. In general, this results in an over-reinforced structure for blades, because less concrete is required. In conventional concrete structures, weight is less important than cost, and it is preferrable to use under-reinforced structures because steel is more expensive than concrete.

Fatigue resistance. - The rotor blades for the MOD-0 wind turbine are required to withstand cyclic airloads which repeat $10^8$ times during a 30-year design life. Unfortunately, there are currently no reliable data on fatigue life of lightweight prestressed concrete to $10^8$ cycles. Maximum fatigue life of conventional concrete structures is of the order of $2 \times 10^6$ cycles. In conventional concrete design, no effort is made to prevent cracking of concrete under tensile stress. Prestressed bars or strands are made of high-strength steel, have a small area ($\sim$2 percent of concrete area), and large elongation after the concrete has cracked. Fatigue tests show that repeated loads above the cracking stress causes failure after around $0.5 \times 10^6$ to $2 \times 10^6$ cycles. Failure occurs as tension failure of the steel bars near the crack locations.

It is observed that isolated bars tested "in air" under the same stress as in the above conventional reinforced concrete case will withstand $10^8$ load cycles. It is, therefore, postulated that a comparable $10^8$ cycle fatigue life

should be obtained if the concrete does not "crack." Thus, the design condition is adopted for rotor blades that the concrete is not permitted to crack under any conditions. This requires more steel area and a higher prestress in the concrete, so that the tension stresses under all load conditions never exceed the compressive prestress.

Another factor affecting fatigue strength is the concrete bond strength. Experience indicates that the fatigue resistance of concrete depends on the efficiency of the bond. Unfortunately, concrete bond strength deteriorates under repeated loading. Furthermore, tests have shown that the bond with lightweight concrete is not as good as with normal-weight concrete of equivalent strength.

The basis of the problem with bond strength in prestressed concrete is the existence of very high bond stresses at the free ends of the bars. This effect is clearly demonstrated by the simplified analysis of appendix B, and a further more detailed discussion of the fatigue strength with reinforced concrete is given in appendix C.

The proposed design for the concrete blade addresses this problem by not depending on bond strength. All bars will have approximately uniform stress throughout their length and will have end fittings to transmit prestressing and operating loads, rather than depending on the steel-to-concrete bond strength. The design conditions of no bond stresses and no "cracking" should then allow achievement of the desired cycle life.

Example. - A simple example of the effect of steel area on blade weight for the condition of no "cracking" (zero tension in concrete) is given in table I. The table shows two designs for a simple prestressed concrete element meeting the same load condition (a tension force of 40 kips and compression force of 30 kips). For the concrete, the prestress is -2.0 ksi, the tension stress is zero, and the compression stress is -3.5 ksi. For design number 1, the steel area is comparable to conventional design practice (2.5 percent). For design number 2, the steel area is increased to 10 percent.

Unit weight for the element is obtained from the equations shown in the table. Values in the table show that over-reinforcing the concrete (10 percent steel area ratio) reduces the total weight by around 20 percent. Theoretically, the minimum weight is achieved at a concrete area of zero. In this case, the steel provides the primary structure, and the concrete provides the molded airfoil shape. Thus, a practical value of steel area for rotor blade applications can be determined from total weight and fabrication considerations (congestion of the volume by excess steel).

Geometry restrictions. - The thickness of wind turbine rotor blades is limited by the requirement to maintain efficient airfoil shapes at all sections. For the MOD-0 blade, the thickness decreases to 12 percent of the chord at the tip. Thus, for much of the outer portion of the blade, the maximum thickness is only several inches. Furthermore, for maximum bending stiffness, the prestressing bars should be as far from the section neutral axis as possible. For these reasons, as well as for the general need to reduce concrete volume and weight, it is grossly impractical to adhere to the relatively con-

TABLE I. - DESIGN EXAMPLE

Loads
- Tension ($P_t$), 40 kips
- Compression ($P_c$), 30 kips

Concrete stress
- Tension load, $\sigma_c = 0$
- Compression load, $\sigma_c = -3.5$ ksi

Steel
- $E_s = 29\,000$ ksi
- $\rho_s = 0.287$ lb/in$^3$

Concrete
- $E_c = 2900$ ksi
- $\rho_c = 0.0579$ lb/in$^3$ (100 pcf)

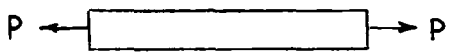


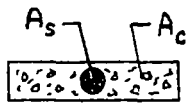


| Parameter | Design 1 | Design 2 |
|---|---|---|
| Steel area, $A_s$, in$^2$ | 0.4 | 1 |
| Concrete area, $A_c$, in$^2$ | 16 | 10 |
| Ratio, $A_s/A_c$ | 0.025 | 0.10 |
| Steel stress, ksi | | |
| Tension load | +80 + 20 = 100 | +20 + 20 = 40 |
| Compression load | +80 - 15 = 65 | +20 - 15 = 5 |
| Concrete stress, ksi | | |
| Tension load | -2.0 + 2.0 + 0 | -20 + 20 = 0 |
| Compression load | -2.0 - 1.5 = -3.5 | -2.0 - 1.5 = -3.5 |
| Weight, lb/in. | | |
| Concrete | 0.925 | 0.578 |
| Steel | .115 | .287 |
| Total | 1.040 | 0.865 |

Elongation: $(P_t + P_c)\dfrac{E_c}{\sigma_c} = E_cA_c + E_sA_s$

Weight: $w = \rho_cA_c + \rho_sA_s$

$$w = \rho_c\left[\left(\frac{P_t + P_c}{\sigma_c}\right) - A_s\left(\frac{E_s}{E_c} - \frac{\rho_s}{\rho_c}\right)\right]$$

servative requirements for concrete wall thickness and prestressing bar cover thickness used in conventional construction design practice. For example, according to the American Concrete Institute Building Code, concrete wall thickness should be at least 3 inches, and bar cover thickness (to protect against fire and other safety effects) should be a minimum of 1 inch.

The design approach for the concrete rotor blade considers that concrete wall thickness can be determined parimarily from strength considerations, since safety aspects are more favorable in wind turbine applications than for long term structures, where little, if any, periodic safety inspections are conducted.

Also, inasmuch as the concrete is designed for no cracking, and since a surface coating is recommended for surface smoothness, the requirement for bar cover thickness can be eased. The thickness relief in blade design is further encouraged by the recent appearance of precast concrete forms such as floor slabs and utility conduits with thinner than standard wall thickness.

## Blade Description

The baseline design for the prestressed concrete blade is shown in figure 2. The external dimensions are approximately those of the existing MOD-0 machine with aluminum blades. The rotor has a tip radius of 62.5 feet and a blade width that tapers linearly from 19 inches at the tip $R_t$ to 54.4 inches at 0.35 $R_t$. The MOD-0 blade has nonlinear variations of thickness and twist along the blade length. For the concrete blade, the thickness and twist vary linearly along the span in order to have single curvature of the surface with straight-line elements in the spanwise direction (along chord percentage lines). The single curvature surface simplifies layout and fabrication and closely approximates the double curvature surface. Reinforcing bars are straight members, and concrete forms can be made of plates with single curvature.

Blade ratio of maximum thickness to chord length is 0.12 at the tip and 0.30 at the base. Blade profiles are symmetrical NACA 230-series low-speed airfoil shapes with maximum thickness at 30 percent chord. The sections are set for a lift coefficient of 0.8 at design conditions.

The concrete section extends from 0.35 $R_t$ to 0.85 $R_t$, a length of 0.5 $R_t$ or 31.25 feet. The concrete portion of the blade provides the necessary beam strength. The trailing edge surface (aft 25 percent of chord) is fiberglass, as is the tip outboard of 0.85 $R_t$. The trailing edge has a very small airload, and thin unsupported fiberglass provides adequate strength at much less weight than a concrete surface. In addition, the fiberglass provides the required thin sharp trailing edge.

The tip section outboard of 0.85 $R_t$ has small bending moments, and a welded steel box spar provides adequate strength and rigidity at lower weight than a concrete blade tip. Inasmuch as the local airloads are high here, the fiberglass surface is internally supported by a foam which fills the blade cavity. At the extreme tip, the blade is less than 2 inches thick, which would require solid construction for reinforced concrete. The joint at 0.85 $R_t$ permits a break in the straight line surface elements, permitting lower twist and taper rates for the tip than for the concrete section.

The blade span between the hub and 0.35 $R_t$ is constructed of a welded steel tube of elliptical or oval cross-section. Each end of this tube is welded to a steel casting. The inboard casting adapts to the bolt circle of the existing MOD-0 hub. The outboard casting forms a transition from the tube shape to the concrete airfoil shape. The transition section connects to the threaded ends of the steel reinforcing bars at 0.35 $R_t$, but the splice nuts do not transmit the bar pre-load to the concrete, since this would cause local

bond damage at the time of removal from the preload fixture. The steel and fiberglass portions represent conventional types of material and fabrication.

A lightweight blade cuff of suitable airfoil section may be added inboard of 0.35 $R_t$. The local air pressures are about 10 percent of those at the blade tip, so unsupported fiberglass skin is adequate. The potential power improvement of this cuff is less than 10 percent at the design wind speed. At off-design wind speeds the cuff section may have an inefficient angle of attack.

The concrete portion of the blade has a few unique design features because of the necessity for tapering the prestressed structure. Details are shown in figure 3. Figure 3(a) is a plan form view of the blade showing the prestressing bars. Preload stresses are transferred to the concrete through bearing plates (fig. 3(b)) welded near each end of each bar. At any cross-section the concrete area is approximately ten times the bar area. If this ratio is constant it provides a uniform distribution of prestress throughout the entire structure. The high ratio of steel to concrete prevents tensile elongation of the concrete under any normal stress condition. It is also considered necessary, for consideration of fatigue life, to provide bearing blocks at the ends of each bar in order to minimize the bond stress between steel and concrete.

Reinforcing mesh is used around the prestressing bars as shown in figure 3(c). The cover thickness for casting around the mesh and bars is a minimum of 0.5 inch on each side of the bar. Concrete wall thickness is typically 0.75 inch.

The length, orientation and diameter of the prestressing bars in straight-line positioning is shown schematically in figure 4. Also shown in the figure is the spanwise variation in blade maximum thickness. Bar locations are also indicated in the concrete portion of the blade cross section shown in figure 5 for several spanwise positions. The blade tailing edge is completed by the attachment of the fiberglass section as illustrated in figure 6.

The concrete proposed is a light aggregate type weighing 100 pounds per cubic foot with a 28-day strength of 6000 psi, a 90-day strength of 7500 psi, and a modulus E of 2,900,000 psi. Various concrete mixes are feasible, but the most important parameter is probably the density. The modulus E is a function of both strength and density. It is desirable for the concrete to have high strain (strength/E) capacity, in order to permit the steel to cycle through a large stress range.

## Loads and Stresses

The concrete blade was designed to meet loading conditions specified in the contract for cyclic airloads in the spanwise direction which might be repeated $10^8$ times. The gravity loads, acting in the chordwise direction with complete load reversal each cycle for $10^8$ cycles, were calculated by the contractor after the blade weight distribution was determined from preliminary design. Stiffness requirements were dictated by the specified values of natural vibration frequency in the chordwise direction (4.32 x rpm) and in the spanwise

direction (2.70 x rpm). These values are essentially the same as those specified for the original aluminum blades of the MOD-0 wind turbine. The centrifugal blade tension forces were also calculated from the blade weight distribution and the normal rotation speed of 40 rpm. Curves for tension force and bending moments for these cyclic conditions are shown in figure 7.

A further loading condition was specified as a gust condition with a blade pitch angle of -20° and a rotor speed of 45 rpm. These loads were to be resisted $10^5$ cycles. However, the contractor chose a more severe load condition in which the airload corresponded to a maximum lift coefficient (at stall) with rotor speed of 45 rpm. With a design blade coning angle of 0.04 radians, a negative airload is more severe since it adds to bending moments from centrifugal forces. This loading condition seems plausible during an emergency shutdown condition when a circuit breaker opens, the electrical load is suddenly removed, the rotor overspeeds, and the blade is quickly feathered through the maximum negative angle of attack. Blade tension forces and bending moments are shown in figure 8 for this noncyclic condition. A more detailed discussion of the loading conditions for the design case and the emergency shutdown case is given in appendix D.

Stresses for the two loading conditions were calculated at various positions along the span of the blade. Details of the calculations are presented in appendix E. For the design cyclic loading condition, the factor of safety for fatigue is given by

$$F_f = \frac{\text{Fatigue limit}}{\text{Maximum stress}} = \frac{\sigma_f}{\sigma_{max}} \qquad (1)$$

Fatigue limits are discussed in appendix C.

Results of the calculations for the design case are shown in table II(a) for the steel at a bar prestress of 20,000 psi. Values are calculated for both the prestressing bars and the welded hub tube. Minimum safety factor in fatigue for the steel is seen to be a very comfortable 2.70.

Stress results for the concrete for the design cyclic load condition are given in table II(b). The concrete prestress is 2000 psi. All values are compression stresses. The factor of safety in fatigue near the blade base is lower than for the steel, with a value of 1.8 at $r/r_t = 0.35$. This region might warrent a closer evaluation, especially in view of the imprecise determination of the fatigue limit for concrete as discussed in appendix C. Perhaps the concrete wall thickness near the blade base should be increased somewhat for the baseline design.

The emergency shutdown loading is considered as a noncyclic load with limiting stresses equal to the ultimate strengths of the materials (115 ksi for the steel bars, 80 ksi for the steel tube in compression, and 7.5 ksi for the concrete in compression). Thus, for this loading case, the safety factor is

TABLE II. - STRESS RESULTS FOR CYCLIC LOADS

AT DESIGN CONDITION

| Radius ratio, $r/r_t$ | Maximum stress, $\sigma_{max}$, ksi | Minimum stress, $\sigma_{min}$, ksi | Fatigue limit, $\sigma_f$ ksi | Factor of safety, $F_f$ |
|---|---|---|---|---|
| (a) Steel (20,000 psi prestress in bars) | | | | |
| 0.052 | +9.68 | -4.76 | 34.6 | 3.57 |
| .20 | +9.25 | -3.49 | 32.7 | 3.53 |
| .334 | +8.96 | -3.06 | 33.5 | 3.74 |
| 0.350 | 27.63 | 17.93 | 74.5 | 2.70 |
| .4375 | 26.88 | 18.66 | 78.1 | 2.90 |
| .55 | 24.82 | 19.64 | 87.0 | 3.50 |
| .625 | 24.36 | 19.70 | 88.8 | 3.65 |
| .7 | 24.37 | 19.25 | 86.8 | 3.56 |
| .8 | 22.20 | 20.4 | *100 | 4.50 |
| (b) Concrete (2,000 psi prestress) | | | | |
| 0.35 | 2.207 | 1.237 | 3.993 | 1.809 |
| .4375 | 2.265 | 1.406 | 4.267 | 1.884 |
| .55 | 2.036 | 1.518 | 4.973 | 2.443 |
| .625 | 2.030 | 1.564 | 5.143 | 2.533 |
| .70 | 2.075 | 1.563 | 5.024 | 2.421 |
| .80 | 1.960 | 1.780 | 6.341 | 3.235 |

*Yield strength.

$$F_u = \frac{\text{Ultimate strength}}{\text{Maximum stress}} = \frac{\sigma_u}{\sigma_{max}} \tag{2}$$

Results of the calculations for the emergency shutdown case are shown in table III. As before, the steel prestress is 20 ksi and the concrete prestress is 2 ksi. For the shutdown case, the factors of safety are seen to be quite satisfactory: above 2.6 for the steel, and above 2 for the concrete.

## Blade Weight

The weight of the baseline blade design was determined from calculations of unit weight of the various elements of the blade along the length of the span. Local cross-sectional areas for the steel, concrete, and fiberglass were determined in conjunction with calculation of local section properties for the stress analysis (appendix E). Figure 9 shows the calculated spanwise distribution of weight for the baseline blade. Total blade weight is 4900 pounds.

TABLE III. - STRESS RESULTS FOR LOADS

IN EMERGENCY SHUTDOWN

| Radius ratio, $r/r_t$ | Tension | | Compression | |
|---|---|---|---|---|
| | Maximum stress, $\sigma_{max}$, ksi | Factor of safety, $F_u$ | Maximum stress, $\sigma_{max}$, ksi | Factor of safety, $F_u$ |
| Blade | Steel bars | | Concrete | |
| 0.35 | 43.2 | 2.66 | 3.62 | 2.07 |
| .4375 | 43.7 | 2.63 | 3.66 | 2.05 |
| .55 | 38.4 | 3.30 | 3.28 | 2.28 |
| .625 | 38.0 | 3.05 | 3.42 | 2.20 |
| .70 | 35.7 | 3.22 | 3.14 | 2.38 |
| .80 | 34.3 | 2.96 | 3.13 | 2.40 |
| Hub tube | Steel | | Steel | |
| 0.52 | 25.28 | 4.55 | 19.08 | 4.19 |

The indicated weight of the prestressed concrete blade is more than twice the weight of the original aluminum blade for the MOD-0 wind turbine. There may be some potential for weight reduction through design refinement. However, in view of the existing deviations from conventional reinforced concrete design practice and the uncertainty of the fatigue data for lightweight concrete, such speculation appears unwarranted at this point.

The heavier weight of the concrete blade, in itself, is not considered a serious detriment, as long as the blades can be manufactured at much lower cost than conventional metal blades. However, it will be necessary to investigate the impact of the heavier blades on the design and construction of the rotor hub, the nacelle, and the supporting tower. This subject will be discussed in a later section of the report.

## Cost Estimate

Estimates were made for the cost of fabricating prestressed concrete blades based on the baseline blade design. Production quantities of 1, 10, and 100 were considered. The tooling cost was also estimated. The cost estimates were based on firm price quotations from various fabricators as well as in-house estimates of some components.

The cost estimation process involved the completion of detailed fabrication drawings, the definition of fabrication methods, and the pricing of all

components involved. For simplicity, the blade fabrication was divided into five components: (1) blade hub assembly; (2) prestressed beam; (3) tip assembly; (4) trailing edges; and (5) final assembly. A discussion of blade fabrication procedures and detailed drawings of the major blade components are given in appendix F (figs. 35 through 44).

A breakdown of the cost estimate for a production quantity of ten blades is shown in table IV. Results of the cost estimates are summarized below:

| Item | Cost, $ |
|---|---|
| Blades | |
| 1 | 33,584 each |
| 10 | 17,579 each |
| 100 | 10,440 each |
| Tooling | 117,549 |

The figures in the summary are "factory" costs (total of quotations from subcontractors, in-house components and final assembly cost), with no fee or profit for the prime contractor.

For a production run of ten blades, the estimated cost of $17,579 for a prestressed concrete blade is substantially lower than the approximately $200,000 cost of an aluminum blade for the MOD-0 wind turbine. It is also interesting to note that for a production of 100 blades, as might be required for a wind turbine "farm," the entire cost per blade, including the tooling cost, would run around $11,600 ($10,440 for blade and $1,175 for tooling).

## MODEL BLADE SECTION

In view of the relatively thin concrete walls in the baseline design, it was desirable to actually construct a model blade section to verify the proposed manufacturing methods. A six-foot length having a typical cross-section and the necessary forms was constructed to study the feasibility of casting concrete in a blade configuration. The section was symmetrical with a maximum thickness ratio of around 20 percent and a chord length of around 3 feet. The parts and procedures of the test casting processes are summarized in the following photographs.

Figure 10 shows the concrete form with one of its two sides hinged open. Both side hinges open for part removal. This 6-foot section form was not prestressed, so that a compressive structure is not involved. The steel form to produce the inner disposable core is shown in figure 11. The form is bolted together with removable ends. In a full size casting, the inner foam core would still be made in approximately 6-foot lengths. The foam core after curing is shown in figure 12. This core is lightweight polyurethane (5 $lb/ft^3$) which would remain in the concrete casting. The procedure to install the foam core into the concrete form is shown in figure 13. The core is placed inside the steel bars which serve as locations for the core.

TABLE IV. - COST ESTIMATE

Production quantity of 10

| Item | Cost, dollars | | |
|---|---|---|---|
| | Material, at cost | Labor, at $15/hr | Total |
| Blade assembly | 10 569 | 7010 | 17 579 |
| Blade hub assembly | 6 135 | 480 | 6 615 |
| Transition casting | 300 | 240 | 540 |
| Adapter fitting | 235 | 240 | 475 |
| Tube | 4 800 | | 4 800 |
| Assembly | 800 | | 800 |
| Prestressed beam | 1 070 | 3360 | 4 430 |
| Concrete | 300 | | 300 |
| Foam | 200 | 240 | 440 |
| Steel | 520 | 480 | 1 000 |
| Inserts | 50 | | 50 |
| Casting | | 1800 | 1 800 |
| Finish | | 600 | 600 |
| Mold preparation | | 240 | 240 |
| Tip assembly | 1 532 | 1200 | 2 732 |
| Knuckle casting | 50 | 120 | 170 |
| Plates and tubes | 100 | | 100 |
| Welding | | 240 | 240 |
| Fiberglass envelope | 1 282 | | 1 282 |
| Foam | 50 | | 50 |
| Assembly | | 600 | 600 |
| Finish | 50 | 240 | 290 |
| Trailing edges | 1 432 | 600 | 2 032 |
| Fiberglass (set) | 1 282 | | 1 282 |
| Hardware | 150 | | 150 |
| Fitting | | 600 | 600 |
| Assembly | 400 | 1370 | 1 770 |
| Blade hub to beam | 50 | 120 | 800 |
| Balance | 200 | 600 | 800 |
| Finish | 150 | 650 | 800 |

Figure 14 illustrates the installation of the steel bars and the steel reinforcing mesh. After the core was installed, the bars were stretched slightly to locate the core. The reinforcing mesh is then installed and tried to the bars. All of the cast-in-place inserts were installed, and the form was closed on the sides, with the top left open for pouring and trowelling.

The closed form is shown in figure 15, with concrete ready in a wheelbarrow. In actual production, the concrete would be cast directly into the top of of the form with the use of special chutes. Vibrators, located on the side of the form, were used to aid the settling of the concrete and the elimination of entrapped air. After curing (24 hr, if heat assisted), the part was removed, and the curing was completed outside of the form.

A section of the 6-foot casting with protruding steel bars is shown in figure 16 (foam core still intact). In an actual full-size construction, these bars would be prestressed to maintain the concrete in a compressive state. Finally, a 2-inch slice cut from the casting with a fiberglass trailing edge section attached is shown in figure 17.

No problems were encountered in the construction of the model section. The mold was successfully filled and the steel bars were properly positioned. The feasibility of casting concrete in the baseline blade configuration was thereby established. However, because of the absence of prestressing in the concrete, the model section could not be used for any strength or property evaluations.

## DYNAMIC ANALYSIS

The second phase of the study effort involved an analysis of the loads and stresses resulting from coupled vibrations of the blades, nacelle, and tower with concrete blades installed (baseline design). It was originally specified that the natural vibration frequency of the concrete blades should be the same as for the aluminum blades of the MOD-0 wind turbine. For the same natural frequencies, the concrete blades would then tend to be heavier and stiffer than the corresponding aluminum blades. The exact nature of the vibration loads with concrete blades, and the possible adverse effect of the transmission of these loads to the nacelle and support tower was not known. Thus, the need for further dynamic analysis.

The dynamic analysis conducted herein compares results for concrete and aluminum blades on the MOD-0 tower. For the concrete blade, the flapping (spanwise) frequency was 2.70 cycles per revolution (2.70 p), and the inplane (chordwise) frequency was 4.32 p. The corresponding frequencies for the MOD-0 aluminum blade are 2.73p and 4.24p, respectively.

Cyclic loads to the nacelle and tower result from a tower wake phenomenon in which the rotor passes through a dead-air region behind the tower and the airload is suddenly reversed. Each rotor blade receives a high impulsive load once per revolution (e.g., ref. 5). A Fourier analysis of the impulse shows almost equal components at 1p (once per revolution), 2p, 3p, 4p, etc. to high frequencies. Thus, even a high harmonic frequency (say 6p) could be excited

by the tower wake airload. A once-per-revolution change also results for the gravity load components on the blade.

In a vibration cycle, the loads reach maximum and minimum values. Results are expressed in terms of steady and cyclic values, where,

$$\text{Steady value} = \frac{1}{2}(\text{maximum} + \text{minimum}) \tag{3}$$

$$\text{Cyclic value} = \frac{1}{2}(\text{maximum} - \text{minimum}) \tag{4}$$

Principal concerns in the analysis are the steady and cyclic loads and moments about the blades (rotor axes) and about the hub (hub axis). These axes are shown in figure 22. Moments about the hub axes indicate effects on the nacelle and tower. Included in the analysis was a quantitative and qualitative evaluation of the effects of a flexible tower, power train, yaw drive, and control system. Particular emphasis was placed on the stiffness of the yaw drive system. A brief description of the computer codes used in the analysis is given in appendix G.

Calculations were made for five cases as defined below:

| Blade | Wind speed, $V_w$, mph | Yaw rate, deg/sec |
|---|---|---|
| MOD-0 aluminum | 26 | 0 |
| | 40 | 0 |
| Prestressed concrete | 26 | 0 |
| | 40 | 0 |
| | 40 | 0.5 |

The case with the yaw rate was included because of a possible intensification of the rotor loads under this condition. The basic geometry of the rotor blades (chord and twist distributions) used in the study is identical to the MOD-0 blades. The precone angle, which was reduced from the MOD-0 value of 7° to 2.29°, was kept at 2.29° in the calculations. The mass and EI distributions were revised to fine tune the first inplane frequency. The mass distribution is shown in figure 9, and the EI variation is obtained from figure 34. The rotor shaft was taken to be rigid in all calculations.

## Shaft Loads

Rotor axes. - Results of the calculation of shaft loads resolved to the rotor axes (fig. 22) are summarized in table V. Values were calculated for the

effects of one blade and a rigid yaw drive system (tower) with the MOSTAB computer code system described in appendix G. The marked increase in blade forces for the concrete blade shown in table V(a) is an expected result of the greater weight of the concrete blade compared to the MOD-0 aluminum blades (around 5000 vs. 2000 lb). In general, the addition of the 0.5°/second yaw rate did not have a significant effect on the calculated forces.

TABLE V! - SHAFT LOADS HARMONIC DATA FOR ROTOR AXES

[One blade only.]

(a) Forces

| Wind speed, mph | Blade system | Force, $F_x$, lb | | Force, $F_y$, lb | | Force, $F_z$, lb | |
|---|---|---|---|---|---|---|---|
| | | Steady | Cyclic | Steady | Cyclic | Steady | Cyclic |
| 26 | MOD-0 | -23 510 | 2028 | 408.7 | 2 150 | -1 542 | 1 044 |
| 26 | Concrete | -72 930 | 4722 | 424.5 | 5 294 | -1 519 | 1 537 |
| 40 | MOD-0 | -23 760 | 2243 | 639.4 | 2 399 | -123.3 | 2 172 |
| 40 | Concrete | -72 950 | 4672 | 498.6 | 5 265 | -580.2 | 2 333 |
| 40 | Concrete 0.5 °/sec | -72 960 | 4677 | 514.7 | 5 312 | -568.6 | 2 638 |

(b) Moments

| Wind speed, mph | Blade system | Torsion, ft-lb | | Flapwise moment, ft-lb | | Chordwise moment, ft-lb | |
|---|---|---|---|---|---|---|---|
| | | Steady | Cyclic | Steady | Cyclic | Steady | Cyclic |
| 26 | MOD-0 | 1 631 | 6176 | 37 740 | 43 880 | -13 670 | 49 670 |
| 26 | Concrete | 372.5 | 5208 | 26 020 | 56 580 | -16 930 | 134 500 |
| 40 | MOD-0 | 2 044 | 7274 | 100 500 | 86 440 | -17 160 | 60 780 |
| 40 | Concrete | 291.2 | 5053 | 68 180 | 84 370 | -17 520 | 134 200 |
| 40 | Concrete 0.5 °/sec | 340.7 | 5126 | 68 450 | 94 160 | -17 980 | 135 700 |

Of particular significance are the results for the flapwise and chordwise moments listed in the second part of the table. Chordwise (inplane) cyclic moments are amplified more than twice for the concrete blades. However, the maximum value (135,700 ft-lb) is not greater than the normal operation chordwise cyclic load ($M_y$ = 145,000 ft-lb at the axis) shown in figure 7. The reduction in steady flapwise moment for the concrete blade indicates how well the precone angle, mass distributions, and design operating conditions are matched. For the cyclic flapwise moment, there is an increase for the concrete blade at the

lower wind speed, with a tendency for the yaw rate to increase the moment again. However, these upper values from the coupled dynamic analysis are not far removed from the normal operation cyclic value in figure 7 ($M_x$ = 83,300 ft-lb). Effect on design blade fatigue life should, therefore, not be significant.

Hub axes. - When loads are resolved to the hub axes (fig. 22) they provide information about shaft torque and nacelle yaw and pitching moments. Results from the harmonic analysis for the hub axes are listed in table VI. The

TABLE VI. - SHAFT LOADS HARMONIC DATA FOR HUB AXES

[Rotor system.]

(a) Forces

| Wind speed, mph | Blade system | Force, $F_x$, lb | | | Force, $F_y$, lb | | | Force, $F_z$, lb | | |
|---|---|---|---|---|---|---|---|---|---|---|
| | | Steady | 2p | 4p | Steady | 2p | 4p | Steady | 2p | 4p |
| 26 | MOD-0 | 4 138 | 185 | 198 | 62.4 | 252 | 198 | 3 747 | 575 | 166 |
| 26 | Concrete | 10 330 | 594 | 320 | 208 | 683 | 320 | 3 712 | 769 | 327 |
| 40 | MOD-0 | 4 206 | 464 | 446 | 286.2 | 561 | 446 | 1 995 | 1 513 | 420 |
| 40 | Concrete | 10 360 | 621 | 454 | 19.1 | 687 | 454 | 2 235 | 1 214 | 508 |
| 40 | Concrete 0.5 °/sec | 10 390 | 661 | 454 | 133 | 724 | 454 | 2 235 | 1 210 | 507 |

(b) Moments

| Wind speed, mph | Blade system | Yawing moment, ft-lb | | | Pitching moment, ft-lb | | | Shaft torque, ft-lb | | |
|---|---|---|---|---|---|---|---|---|---|---|
| | | Steady | 2p | 4p | Steady | 2p | 4p | Steady | 2p | 4p |
| 26 | MOD-0 | 7 073 | 23 100 | 11 370 | 36 300 | 32 550 | 11 370 | 28 200 | 5 626 | 16 770 |
| 26 | Concrete | 5 484 | 44 700 | 26 300 | 37 100 | 28 610 | 26 310 | 26 880 | 6 302 | 5 691 |
| 40 | MOD-0 | 11 550 | 42 990 | 29 380 | 57 450 | 66 260 | 29 380 | 26 150 | 14 480 | 38 240 |
| 40 | Concrete | 7 832 | 68 140 | 40 750 | 50 490 | 44 700 | 40 750 | 26 200 | 10 780 | 8 957 |
| 40 | Concrete 0.5 °/sec | 11 320 | 76 050 | 40 730 | 60 320 | 52 360 | 40 730 | 26 120 | 11 020 | 9 597 |

values for the 0p harmonic are steady loads. For the steady forces (table VI(a)), the heavier concrete blades, as expected, increased the tension considerably, but had little effect on the torsion.

As before, the moment results of part (b), which indicate moments on the nacelle, are most significant. For the shaft torque, the steady values change very little. This is expected inasmuch as all cases are designed to produce the same power. The cyclic values, however, either increase or decrease for the concrete blades. There is some load aggravation due to the yawing rate for the 2p and 4p excitation.

Steady values of the pitching moment showed no large variations. The 2p loads actually decreased for the concrete blades, but the 4p results showed

a marked increase at both wind speeds. Furthermore, the addition of the yaw rate produced significant increases in steady and 2p loads. The pitching moment may, therefore, be an important design factor, since the direction of the yawing motion will tend to push the blades toward the tower.

For the yawing moment, the steady values decreased for the concrete blade. However, there was a considerable amplification of the 2p and 4p loads for the concrete blades at both wind speeds. The behavior of this moment was sufficiently interesting to warrant further study, as described in appendix H. A simple one-degree-of-freedom analysis was conducted which identified the factor which caused the increase in harmonic activity for the concrete blade. Simply stated, the increased flapping inertia of the heavier concrete blades decreased the modal damping ratio, thus allowing higher 2p and 4p loads to develop. In a broader sense, this observation may dictate limits on the vibration properties of the blade configuration.

## Nacelle Moments

In view of the implication of increased nacelle moments as obtained from the hub axes load results presented in the preceeding section, further calculations of nacelle dynamic pitching and yawing moments were made with the WINDLASS computer code system described in appendix G. These codes were used to assess the effects of a flexible drive shaft, yaw drive, tower, and control system on the nacelle pitching and yawing moments. Three conditions were considered: "rigid" - all rigid system (from MOSTAB code execution); "stiff" - relatively high yaw drive stiffness value (WINDLASS execution); and "soft" - low value of yaw drive stiffness (WINDLASS execution). In these calculations, the loads resolved to the hub axes are due to an entire rotor system. Results of these harmonic calculations are summarized in table VII.

For the nacelle pitching moment (part (a) of the table), the steady moments with the concrete blades tend to decrease sharply and then rise somewhat as the support stiffness is relaxed. In contrast, the cyclic moments increase slightly and then fall off. The steady moments decrease in going from the MOD-0 aluminum blade system to the concrete blades. However, when the yaw rate is added, the steady pitching moment increases again and becomes greater than for the MOD-0 case as the support stiffness is relaxed. The cyclic moments for the concrete blades first decrease and then increase, compared to the MOD-0 case, as the yaw rate is added. However, the maximum concrete cyclic moments are not greater than for the MOD-0 blades.

Results for the nacelle yawing moment are given in part (b) of table VII. The principal observation is the pronounced increase in the cyclic values of yawing moment with the concrete blades (order of 100 000 ft-lb) for all stiffness states. As indicated in the previous section, the increase in cyclic loads (2p frequency) with the concrete blades results from the accompanying reduction in blade damping ratio. Such high levels of nacelle yawing moment would be completely unacceptable if the present concrete blades were installed on the MOD-0 tower.

TABLE VII. - NACELLE PITCHING AND YAWING MOMENTS[a]

[Complete rotor system.]

| Wind speed, mph | Blade system | Support system | | | | | |
|---|---|---|---|---|---|---|---|
| | | Rigid | | Stiff | | Soft | |
| | | Steady | Cyclic | Steady | Cyclic | Steady | Cyclic |
| (a) Pitching moment | | | | | | | |
| 26 | MOD-0 | 44 800 | 34 320 | ------ | ------- | ------- | ------- |
| 26 | Concrete | 48 120 | 42 510 | 25 575 | 43 165 | 25 660 | 41 180 |
| 40 | MOD-0 | 79 570 | 72 070 | 35 190 | 75 200 | 31 310 | 86 160 |
| 40 | Concrete | 67 080 | 66 470 | 32 915 | 67 585 | 32 820 | 64 920 |
| 40 | Concrete 0.5 °/sec | 79 050 | 70 770 | 39 780 | 72 620 | 40 330 | 70 590 |
| (b) Yawing moment | | | | | | | |
| 26 | MOD-0 | -14 720 | 25 710 | ------ | ------ | ------- | ------- |
| 26 | Concrete | -7 670 | 61 340 | -3 260 | 61 220 | -2 220 | 65 960 |
| 40 | MOD-0 | -22 350 | 57 870 | 680 | 58 740 | -14 960 | 58 400 |
| 40 | Concrete | -11 210 | 94 000 | -4 390 | 93 850 | -2 640 | 99 710 |
| 40 | Concrete 0.5 °/sec | -18 350 | 100 400 | -4 230 | 100 200 | -20 900 | 105 510 |

[a]All values in ft-lb.

The cyclic hub loads of a rotor system depend on the blade natural flapping frequency as well as on the blade damping ratio. The dependence of the hub yawing moment on flapping frequency was explored in appendix H based on a simple one-degree-of-freedom model. The results of the analysis indicated that substantial reductions in hub yawing moment might be obtained from a relatively modest (15 to 18 percent) reduction in the flapping frequency of the concrete blade. As discussed in appendix H, reducing the flapping frequency from 2.7 to 2.2 might possibly result in concrete-blade system hub moments to within around 10 percent of the MOD-0 values. However, this result was drawn from a simple one-degree-of-freedom model, not a full 4- or 6-degree-of-freedom analysis. Therefore, a full analysis such as MOSTAS-B would be required to completely assess the effects of the reduced blade flapping frequency.

## Modification Options

Several approaches are available to deal with the problem of excessive nacelle moments that were shown to result from the use of a rotor with baseline concrete blades with a high value of flapping frequency. The options involve modifications to the blades, the support structure, or both.

Component redesign. - The most obvious option is to redesign the affected components on the MOD-0 structure to accommodate the increased dynamic loads. However, this does not seem to be a reasonable engineering solution for the present situation (but might be feasible if additional similar towers were constructed).

Downwind installation - flexible blades. - The principal design modification indicated for the concrete blades is a reduction in natural flapping frequency. The proposed reduced flapping frequency should largely bring the hub moments with the concrete blades more in line with those of the original MOD-0 rotor system. The original design specification of a value close to that of the MOD-0 aluminum blades was somewhat arbitrary, and a reduction in the design value, per se, poses no problem. Inasmuch as the indicated reduction is rather modest (from 2.7 p to around 2.2 p), the design changes for the concrete blade should not be drastic. The desired reduction in flapping frequency can readily be obtained from a redesign of the blade hub tube (fig. 2). A small reduction in blade weight might even result. Furthermore, such an increase in blade flexibility can well support the static weight of the blades when feathered in the horizontal position without noticeable tip droop. The change in design to accommodate a more flexible blade should not increase the blade cost.

There is reason for consideration of a flapping frequency reduction to a value around 1.6/rev. Some modern wind turbine designs have teetered or hinged blade hubs so that the blades are free to flap. For these configurations, the flapping frequencies are around 1.6/rev. A reduction to this value of flapping frequency for prestressed concrete blades might also be considered if the 2.2/rev level is too close to a strong 2/rev excitation. Concrete blades at the 1.6/rev level might well show a noticeable tip droop when feathered horizontally.

For the more flexible concrete blades installed in the downwind position, only nominal changes would be required for the support tower. The blade should be coned with the tips downwind at some angle between 2.29° and 4° from the plane of rotation. This requires that the blade root fitting attaches with a bend of 3° to 4.71°, placing the blade center of gravity some 1.44 to 2.26 feet from the blade feathering axis. Using the value of 2.26 feet, the required pitch control moment is 21,200 sin $\beta$ (ft-lb) for each blade at operating rotor speed. This seems a reasonable value for the present system, although the blades would probably be swept slightly so that no hydraulic pressure would be required to hold the blades in operating pitch. During feathering, the required torque would reduce with speed of rotation.

The rotor axis can be tilted to permit tower clearance of the blades. A bevel ring above the turntable appears a fairly simple way to do this. The downstream tower system is shown in figure 18. The rotating blades have ap-

proximately the same tower clearance as at present. When feathered, the blades are farther from the tower. In the configuration of figure 18, all cyclic loads to the pod and tower should be comparable to the present loads. Steady loads from the added blade weight are less than the reduction of dynamic loads resulting from the more flexible blades.

Upwind installation - stiff blades. - This configuration basically corrects the conditions which cause the load increase (resonant vibrations excited by the tower wake). With the rotor blades mounted upwind of the tower, the loads on the hub, shaft, and bearings would be lower than with the downwind MOD-0 installation with aluminum blades. The rotor axis should be tilted upward so that the blades clear the tower. The various effects of tilting the rotor appears small compared to the tower wake effect. An upwind rotor with no coning angle (flat rotor) is shown in figure 19. The blade center of gravity is about 3.23 feet from the feathering axis, and the required pitch control torque is 30,300 sin $\beta$ ft-lb. This probably approaches the limit of the present system.

TABLE VIII. - EFFECTS OF VARIOUS CONCRETE BLADE CONFIGURATIONS ON MOD-0 TURBINE INSTALLATION

| Characteristics | Rotor downstream | | Rotor upstream | |
|---|---|---|---|---|
| | Stiff blades (frequency 2.7p) | Flexible blades (freq. 2.2p - 1.6p) | Flat rotor disk | Coned rotor disk |
| Figure number | 18 | 18 | 19 | 20 |
| Cone angle, deg | 2.39 | 2.39 | 0 | -2.39, -7 |
| Coning method | Blade Root angle | Blade Root angle | Blade Root angle | Hub Change |
| Turntable tilt ring angle, deg | 5 | 5 | 7 | 10 to 14 |
| Overloaded components[a] | Hub Pitch control Yaw drive Tower | Non | Pitch control mechanism | None |
| Component changes required | Tilt ring hub, pitch control, yaw drive systems | Tilt ring | Tilt ring pitch control mechanism | Tilt ring pitch control gears, hub |

[a]Higher loads than for present aluminum blades in MOD-0 wind turbine.

A better configuration is shown in figure 20. Here, the rotor is upstream, but the blades are coned downstream so that centrifugal forces again relieve airload bending moments. Further tilt of the rotor axis is necessary to provide blade clearance from the tower. The hub mechanism must be changed. It appears possible to use all existing hub parts except the three bevel gears if the cone angle is changed from 7° away from to 7° toward the tower. The hub housing is simply reversed, as both ends now use a bolt circle of 24 5/8ths inch bolts. The existing and proposed hub mechanism are shown in figure 21. A summary of the factors involved in the several modification options is given in table VIII.

## CONCLUDING REMARKS

The preliminary analytical evaluation of a prestressed concrete blade for wind turbines described herein has revealed no apparent difficulty or problem in achieving a satisfactory design with a large potential reduction in fabrication cost. These results were obtained, however, based on some deviations of the design approach from conventional concrete design practices for concrete wall thickness and reinforcing bar cover thickness. Furthermore, the blade design was based on the use of a lightweight (low-density) concrete formulation, for which ample reliable property data are largely lacking. Of particular concern with lightweight concrete are the fatigue strength and the creep and shrinkage characteristics.

Any further serious pursuit of prestressed concrete blade construction should, therefore, first consider further investigation and experimental verification of these factors. Consideration might also be given to the use of fibrous concrete which has excellent fatigue resistance. A necessary further step is the construction of a large-scale or full-scale model blade with prestressing. The effects of creep and shrinkage during the curing process after casting could then be determined. Subsequent testing of such a model can establish the structural behavior of the blade under load, and can also verify the design stress calculations and material properties. Specimen tests of the concrete formulation in prestressed beams without cracking are also required to determine long-term fatigue strength.

Close attention to the value of the blade flapping frequency may be required in concrete blade design in order to minimize potential adverse rotor-tower dynamic coupling effects. Consideration should also be given to mounting concrete-bladed rotors on the upwind side of the tower.

## APPENDIX A

## SYMBOLS

| | |
|---|---|
| $A$ | area |
| $\bar{A}$ | equivalent area for steel |
| $C$ | chord length |
| $C_d$ | drag coefficient of airfoil section |
| $C_{d,t}$ | airfoil drag coefficient for thick trailing edge |
| $C_\ell$ | lift coefficient of airfoil section |
| $C_p$ | power coefficient, $\Delta P/P_i$ |
| $E$ | elastic modulus |
| $F$ | factor of safety for stress, or force |
| $G$ | shear modulus |
| $I$ | moment of inertia |
| $\bar{I}$ | equivalent moment of inertia for steel |
| $k$ | constant in equation developments |
| $L$ | load |
| $M$ | moment |
| $m$ | mass flow |
| $P$ | load, or power |
| $P_i$ | ideal power |
| $p$ | harmonic integer, per revolution |
| $Q$ | rotor torque |
| $q$ | dynamic pressure |
| $R$ | radius of bar |
| $r$ | radius along blade |
| $r_t$ | radius at blade tip |

| | |
|---|---|
| $T$ | centrifugal force |
| $T_x$ | axial thrust |
| $t_e$ | blade trailing edge thickness |
| $t_{max}$ | blade maximum thickness |
| $V_w$ | approaching wind velocity |
| $V_s$ | downstream slipstream velocity |
| $V_T$ | rotor tangential velocity |
| $W$ | gravity (weight) load |
| $w$ | weight per unit length |
| $x$ | direction along longitudinal axis of member, or along longitudinal centroidal axis of blade |
| $y$ | direction perpendicular to blade axis |
| $\beta$ | angle between blade chord line and plane of rotation |
| $\Delta$ | change in quantity |
| $\delta$ | ratio of vibratory to static displacement |
| $\mu$ | bond stress between concrete and steel |
| $\nu$ | shear stress in concrete |
| $\xi$ | axial tension strain, or damping ratio |
| $\rho$ | density |
| $\sigma$ | stress in material |
| $\sigma_{max}$ | maximum stress for cyclic load |
| $\sigma_{min}$ | minimum stress for cyclic load |
| $\sigma_u$ | ultimate strength of material |
| $\Omega$ | rotor angular velocity |
| $\omega$ | blade natural frequency |

Subscripts:

| | |
|---|---|
| c | concrete |
| f | fatigue limit |
| L | power loss |
| o | prestress condition |
| s | steel, or slipstream |

## APPENDIX B

## AERODYNAMIC ANALYSIS

The use of crude airfoil shapes with rough surfaces and blunt trailing edges could result in significant reductions in blade fabrication cost. However, such factors may seriously compromise the aerodynamic efficiency of the rotor design. It was desirable, therefore, to conduct a simplified aerodynamic analysis to determine the general sensitivity of turbine power loss to blade aerodynamic performance, and, more specifically, to the effects of blade surface roughness and trailing edge thickness. The analysis first defines the relationship between rotor power loss and blade aerodynamic performance, and then evaluates the power losses associated with surface finish and trailing edge thickness.

### Rotor Power

The rotor aerodynamic power can be established from conventional simplified propeller momentum theory. Under normal operation, the slipstream flow across the rotor blades looses kinetic energy, so that the exit slipstream velocity $V_s$ is less than the approaching wind velocity $V_w$. Part of the kinetic energy appears as useful aerodynamic power $P$. The remainder is absorbed mainly in overcoming the aerodynamic drag of the rotor blades $\Delta P_d$ and in imparting rotation to the slipstream $\Delta P_s$ due to the deflection of the airflow by the blades. Rotor drag is taken as the blade profile drag, since the very high aspect ratio of a wind turbine rotor blade renders the induced drag small compared to the profile drag.

Maximum power. - For flow across the rotor disk, there is an optimum relationship between the downstream velocity $V_s$ and the upstream velocity $V_w$ that results in the maximum power to the rotor. This is obtained in the following development which assumes initially that the slipstream rotation is negligible. The mass flow per second through the rotor is

$$m = \rho A V_{av} \tag{B1}$$

where the average velocity at the rotor is

$$V_{av} = \frac{1}{2}(V_w + V_s) \tag{B2}$$

The axial thrust $T_x$ on the rotor is equal to the change in momentum per second

$$T_x = mV_w\left(1 - \frac{V_s}{V_w}\right) \tag{B3}$$

The power of the ideal rotor is equal to the product of the thrust and average velocity, or to the product of the rotor torque $Q$ and the rotor angular velocity $\Omega$,

$$P_i = T_x V_{av} = Q\Omega \tag{B4}$$

For the design operating condition of the rotor, the ratio of wind velocity to rotor tangential velocity $V_w/V_T$ is of the order of 0.1. Thus, the aerodynamic drag forces will be within 0.1 radian from the plane of rotation, and will be assumed in this plane. Accordingly, the drag forces have a total value of very nearly $T_x(C_d/C_\ell)$ and a moment arm of $2/3\ r_t$, with a power loss

$$\Delta P_d = Q_d\Omega = T_x\left(\frac{C_d}{C_\ell}\right)\frac{2}{3}\ (r_t\Omega) \tag{B5}$$

The rotor aerodynamic power is obtained by subtracting the drag loss $\Delta P_d$ from the ideal power $P_i$ (eq. (B4)) to give

$$P = P_i - \Delta P_d = T_x\left(V_{av} - \frac{C_d}{C_\ell}\frac{2}{3}\ V_T\right) \tag{B6}$$

The optimum ratio $V_s/V_w$ can now be evaluated by expressing equation (B6) in terms of this ratio,

$$P = T_x V_w\left[\frac{1}{2}\left(1 + \frac{V_s}{V_w}\right) - \frac{2}{3}\left(\frac{C_d}{C_\ell}\right)\left(\frac{V_T}{V_w}\right)\right] \tag{B7}$$

Furthermore, by expressing $T_x$ in terms of $m$ from equation (B3) and then $m$ in terms of $V_s/V_w$ from equations (B1) and (B2), the power equation becomes

$$P = \frac{1}{2}\rho A V_w^3\left\{\frac{1 - \left(\frac{V_s}{V_w}\right)^2}{2}\left[\left(1 + \frac{V_s}{V_w}\right) - \frac{4}{3}\left(\frac{C_d}{C_\ell}\right)\left(\frac{V_T}{V_w}\right)\right]\right\} \tag{B8}$$

Ideal power. - The ideal rotor power is defined as the maximum aerodynamic power generated for the condition of zero drag. For zero drag, equation (B8) becomes

$$P_0 = \frac{1}{2}\rho A V_w^3\left\{\frac{1}{2}\left[1 - \left(\frac{V_s}{V_w}\right)^2\right]\left(1 + \frac{V_s}{V_w}\right)\right\} \tag{B9}$$

Differentiating equation (B9) with respect to the ratio $V_s/V_w$ and setting the derivative equal to zero produces

$$\frac{V_s}{V_w} = \frac{1}{3}, \qquad \text{so that} \qquad V_{av} = \frac{2}{3} V_w \tag{B10}$$

The theoretical maximum power $P_i$ is then obtained from equation (B9) as

$$P_i = 0.5926 \left( \frac{1}{2} \rho A V_w^3 \right) \tag{B11}$$

Power ratio. - The power ratio for the effect of aerodynamic drag is defined as $P/P_i$ and is given from equations (B8) and (B11) as

$$\frac{P}{P_i} = \frac{\dfrac{1 - (V_s/V_w)^2}{2} \left[ \left( 1 + \dfrac{V_s}{V_w} \right) - \dfrac{4}{3} \left( \dfrac{C_d}{C_\ell} \right) \left( \dfrac{V_T}{V_w} \right) \right]}{0.5926} \tag{B12}$$

Plots of equation (B12) are shown in figure 23 for several values of the drag parameter $(C_d/C_\ell)(V_T/V_w)$. Maximum power ratio decreases with increasing drag. Also, the value of $V_s/V_w$ at maximum power increases with increasing drag. However, the ideal value of $V_s/V_w = 1/3$ is very close to the peaks of the curves for all values of drag parameter considered. Thus, for simplicity, a fixed value of slipstream velocity ratio can be taken for use in further analysis of rotor power. With $V_s/V_w = 1/3$, equation (B12) for the power ratio due to profile drag becomes

$$\frac{P}{P_i} = 1 - \left( \frac{C_d}{C_\ell} \right) \left( \frac{V_T}{V_w} \right) \tag{B13}$$

Power loss coefficient. - In singling out the effect of aerodynamic losses on rotor power, it is illuminating to work in terms of a power loss coefficient, where,

$$C_{p,L} = \frac{\Delta P_L}{P_i} \tag{B14}$$

For the wind turbine rotor, two major sources of aerodynamic power loss are considered: the blade profile drag; and the rotational energy of the slipstream. Thus,

$$C_{p,L} = \frac{\Delta P_d}{P_i} + \frac{\Delta P_s}{P_i} \tag{B15}$$

For the profile drag, from equation (B13),

$$\frac{\Delta P_d}{P_i} = \left(\frac{C_d}{C_\ell}\right)\left(\frac{V_T}{V_w}\right) \tag{B16}$$

For the slipstream rotation, the downstream air of mass m has angular momentum about the rotor axis equal to the rotor torque Q. The torque Q varies inversely with the angular velocity $\Omega$, since $Q\Omega = P$. The rotational kinetic energy of the slipstream varies inversely with $\Omega^2$. With the preceeding considerations and a few reasonable approximations (e.g., vortex core about 0.2 $r_t$), the kinetic energy of rotation of mass m represents a loss in rotor power given by

$$\Delta P_s = \left(\frac{1}{2}\rho A V_w^3\right)\frac{1}{3}\left(\frac{V_w}{V_t}\right)^2 \tag{B17}$$

or

$$\frac{\Delta P_s}{P_i} = \frac{0.333\left(\frac{V_w}{V_T}\right)^2}{0.5926} \tag{B18}$$

The total power loss coefficient is then, from equations (B16) and (B18)

$$C_{p,L} = \left(\frac{C_d}{C_\ell}\right)\left(\frac{V_T}{V_w}\right) + 0.5624\left(\frac{V_w}{V_T}\right)^2 \tag{B19}$$

Equation (B19) for the power loss coefficient is plotted in figure 24 as a function of velocity ratio $V_w/V_T$ for several values of lift/drag ratio $C_\ell/C_d$. The plot shows the power loss coefficient to increase rapidly as blade profile lift/drag ratio is decreased. Also shown in the figure is the relatively small contribution of the slipstream rotation. The slipstream rotation loss, however, is sufficient to produce a minimum value in the power loss coefficient curves. For the range of lift/drag ratios considered, minimum $C_{p,L}$ occurs for values of $V_w/V_T$ between 0.20 and 0.28.

The design point of the MOD-0 wind turbine is a wind velocity of 18 mph (26.40 ft/sec) and a tip speed of 261.8 ft/sec, for a value of 0.1008 for $V_w/V_T$. As shown on figure 24 by the dot-dash line, such a ratio makes the rotor very sensitive to lift/drag ratio. Since slipstream rotation is very small in this region, the power loss coefficient is practically inversely proportional to the lift/drag ratio.

The sensitivity of $C_{p,L}$ to $C_\ell/C_d$ can be considerably reduced if the design rotational speed is reduced at least in half to give $V_w/V_T = 0.2$. However, this would require a doubling of the blade torque to maintain the same power. This, in turn, would require an increase in the number of blades, which would be unacceptable costwise. Thus, if cost considerations dictate operation at the design conditions shown in figure 24, extreme care must be exercised to achieve maximum airfoil efficiency (i.e., highest value of lift/drag ratio).

## Airfoil Characteristics

Airfoil sections considered for wind turbine rotor application should have very high aerodynamic efficiency. Such airfoils are typified by the NACA low-speed 65-series and 5-digit series sections (ref. 6). These airfoils have small amounts of camber well forward on the blade and maximum negative stalling lift coefficients greater than -1.0. The $65_3$-series airfoils (laminar flow sections) are more sensitive to surface roughness than the 23 000-series airfoils. Also, the 23 000-series airfoils have higher values of maximum lift coefficient than the $65_3$-series airfoils.

Both airfoil sections have their centers of pressure well forward. For the 2300 sections, the aerodynamic center is at the quarter chord point. Since these airfoils have relatively small amounts of camber (maximum 2 percent of chord), the profiles tend to approach symmetrical distributions about the longitudinal centroidal axis (slightly rotated from chord line) as the section maximum thickness ratio increases beyond around 12 percent. The closeness between a 23 012 airfoil and a symmetrical 0012 airfoil was demonstrated in figure 38 of reference 4. Thus, since the concrete blade design has maximum thickness ratios greater than 12 percent, section symmetry can be assumed to simplify blade structural design and construction.

Variations of drag and lift coefficients for several low-speed airfoil sections are shown in figure 25(a), as replotted from reference 6. Data are given for smooth blades and for blades with standard surface roughness for a range of section maximum thickness ratio. The data in figure 25 are taken for a Reynolds number of $3 \times 10^6$, which is approximately that for the design operation of the MOD-0 machine. Lift/drag polars are also shown in figure 25(a) by the dot-dash lines, and data variations of lift/drag ratio $C_\ell/C_d$ are shown in figure 25(b). It is seen that $C_\ell/C_d$ values from around 80 to 120 can be obtained with the smooth airfoils, and from 50 to 60 for the sections with standard roughness. Peak values of lift/drag ratio occur for lift coefficients between 0.8 and 1.0. The design value of $C_\ell$ is taken at 0.8 for the MOD-0 rotor as shown in figure 25. The blades then operate very close to their maximum values of lift/drag ratio and have some margin for operation at higher angles of attack.

The loss in rotor aerodynamic power resulting from the airfoil section properties was calculated from equations (B14) and (B19) for the airfoil data of figure 25. Calculation of power loss was made for a range of wind speeds $V_w$ from 10 to 22 mph. Drag values over this range were determined from the variation in lift coefficients $C_\ell$ with $V_w$ considered in the design analysis for

the MOD-0 machine. This variation called for $C_\ell = 0.48$ at 14 mph, $C_\ell = 0.8$ at 18 mph (design point), and $C_\ell = 1.2$ at 22 mph. For the 125-foot diameter rotor of the MOD-0 turbine, the ideal power $P_i$ is 210 kW at the design point, and proportional to $V_w^3$ for lower values. Above the design wind speed, power is generally held constant through appropriate pitch changes.

Results of the power loss calculations are shown in figure 26(a) for the smooth and rough airfoils of figure 25. At design wind speed, power losses of around 20 kW are indicated for smooth airfoils and around 40 kW for airfoils with standard roughness. The impact of these profile drag losses on the available mechanical power output of the rotor is shown in figure 26(b). The calculation of available power assumed 25 kW of other aerodynamic and mechanical losses. The shaded area represents the band of power loss for the best and poorest airfoils with 18 percent maximum thickness provide a good representation of total rotor performance, since that value corresponds to the section of the concrete blade design at $r/r_t = 0.75$. This location is the midpoint of the outer half of the blade radius which generates the major portion of the rotor power.

Figure 26 clearly illustrates the importance of profile efficiency and surface condition to rotor power output, especially at reduced wind speeds. Wind speed affects ideal power to the third power, but drag power loss to only the second power. Although it is not clear how to relate the "smooth" and "standard roughness" of the metal airfoil sections of reference 6 to the concrete blade sections considered herein, it is quite clear that surface condition should be a very important consideration for concrete blades. Specifically, the blade contours should be precise, and the surface should not corrode or wrinkle in use, and should be as smooth as possible. Appropriate surface coatings should be considered for concrete blades.

## Trailing Edge Thickness

Since a concrete blade cannot be cast to a sharp trailing edge, it was of interest to evaluate the effect of blunt trailing edges on profile drag and rotor power loss. Data for profile drag coefficient for airfoil sections with thickened or cut-off trailing edges are given in reference 7 (p. 3.21). For values of ratio of trailing edge thickness to chord length of around 0.03, reference 7 presents an empirical expression for increase in profile drag as

$$\Delta C_d = C_{d,t} - C_d = \frac{k\left(\frac{t_e}{C}\right)^{4/3}}{(C_d)^{1/3}} \qquad \text{(B20)}$$

where $C_{d,t}$ is the profile drag coefficient with a thickened trailing edge. For application to the concrete blade design, with $k = 0.14$, equation (B20) is expressed as

$$\Delta C_d = \frac{0.14}{(C_d)^{1/3}} \left( \frac{t_e}{t_{max}} \right)^{4/3} \left( \frac{t_{max}}{C} \right) \tag{B21}$$

For the representative blade thickness ratio of 0.18, take $C_d = 0.010$ for a smooth blade, and for a standard roughness blade, take $C_d = 0.015$. The calculated variation of drag coefficient with trailing-edge thickness ratio $t_e/t_{max}$ is shown in figure 27(a) for smooth and rough blades. The corresponding variation of power loss with trailing edge thickness $t_e$ is given in figure 27(b). This calculation was made for the design conditions and for $C = 32.5$ inches and $t_{max}/C = 0.18$, which characterizes the blade at $r/r_t = 0.75$. Significant increases in power loss are observed; around 20 kW for a $1\frac{1}{4}$-inch-thick-trailing-edge. Thicknesses greater than this value would probably result in progressively greater power losses. Therefore, if maximum power output over a wide range of wind speeds is desired, conventional thin trailing edges are necessary. For concrete blades, this means that some other material must be used to achieve the desired trailing edge configuration.

## APPENDIX C

### FATIGUE RESISTANCE OF CONCRETE BLADES

Conventional reinforced concrete structures have cross-sections in which the steel area is of the order of 1 or 2 percent of the concrete area. In most cases, the stresses do not often exceed 50 percent of the yield stress, and cyclical loads which might cause fatigue are very low. Concrete fatigue test data are consequently not as prevalent as fatigue data for metals which have long been used in machine parts with cyclical loading. The proposed wind turbine blades have cross-sections in which the steel area is about 10 percent of the concrete area; consequently much of the experimental data for "under-reinforced" beams must be extrapolated for "over-reinforced" beams.

Numerous papers are presented in the publication of reference 8 which is dedicated to Dr. Paul W. Abeles, an international authority on concrete design. The test data for flexural fatigue are predominantly for under-reinforced beams. Typical failures are tension failures of the reinforcing steel at locations corresponding to concrete cracks. The test data have more scatter than similar data for metal fatigue specimens. Reinforcing bars or wires often fail in fatigue at lower stressses or fewer cycles when parts of a concrete beam than as identical bars or wires tested by themselves ("in-air" rather than in concrete) with identical load-cycles. This anomaly is explained in paper SP41-12 of reference 8 (p. 279), by P. W. Abeles, E. I. Brown, II, and C. H. Hu. From the synopsis: "Results indicate that when bond is poor and excessive cracking occurs, there can be no consistent results in fatigue tests; but when bond is good, the fatigue life of beams may be expected to be greater than that of the steel strands in air." These authors attribute the poor bond strength of various test beams to the fabrication procedure.

Another paper in reference 8 by N. M. Hawkins (p. 203) discusses the poor fatigue properties for bond stress described in an earlier paper: "Nordby (ref. 9) observed that for data published prior to 1958, results on bond fatigue were extremely erratic. He surmised that there was probably no endurance limit in bond and that failures at as little as 50 percent of the flexural capability were possible after several million loading cycles."

However, another consideration indicates that there is always a very high bond stress at the end of a prestressed bar or strand which exceeds the normal allowable stress for concrete bond. After a large number of repeated loadings (500,000 to 1,000,000 cycles), progressive bond failure will occur for loads above 50 percent of the static strength.

When a prestressed concrete member is removed from the loading fixture, the external tension force on the reinforcing bar or strand is removed. The member becomes shorter, reducing the bar tension force and producing a compression force in the concrete equal to the residual tension force in the bar. At the free end of the member, the axial loads must be zero, and the load must be transferred from the steel to the concrete by bond and shear stresses in the concrete. The bond and shear stresses are high near the end and decrease as the

axial loads build up along the length of the bar. This phenomena will be shown in the following analysis.

## Bond Stress

A simplified structure will be assumed as shown in figure 18(a). A cylindrical member of area $A_c$ is assumed to resist a uniform compressive stress $\sigma_c$ in the concrete to balance the residual steel tension pressures $\sigma_s$ on the steel area $A_s$. The resultant load is

$$P = A_s\sigma_s = A_c\sigma_c \tag{C1}$$

The total load $P$, the concrete shear stress $\nu$, and the bond stress $\mu$ (shear stress when $r = R_1$) all vary with $x$, as shown in figure 18(a).

A further simplification is shown in figure 18(b) for obtaining the shearing deformation. The concrete is assumed to resist a constant axial shear force between radii $R_1$ and $2R_2/3$, with axial compression strain of $\sigma_c/E_c$ at $2R_2/3$, and axial tension strain $\sigma_s/E_s$ at $R_1$. The sum of the axial strains in a length $dx$ is $d\xi$ (as shown in fig. 18(b)) which is defined as

$$d\xi = \frac{P\ dx}{A_sE_s} + \frac{P\ dx}{A_cE_c} \tag{C2}$$

where $E_s$ is steel elastic modulus, and $E_c$ is the modulus for concrete. The shear stress $\nu$ at radius $r$ is found by equating the axial forces shown in figure 18(b).

$$dP = 2\pi r\nu\ dx \tag{C3}$$

The total strain from the shear is found as

$$\xi = \int_{R_1}^{2R_2/3} \frac{\nu}{G_c}\,dr = \frac{dP}{dx}\,\frac{\ln\left(\frac{2R_2}{3R_1}\right)}{2\pi G_c} \tag{C4}$$

where $G_c$ is the shear modulus of the concrete. Equation (C4) is differentiated, and the value of $d\xi/dx$ equated with that from equation (C2) to give

$$\frac{d^2P}{dx^2} = k^2P \tag{C5}$$

where

$$k^2 = \frac{2\pi G_c}{\ln(2R_2/3R_1)} \left( \frac{1}{A_s E_s} + \frac{1}{A_c E_c} \right) \tag{C6}$$

The solution of equation (C5) for boundary conditions $P = 0$ at $x = 0$ and $P = P_0$ at $x = \infty$ is:

$$P = P_0(1 - e^{-kx}) \tag{C7}$$

The shear stress distribution is obtained from equations (C3) and (C7) as

$$\nu = \frac{P_0 k}{2\pi r} e^{-kx} \tag{C8}$$

The corresponding solution for bond stress is obtained when $r = R_1$. In this case

$$\mu = \mu_0^{-kr_1(x/R_1)} \tag{C9}$$

where k, defined in equation (C6), is expressed as

$$(kR_1)^2 = \frac{2(G_c/E_c)}{\ln(2R_2/3R_1)} \left( \frac{E_c}{E_s} + \frac{A_s}{A_c} \right) \tag{C10}$$

For a general noncircular structure, since the concrete stress adjacent to the steel is known, an effective concrete area is used as

$$\frac{A_c}{A_s} = \frac{\sigma_s}{\sigma_c} = \frac{\sigma_{s,0}}{\sigma_{c,0}} \tag{C11}$$

Solutions for the bond stress in terms of the ratio $\mu/\sigma_{s,0}$ against dimensionless distance ratio $x/R_1$ are shown in figure 29. The calculation was made for $G_c/E_c = 0.38$ and $E_c/E_s = 0.1$. Values of $\sigma_{c,0}/\sigma_{s,0}$ from 0.025 to 0.1 are shown. The value of 0.025 corresponds to steel bar area ratios used in conventional reinforced concrete practice. The value of 0.1 is the bar situation for the baseline concrete blade. In figure 29, the bond stress for a system of N bars is $1/\sqrt{N}$ times the values shown.

The curves of figure 29 reveal that approximately half of the area under the curves is left of $x/R_1 = 2$. This indicates that half of the force $P_0$ is transferred by shear and bond in one bar diameter from the end. Some local deformations are probably produced under such conditions, so that the assumptions of the simplified model are not completely valid. Nevertheless, the calculation

gives a conservative indication of the magnitude of the stresses near the end of prestressing bar.

Calculated maximum bond stresses at the end of the bar ($x/R_1 = 0$) are listed in the table below for several conditions. Bond stress is expressed as a ratio of the steel prestress ($\mu_0/\sigma_{s,0}$) and of the concrete prestress ($\mu_0/\sigma_{c,0}$). Calculations were made for two values of modulus ratio $E_c/E_s$.

BOND STRESSES AT END OF BAR

| Prestress ratio, $\sigma_{c,0}/\sigma_{s,0}$ | $E_c = 0.15\ E_s$ | | | $E_c = 0.1\ E_s$ | | |
|---|---|---|---|---|---|---|
| | $kR_1$ | $\mu_0/\sigma_{s,0}$ | $\mu_0/\sigma_{c,0}$ | $kR_1$ | $\mu_0/\sigma_{s,0}$ | $\mu_0/\sigma_{c,0}$ |
| 0.1 | 0.4925 | 0.2462 | 2.46 | 0.440 | 0.220 | 2.20 |
| .05 | .3713 | .1856 | 3.71 | .332 | .161 | 3.22 |
| .025 | .3047 | .1524 | 6.10 | .258 | .129 | 5.16 |

For conventional prestressed concrete structures ($\sigma_{c,0}/\sigma_{s,0} = 0.025$), the end bond stress is more than five or six times the concrete prestress. Such high stresses obviously causes local failure in bond or concrete shear. After local failure the loads redistribute over more length of the bar, and for single static loading the full strength of the bar may be developed in bond. Cyclical loading, however, produces progressive failure as a result of local stress concentrations. Fatigue tests show many satisfactory structures for 500,000 cycles, but there is little indication that such bonded bar ends are suitable for the required $10^8$ cycles of the wind turbine blades.

Allowable stresses for conventional structures are often obtained from tests of specimens which have the same type of local stress concentration. Consequently, prestressed structures with bonded bars or strands show satisfactory static strength, but often have questionable fatigue properties after numerous load cycles. After local bond failure at bar ends, the stress peaks at other points, and bond failure progresses down the bar.

For the concrete baseline blade design, for which the steel-to-concrete area ratio is 0.1, the table shows the end bond stress to be considerably less than for the conventional structure case. Ratio of end bond stress to concrete prestress is only a little over 2 to 1. Some degree of reduction, of course, is expected, since there is more steel area to distribute the prestress load. Local stress concentrations should, therefore, be lower for the blade construction than for the conventional structure. Although test data are not available, these simplified test results imply a possible reduced deleterious effect of bond stresses on fatigue life for prestressed concrete blade construction.

## Cracking

The preceding analysis does not completely explain the reasons why concrete structures do not survive as many load cycles as comparable metal structures. The conventional concrete beam without prestress (fig. 30) does not have the same bond stress distribution as shown in figure 29, because the bar load builds up gradually between supports and load points with a constant bond stress distribution. Tension cracks (too small to be apparent) occur at the first loading, and open and close with cyclical loading for the lifetime of the structure. For normal bridge and building structures, this causes no structural deficiency - many bridges are satisfactory after 50 or more years of service. Such concrete, however, will not survive the type of cyclical loading required for a wind turbine blade. Fatigue tests again show failures in the steel rods at fewer cycles than the rods would survive when tested in air.

Analysis of the local stresses near a concrete crack shows similar high bond stresses to those in figure 29. The cracking spacing is several bar diameters, and the bars have uniform axial strain, whereas the concrete has axial stress between cracks but none at the cracks. For strain compatibility the local bond stress must peak at the cracks. Fatigue tests show progressive bond deterioration, with final bar failures at crack locations.

If the structure is designed with the concrete prestress always higher than the subsequent cyclical tension loads, cracks will never open up under load. It is feasible then to prestress the concrete high enough so that even the extreme loads (emergency shut-down condition) do not cause cracking. However, many fatigue specimens of prestressed beams have survived over 2,000,000 cycles when loaded above the cracking stress, and it appears reasonable to expect fatigue properties similar to metal if the cyclical loads are kept well below those at which cracking occurs. If cracking is permitted for noncyclical occasional high loads, the concrete prestress can be lower, and the concrete then cycled about a lower steady stress level. Assuming the same Goodman diagram for allowable fatigue stress, the lower steady stress level indicates a higher factor of safety in fatigue.

## Design Approach

The proposed concrete turbine blade does not depend on concrete bond strength. Reinforcing steel bars have nuts and bearing plates at each end, so that the bar tension is transferred through the nut and plate to the concrete in compression, rather than through bond shear. Airloads on the turbine blade produce small shearing stresses in the concrete, but because of blade taper, most of the shear load is resisted by the transverse components of the tension and compression forces in the bars and the concrete.

The proposed blade has bearing plates at all bar ends, as shown in figure 31(a). The bar tension remains constant at the preload value, rather than decreasing to zero at the end as shown for the bonded bar of figure 31(b). The bar end strength may be developed by welding, as shown, or by a nut. The same nut is not used for preloading, since even a single release of the load will

cause bond failure. These measures should adequately eliminate the bond stress effect on fatigue life for the rotor blade.

The question of concrete cracking is addressed in the design approach by designing the rotor blade with sufficient prestress so that the concrete is not subject to any tension stress, even under the most severe loading conditions.

The analysis of the stresses and factors of safety for the baseline design of the prestressed concrete blade requires data on the limiting stress for fatigue for the blade materials. For steel, the limiting stress for fatigue is that proposed by U.S. Steel for T-1 steels of 100,000 psi minimum yield strength with ground welds (ref. 10):

$$\sigma_{f,s} = \frac{45{,}000}{1 - 0.61(\sigma_{min}/\sigma_{max})} \tag{C12}$$

Specific comparable fatigue data are currently unavailable for lightweight concrete. For the concrete, the expression for limiting strength for fatigue was developed from extrapolation of experimental data for conventional "under-reinforced" beams as

$$\sigma_{f,c} = \frac{2500}{1 - 0.667(\sigma_{min}/\sigma_{max})} \tag{C13}$$

The generation of appropriate fatigue data for the specific concrete to be used in blade construction is a necessary prerequisite for serious design consideration.

## APPENDIX D

## DESIGN LOADING CONDITIONS

The maximum airloads on the wind turbine blades occur as the airfoil sections approach the stalling angle of attack, giving a maximum value of the aerodynamic lift coefficient. This situation occurs (infrequently) in severe wind gusts. The blade pitch setting for normal operation provides about one-half the maximum (stalling) angle of attack, and the winds must have gusts to more than double the average velocity to produce the maximum positive load condition. The blades are normally coned so that the plane of the tip path is downstream from the hub. Consequently, the centrifugal forces produce blade bending moments which counteract the normal operating aerodynamic bending moments. The wind gusts may then vary the local wind velocity from zero to double the average value, producing blade bending moments of equal negative (upstream loads) and positive (downstream loads) magnitudes. A similar negative bending moment occurs more frequently as the lower blade passes through the tower wake in which the local dead air region may have a very small downstream velocity.

The blade pitch setting for normal wind turbine operation is such that the airfoil chord is at a small angle to the plane of rotation. Therefore, a large negative angle of attack cannot occur even though the axial flow velocity is zero. The negative stalling angle of attack can occur only during shut-down conditions. In a normal shut-down procedure, the blade pitch would be feathered gradually as the power generated decreases. The electrical power is disconnected when approximately zero power is generated at synchronous rotational speed. The blade pitch is then gradually decreased as rotation stops with the blade in full-feathered position.

An emergency shutdown occurs when a malfunction causes a power disconnect. For example, lightning strikes may cause circuit breakers to suddenly disconnect the electrical load on the wind turbine. The turbine then tends to overspeed until slowed by mechanical or aerodynamic braking. For redundancy and reliability, both types of braking will probably operate concurrently. It is assumed that the rotor overspeeds from 40 to 45 rpm by the time the blade pitch is feathered to the negative stalling angle. A maximum negative airload bending moment is then added to the centrifugal force bending moments. This load condition produces blade bending moments which are considerably higher than those for positive airloads provided that the blade coning angle is selected to minimize the bending moment under nominal operating conditions. The prestressed concrete blade is designed for a coning angle of 0.04 radians (2.292°).

The highest blade bending moment occurs with the blade section near the stalling lift coefficient and with the rotor speed at 45 rpm. This load condition can be eliminated if a reliable mechanical brake can quickly absorb the rotor power after the electrical load is suddenly removed, thus permitting shutdown by a gradual blade feathering procedure. However, this cannot be positively assumed. Furthermore, even though mechanical brakes can protect the blades from this loading, other severe wind conditions may combine to cause

similar loads on the blades. Thus, the maximum possible load must be for the maximum positive or negative lift coefficient.

Local air pressures on the blade are readily calculated for the rotational speed of 45 rpm. The dynamic pressure q is 82 psf at the blade tip, and varies approximately as the square of the radius [$q = 82(r/r_t)^2$]. A hurricane wind of 110 mph would produce dynamic pressures of 31 psf which are larger than those from rotation at points on the blade where $r/r_t < 0.61$. Also, the rotational speeds do not produce high pressures on the blade trailing edges, whereas the hurricane wind blowing from the aft direction may produce high loads on the trailing edge. The hurricane wind of 110 mph will be considered as a design condition to determine the local strength of the trailing edge and inboard sections.

The chordwise pressure distribution varies with the airfoil section, the angle of attack, and whether the flow is forward or reversed (winds from trailing edge). For simplicity, since the blade profiles are essentially symmetrical, the distribution of figure 32(a) will be used for all conditions. This distribution gives the correct total load, a center of pressure at 0.25 C, and conservatively high forward and aft pressures. The local air pressures for the hurricane conditions are shown schematically in figures 32(b). A stalling coefficient of lift of -1.0 is considered conservative for negative angle of attack (fig. 25) and for reversed flow of the ground wind.

For the emergency shutdown condition, gravity forces affect the spanwise bending moments appreciably. During normal operation, the gravity moments are essentially perpendicular to the airload moments and have a negligible component about the X-axis. During shutdown, the blade angle $\beta$ for negative blade stall is of the order of 20° (at $r/r_t = 0.75$) for the strongest wind which can produce a uniform high lift coefficient. In very strong winds, the inboard portions of the blade are stalled before the outboard portions reach high angles of attack. The gravity force W has a spanwise component W sin $\beta$ (fig. 32(c)), which adds to the airload on the ascending blade. For the descending blade these forces subtract, so the maximum spanwise bending moment always combines with a rearward force chordwise moment from W cos $\beta$.

The bending moments for fatigue loading of $10^8$ cycles under normal cycle operation are shown in figure 7. The spanwise bending moment is taken directly from the specifications for the original aluminum blades for the MOD-0 100-kW wind turbine. The chordwise bending moment is equal to the gravity moment times the undamped dynamic amplification factor of $[1 - (\omega/\Omega)^2]^{-1}$. The centrifugal force for 40 rpm is also shown in figure 7. Since the effect of centrifugal force on chordwise bending moment is small, it is conservatively neglected. The blade has equal strength for positive or negative beamwise bending, inasmuch as the blade structure is symmetrical about the X-axis.

The maximum static load bending moments are plotted in figure 8 as calculated for the condition of emergency shut-down. Airload moments for $C_\ell = -1.0$ and 45 rpm are combined with centrifugal force bending moments on a blade coned downstream at 0.04 rad and deflected upstream under loads, and also with gravity bending moments from loads shown in figure 32(c). Also shown in figure 8 is the

centrifugal force due to rotation at 45 rpm.

The allowable stresses for gust loads of $10^5$ cycles are approximately the same as for static loads. Consequently, the bending moments for the emergency shutdown case, which are more than double those of the original specifications for $10^5$ cycles, are more severe. Thus, the originally specified alternate gust load condition of $10^5$ cycles is not critical.

## APPENDIX E

## BLADE STRESSES

The blades were analyzed for the loads developed in appendix D for conditions which will be summarized here. The cyclical loads of figure 7 occur every revolution of normal operation from gravity, wind and centrifugal forces for a design life of $10^8$ cycles. The loads of figure 8 are noncyclical, and are based on an assumption of maximum negative (stalling) airloads at an overspeed of 45 rpm. This was termed an emergency shutdown condition, which produces bending moments which are more than double those specified in the original gust load specifications. Since the allowable stresses for $10^5$ cycles specified for this gust load condition are approximately those for noncyclical loads, the emergency shutdown condition conservatively replaced the originally specified gust condition in this analysis.

The locations of the reinforcing bars in the blade cross section along the concrete beam length are shown in figure 33. Inasmuch as the selected airfoil shape is very nearly symmetrical, it will be assumed for simplicity that the bars are symmetrical about the centroid axis (slight rotation from chord line). The blade span was then divided into a number of segments, and the local moments of inertia I were calculated about the x (chord) axis and the y (normal) axis. For the composite sections (concrete beam), the area and moments of inertia for each segment were determined for an all-steel beam which would have the same flexural stiffness (EI) as the reinforced concrete beam as

$$\overline{A} = \frac{\sum EA}{29 \times 10^6} \tag{E1}$$

$$\overline{I}_x = \frac{\sum EI_x}{29 \times 10^6} \tag{E2}$$

$$\overline{I}_y = \frac{\sum EI_y}{29 \times 10^6} \tag{E3}$$

The resulting equivalent values are shown in figures 34(a) and (b), respectively. The area distribution, in conjunction with the local material density values, were then used to calculate the blade weight.

The blade is designed so that the concrete area is ten times the steel area at all cross-sections. A residual prestress (after concrete shrinkage) of 20,000 psi in the steel produces a uniform compression stress of 2000 psi in the concrete. Subsequent applied loads are superimposed on the prestress loads. The applied load stresses are calculated as follows:

$$\sigma_s = \frac{T}{A} \pm \frac{M_x y}{I_x} \pm \frac{M_y x}{I_y} \qquad \text{(E4)}$$

where $T$ is the centrifugal force due to rotation.

Concrete stresses are one-tenth the steel stresses for corresponding $x$ and $y$ values. The axial load is always positive. Since the cross-section is symmetrical about the X-axis, the moments $M_x$ produce equal and opposite stresses in top and bottom surfaces. The bending moments $M_y$ are primarily from gravity, so are fully reversible on the ascending and descending blades when the X-axis is parallel to the plane of rotation. However, for the emergency shutdown condition, the ascending blade is more highly loaded than the descending blade, because gravity components add to airloads on the ascending sweep. This results from the blades operating at a negative angle of attack for this condition.

The blade stresses from the cyclical loads are summarized in table II. The stresses were calculated from equation (E4) for combinations which produce the maximum and minimum stresses at each blade cross-section. These stresses were then compared with limiting cyclical stresses obtained from equations (C12) and (C13), and the factors of safety for fatigue were calculated as described on page 9. A minimum value of 1.809 was obtained.

Similar stress calculations for the emergency shutdown condition are summarized in table III. Factors of safety are based on ultimate strengths of 115 000 psi for steel and 7500 psi for concrete (pg. 10). All factors of safety exceed 2.0 for this load condition.

## APPENDIX F

## BLADE FABRICATION

In order to evaluate the feasibility of fabrication of a prestressed concrete rotor blade and also obtain realistic cost estimates, it was necessary to proceed into detailed component drawings and specific fabrication techniques for manufacturing these components for the baseline blade design. Examples of this effort are presented herein. The major components are identified in the isometric drawing of the complete blade assembly in figure 2.

### Blade Hub Assembly

The blade hub assembly is manufactured from two steel castings and a steel tube which are welded together. A view of the hub assembly is shown in figure 35. The detailed drawing for the tube weldment with gross dimensions is shown in figure 36. This section is a fabricated part utilizing steel plates which are formed into shape and then welded into an assembly.

A sectioned view of the casting which becomes the transition between the steel hub tube and the prestressed concrete beam is shown in figure 37. The drawing for the steel casting which forms the inner extremity of the blade is shown in figure 38. This adpater fitting bolts to the existing rotor hub or adapter piece.

The steel castings are cast from a special grade steel utilizing simple patterns. The flange ends of the steel castings are surfaced by a Blanchard grinding operation which provides the mounting and reference surface for subsequent operations. The mounting holes in the castings are drilled by means of conventional drilling equipment. Limited quantities utilize a simple drill plate jig for hole location.

The steel tube is fabricated from steel plate utilizing six separate pieces. Each piece is press brake formed into its proper shape using templates as gages. The formed steel plates are welded into half longitudinal sections with stiffeners welded into place. The welds are both inside and out and are full penetration in accordance with proper welding techniques. The circumferential welds are ground both inside and out. The halves are then welded longitudinally both inside and out.

The blade hub assembly is then formed by welding the machined steel castings to the welded steel tube. These three parts are held in their respective positions by means of simple welding positioning fixtures. All parts are first tack welded into place and then completely welded using proper welding techniques. The blade hub assembly is now complete and ready for finishing.

## Prestressed Beam

Cross-sections of the concrete beam at several radial locations are shown in figure 39. The beam is fabricated from concrete and steel utilizing a special self-stressing concrete form. The procedure is as follows:

The inside profile of the beam is defined by an expendable polystyrene core. This core is cast in a mold built especially for this purpose. The mold is hinged for part removal and is constructed of steel. To cast a core, it is necessary to close the mold and inject the proper combination of foam materials. These materials expand and cure inside the mold to form a rigid structure. The foam core is then inserted into the open self-stressing concrete form. It is positioned by plastic standoffs that protrude through the finished concrete beam and set the concrete thickness throughout the beam. The plastic standoffs are positioned on approximate one-foot centers.

The longitudinal steel stress bars are positioned in the concrete form from one end to the other. Their position is determined by templates on both ends of the casting. These plates stay with the casting and become stress abutments for the steel bars. The steel stress bars that stop off short are temporarily held in position by ties. The reinforcing wire mesh is installed using the steel stressing bars as locators. It is properly positioned and tied as required. The side skins of the self-stressing form are then closed which further positions the foam core by means of the plastic standoffs.

Lateral stressing jigs are installed in slots provided in the main form. These bars fasten to the short steel stressing bars and are stressed along with the through bars. The steel bars are now stressed using conventional hydraulic stressing jacks at one end of the self-stressing foam. Each bar is stressed to its predetermined stress level and locked into position with special hardware. Figure 40 is an isometric illustration showing the method of terminating the prestressed bars inside of the prestressed beam. This concept allows for the steel to be prestressed yet not be continuous to the end of the prestressed beam. The view also shows the steel form and the plastic innercore in place. The innercore defines the inside configuration of the prestressed concrete beam, and the outer steel form defines the outside configuration.

The concrete is poured, utilizing conventional techniques, into the open top of the self-stressing form. Vibrators are utilized to minimize air entrapment. The top surface (back edge) is hand troweled for proper finish. Test cylinders are cast for control purposes. After curing, the self-stressing form is opened for part removal. The part is lifted by means of lugs which have been cast into place for this purpose. The mold is then cleaned and oiled for the next cycle.

## Tip Assembly

The blade tip assembly consists of a metal spar assembly and a contoured fiber-glass envelope which defines the airfoil shape. The steel spar is fabricated from sheared plate and welded into its form in a weld jig. It is also

welded to a steel knuckle casting which has been previously drilled for its mounting holes. The blade tip spar and its attachment, which constitute the construction from the outward end of the concrete beam to the blade tip, is shown in figure 41. The steel spar is assembled onto the small end of the previously completed concrete beam. The structural steel spar is fastened to the protruding prestressed bars and becomes the load bearing member for the blade tip. Details of the spar beam weldment are shown in figure 42.

The cast flange end attachment knuckle is shown in figure 43. This casting is welded to the inner end of the spar beam and bolted to the protruding prestressed bars at the outer end of the concrete beam.

The fiberglass envelope is constructed in female half molds by means of chopper gun layup. The mold is first cleaned and prepared with a release agent, and Gel-Coat is applied with a spraying technique. A fiberglass and resin matrix is applied with a conventional technique chopper gun and roll-out procedure to obtain the desired thickness. The two halves are allowed to cure, trimmed and bonded together utilizing glass tape and hand layup procedure. The part is finished by filling and sanding as required. The section is shown in figure 44(a).

The fiberglass envelope is positioned over the steel spar by means of a jig and is attached to the end of the concrete beam by means of drilling and tapping in place. Polyurethane foam is then cast between the steel spar and the inner surface of the fiberglass envelope and allowed to cure. The tip is now integral with the concrete beam.

## Trailing Edges

The fiberglass trailing edges are fabricated in a female mold utilizing techniques similar to those for the fiberglass tip envelope. The fiberglass trailing edge is constructed in three lengths, as shown in figure 44(b). The trailing edges are attached to the previously completed concrete beam by means of aluminum angles and related hardware, as shown in figure 6. These aluminum angles are adjusted and locked into proper position. The trailing edges are positioned utilizing appropriate jigs and then fastened to the aluminum angles by means of drilling and blind riviting.

## Assembly

The assembly of the blade hub and the concrete beam is accomplished by means of appropriate holding fixtures and slings. The assembly is moment balanced in a balancing fixture. This fixture has the ability to indicate bending moment at the mounting flange when the part is cantilevered from that point. Adjustments to the moment and weight are accomplished by adding weights to receptacles provided in the structure. The assembly is now ready to be cleaned and finish coated. The coating will be spray gun applied utilizing conventional techniques.

## APPENDIX G

## COMPUTER CODES FOR SHAFT LOADS

The coupled dynamic analysis of the wind turbine system was conducted with the use of seven computer codes: MYRAC, MOSTAB, PROCESS, ROLIM, WINDLESS, DYNAM2, and RECOV2. For purposes of discussion and output, these programs are discussed in three groupings.

### MYRAC

The Myklestad Rotor Analysis Code (MYRAC) is a simple rotor blade modal analysis computer program, developed primarily as a quick analysis aid for rotor blade designers. MYRAC performs a Myklestad analysis for one-dimensional beam motion and for rotating beams with arbitrary bending stiffness and mass distribution. The distributed properties are read into MYRAC as tables.

MYRAC incorporates the transfer matrix method originally devised by N. O. Myklestad, extended for the analysis of rotating beams. This method provides for the computer calculation of beam modeshapes or eigenvectors, and frequencies or eigenvalues. The modeshape is calculated in four simultaneous forms: deflection, slope, beam bending moment, and section shear force, all specified as a function of blade radius. These functions are particularly useful for design, since, in addition to the fundamental dynamic properties they reveal, they also show moment and stress distributions when the blade is excited in its normal modes of vibration.

MYRAC computes modeshapes and frequencies for out-of-plane ("flapwise" or "beamwise") motion, for inplane ("chord" or "edgewise") motion, and for torsional motion. The code also produces the blade tension distribution, weight, second mass moment of inertia about the shaft, and "gravity droop" shapes in the flapwise direction. Examples of calculated stress distribution and modeshapes are shown in figure 45. The chordwise stress distribution in the example of figure 45(a) indicates where redefinition of mass or moment of inertia distributions might be considered (e.g., steel/concrete interface, blade tip). Also, after careful redefinition of the mass and EI distribution of the blade, the first inplane and the first flapping frequencies of the concrete blade were computed as follows for comparison with the MOD-0 aluminum blades:

| Blade | First flapping | First inplane |
|---|---|---|
| Concrete | 2.698p | 4.319p |
| MOD-0 (Al.) | 2.73p | 4.24p |

### MOSTAB-HFW/PROCES-PD/ROLIM

The High Frequency Analysis Wind Energy version of the MOdular STABility derivative computer code is one in a series of comprehensive computer programs

designed to analyze rotor systems, VTOL aircraft, and a wide range of general aerodynamic problems. The modular design of the program permits generalization of function for many of the subroutines, and thus permits the user to analyze a wide variety of aerodynamic problems with the same computer code. The MOSTAB-HFW version features use of an aeroelastic rotor blade, an interference velocity coupling matrices, user-defined wake profiles and tower shadow options. These combine in a rigorous manner to yield shaft loads, blade loads, stability derivatives and deflections which are printed out, either in MOSTAB-HFW or its post-processor, PROCES-PD.

PROCES-PD is a MOSTAB post processor which prints out distributed blade loads and aerodynamic data as a function of radius and azimuth angle and the integrated loads applied to the shaft in rotor axes. PROCES takes this single blade data, synthesizes an entire rotor system from the data, then demodulates this information from the rotor (rotating) axes to the hub (fixed) axes. The hub loads can then be transferred to any convenient point with a simple geometric transformation matrix. Various loads tables resolved to blade, rotor and hub axes (as shown in fig. 22) are also printed out. Most of the rigid shaft loads values used in this analysis come from this program.

The ROtorcraft LInear Modelling program (ROLIM) of rotor analysis reads a file written by MOSTAB-HFW and assembles a rigorous linear math model for a rotor system. This file is then used in the WINDLASS system as it assembles the entire rotor, pod, tower, etc. into one large set of simultaneous, coupled differential equations.

Examples of shaft loads resolved to rotor axes and hub axes are given in tables V and VI. Loads referenced to blade or rotor axes are loads developed by a single blade. Only those loads resolved to hub axes are for an entire rotor. In all cases, results are for a rotor (or blade) mounted on a rigid shaft.

## WINDLASS/DYNAM2/RECOV2

The WIND-turbine Linear Analysis Software System (WINDLASS) couples together component mathematical models developed by MOSTAB/ROLIM and NASTRAN into a dynamic math model of an entire wind turbine system. This dynamic model is then written to a file which can be solved for, using various solution techniques. Furthermore, by option, the system provides for eigenanalysis yielding immediate assessment of the system stability.

Once created, the coupled dynamic model file, DYNFIL, can be accessed whenever required to compute system loads and motions under a variety of dynamic loadings. The DYNAM2 program accesses DYNFIL and computes system frequency response under the influence of harmonic shaft loads or other sinusoidal forces. This program places additional files on DYNFIL (or an alternate file, if desired) which are read by RECOV2 and converted to time histories.

RECOV2 recovers time histories from the DYNAM2 harmonic response results for all system variables. RECOV2 provides basic printed time history tables

of the independent and eliminative variables, and, on option, recovers loads in the moving blade reference system.

The WINDLASS program group was used mainly to calculate nacelle pitching and yawing moments. Execution was done with a relatively high stiffness value ("STIFF") and a relatively low stiffness value ("SOFT"). The axis system for these loads is the same axis system used in the MOSTAB execution for the rotor. An example of the variation of these loads with time as computed by the code is shown in figure 46. Results are shown compared to the corresponding loads obtained from the MOSTAB program. The WINDLASS/DYNAM2/RECOV2 output also includes other hub loads, distributed blade loads (as function of azimuth angle), and the yaw drive (tower) loads.

## Summary of Results

Several design cases were calculated by the computer codes described above, as outlined in the main text. The purpose of the calculations was to compare the loads produced by a rotor with baseline design concrete blades with the loads of the original MOD-0 rotor with aluminum blades. The principal results of the calculations are summarized below:

· Increasing the blade weight, and thus the inertia, has a direct influence on the cyclic loads produced by a rotor. The amount of modal damping is inversely proportional to the blade inertia. Thus, while steady values of blade flapping moment may remain fairly constant, the cyclic values will surely increase. This phenomenon becomes a significant factor with regard to acceptable blade weight.

· The yawing (weathercocking) moment and pod nacelle pitching moment are apparently the most critical design loads if the baseline concrete blade concept is to be feasible. Of these, the yawing moment is the most sensitive to blade weight. The cyclic fatigue due to the yawing moment and applied to the tower structure is significantly greater when the concrete-bladed rotor is used. This effect is directly attributable to the increased blade weight, but may be controllable with blade flapping frequency.

· The magnitude of the hub yawing moment is controllable by the value of the blade flapping frequency. The actual dependence of the yaw moment on modal damping ratio and blade flap frequency is a complex function, but for the given damping ratio of 0.10089 for the concrete-bladed rotor, a blade flapping frequency of 2.20 appears to be optimum. This value brings the loads of the rotor to within 11 percent of the MOD-0 loads at possible cost of raising the steady loads around 60 percent.

· While some sensitivity to the yaw drive stiffness is noted from the WINDLASS calculations, the loads predicted by MOSTAB are generally accurate enough to assess the effects of using concrete blades on a wind-turbine system such as the MOD-0 system. The yawing moment was the most sensitive to the relaxation of the rigid shaft assumption with loads often amplified by 7 percent.

• The nacelle pitching moment is the most sensitive load with respect to a pod yawing ratio. A clockwise rotation of the pod (when viewed from above) produces pitch moments which will tend to bring the bottom blade in toward the tower. The reduced precone angle enhances the potential blade/tower clearance problem. One method to correct this problem may be to elevate the shaft.

• All of the hub loads demonstrate a reduced sensitivity to windspeed. This is due to the increased blade weight. The cyclic inplane loads of the blades are generally insensitive to wind speed over the 26 to 40 mile per hour range and are not affected greatly by the introduction of a pod yawing rate. The magnification of the loads over the nominal value is related approximately linearly to the increase in blade inertia.

• The steady flap bending moments for the blades do not appear to be a function of blade weight. Indeed, the concrete blade loads are lower than the MOD-0 nominal loads, indicating the advantage of properly selecting the precone angle. A yaw rate of 0.5 °/sec did not appreciably affect these loads.

• The cyclic flap bending moment for the concrete-bladed rotor is about 30 percent greater than MOD-0 for the low wind speed case, but is approximately equal to the MOD-0 values at the higher wind speed. Fatigue life will probably not be severely hampered by this.

• The cyclic shaft torque loads were significantly less with the concrete-bladed rotor compared to the current MOD-0 rotor system. This is, of course, due to the increased inertia of the rotor. This phenomenon may actually benefit the power quality by reducing the power ripple factor.

## APPENDIX H

## ANALYSIS OF HUB YAWING MOMENT

The harmonic results from the coupled dynamic analysis of the concrete blade were compared to the original MOD-0 aluminum blades in the text (tables VI and VII). The principal observation was a large and serious increase in the harmonic components of the hub yawing (weather-cocking) moment developed by the rotor with concrete blades. In table VI, from the MOSTAB code, the yawing moment amplification for the concrete blade was between 1.6 and 1.9 for the second harmonic (2p) and from 1.4 to 2.3 for the fourth harmonic (4p). In table VII (WINDLASS code), the nacelle yawing moment amplification varied from around 1.6 to 2.4 for the cyclic (2p) values.

The nature of the increased 2p and 4p load levels is illustrated in figure 47. The figure shows the variation of blade flapping angle $\beta$ with azimuth angle in a rotating axis system for both the MOD-0 rotor and the concrete-bladed rotor operating at the same conditions. For the concrete blade, $\beta$ was scaled by the ratio of the inertias to aid in the comparison. Clearly evident is the pronounced 3p (three per revolution) displacement activity of the concrete blade and the more attenuated activity of the MOD-0 blade. When this signal is transformed into the fixed system of the hub coordinates, it contributes to the 2p and 4p signals.

Accordingly, simple 1-degree-of-freedom mathematical models of a flapping blade of a rotor system were developed to further investigate the origins of the blade flapping, and ultimately, of the hub yawing loads. Measured wind turbine data and simple analysis had indicated that the hub flapping bending moment and the out-of-plane flapping angle track each other quite well. Thus, a simple model of this moment can be made by writing and solving the modal equation for a simple rigid hinged beam.

### Models

Damped oscillator. - An examination of hub moments due to blade vibration was made based on a model for a 1-degree-of-freedom damped oscillator with a step input to simulate the tower wake effect. In this development, the flapping coordinate $\beta$ was used to model flapping moment at the blade root (axis).

The model of a flapping blade of a rotor system starts by considering the simple rigid rotating hinged beam pictured on the following page.

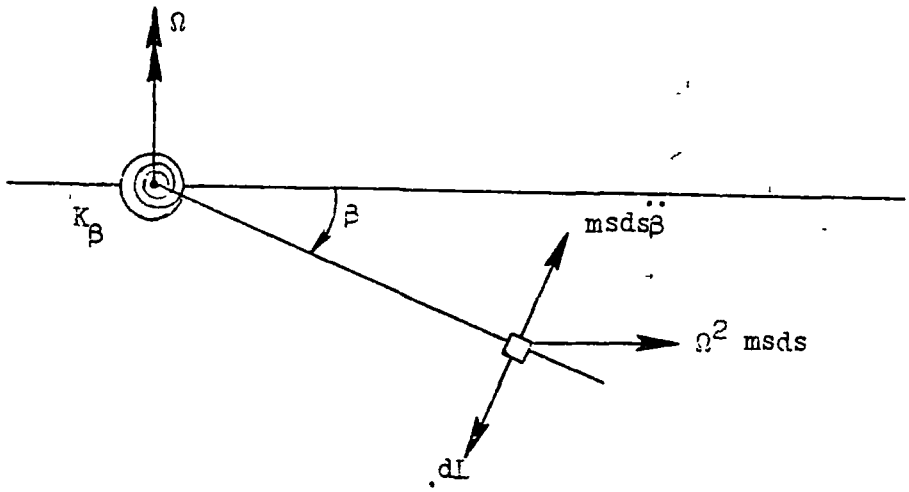


Then

$$dM_H = (sdL - ms\ ds\ \ddot{\beta}) - \beta s\Omega^2 ms\ ds \tag{H1}$$

Integrating both sides yields

$$M_H = K_\beta \beta = \int sdL - \ddot{\beta} \int ms^2 ds - \Omega^2 \beta \int m\dot{s}^2 ds \tag{H2}$$

The second and third integrals are simply the flapping inertia of the blade I, so that equation (H2) is reduced to

$$I\ddot{\beta} + \omega^2 \beta = \int dL \tag{H3}$$

where

$$\omega^2 = \left(\frac{K_\beta}{I} + \Omega^2\right)$$

In real life, the rotor undergoes some aerodynamic modal damping, so equation (H3) has the modal damping term $\Lambda_\beta^{\cdot}$ added:

$$\ddot{\beta} + \left(\frac{\Lambda_\beta^{\cdot}}{I}\right)\dot{\beta} + \omega^2 \beta = \frac{a_e(t)}{I} \tag{H4}$$

where

$a_e(t)$ = aerodynamic excitation. This function will be the same for any rotor system and will be independent of $\beta$, its derivatives, or $I$

$\Lambda_{\dot{\beta}}$ = aerodynamic damping coefficient. This is independent of the mass properties and will be constant with time

The vibratory displacement is thus a function of the blade flapping inertia $I$ and the blade flapping natural frequency $\omega$. The former depends primarily on blade weight, and the latter varies primarily with blade material and geometry.

Vibratory load analyses are usually conducted in terms of the modal damping ratio $\xi$ defined as

$$\xi = \frac{\Lambda_{\dot{\beta}}}{2I\omega} \tag{H5}$$

The modal damping coefficient defines how quickly the oscillatory behavior of a system will die out. If $\xi = 0$, no damping is available and a particle in motion undergoes simple harmonic motion with undiminished amplitude. If, however, $\xi = 1$, critical damping has been achieved and a particle in motion would "creep" back to its equilibrium point with no oscillatory motion. Thus, if $\Lambda_{\dot{\beta}}/I$ is set equal to $2\omega\xi$, the problem is nondimensionalized. A convenient parametric study may then be conducted from solution of the equation

$$\ddot{\beta} + 2\omega\xi\dot{\beta} + \omega^2\beta = \frac{a_e(t)}{I} \tag{H6}$$

A simple computer program solved the problem modelled by equation (H6). An excitation signal, $a_e(t)/I$, was input in such a manner as to simulate the effects of the tower wake. For this simple model, no wind shear effects were introduced. The blade motion was Fourier analyzed after convergence, and from these values, a rotor was synthesized and Fourier coefficients of the hub "loads" were produced.

The calculated behavior of the steady, 2p, and 4p loads as functions of damping ratio $\xi$ are shown in figure 48 for first flapping frequencies of 2.73 and 2.70, which are representative of the MOD-0 aluminum and the concrete blades, respectively. The Fourier coefficient value shown plotted in the figure reflects the magnitude of the vibratory hub moments. Also shown on figure 48 are the values of damping ratio for the MOD-0 and the concrete blades. It is clearly seen that the hub moments for the concrete blade, as reflected in the Fourier coefficient values, are substantially greater than for the MOD-0 blades for the 2p and 4p harmonics. This is a direct result of the greater flapping inertia of the concrete blade caused by its greater weight.

Simple vibrating mass. - In view of the strong dependence of the vibratory loads on blade damping ratio, it would be convenient to have a simple calculation procedure for parametrically exploring the effects of $\xi$ as well as natural frequency $\omega$. Accordingly, a second mathematical model was considered to examine the effects of resonant vibrations on displacement as follows. A

mass $m$ with natural frequency $\omega$ excited by an oscillating force of frequency $p$ has a displacement of $\delta$ times the static displacement. This is expressed for a simple single-degree-of-freedom model as

$$\delta = \frac{1}{\sqrt{\left[1 - \left(\frac{p}{\omega}\right)^2\right]^2 + \left[2\xi\left(\frac{p}{\omega}\right)\right]^2}} \tag{H7}$$

where $\xi$ is the damping ratio. This ratio, as before, is obtained by dividing the aerodynamic damping force by the critical damping $2\omega m$ where $m$ is proportional to the inertia.

For the concrete blade, from the MOSTAB calculations, the damping ratio is 0.101, and for the MOD-0 aluminum blade, the damping ratio is 0.267. The value of $\xi$ for the concrete blade is around 0.38 of the MOD-0 value. This is about the inverse ratio of the blade weights. With the natural flapping frequencies about the same for both blades ($\omega$ = 2.73 for MOD-0, and $\omega$ = 2.70 for concrete), it is expected that the damping ratios would vary inversely with the blade weight.

With the above values for $\omega$ and $\xi$, values of displacement amplification $\delta$ were calculated from equation (H7) to give

| Harmonic | Displacement amplification, $\delta$ | |
|---|---|---|
| | MOD-0 | Concrete |
| 1p | 1.125 | 1.155 |
| 2p | 1.650 | 2.112 |
| 3p | 1.606 | 3.082 |
| 4p | .718 | .812 |

The displacement amplification is seen to be more severe for the concrete blade for the second and third harmonics. When it is considered that the 3p amplification of the displacement ratio contributes to the 2p and 4p values in the fixed coordinate system, these results are in general keeping with those of the more complex damped oscillator model of equation (H6).

Load ratios. - To summarize the results from the preceeding models of the blades, use will be made of the ratio of concrete system hub moment to MOD-0 system hub moment. This ratio is obtained from the ratio of Fourier coefficients from the computer output. These load amplification ratios are then compared with the corresponding ratios obtained earlier from the comprehensive MOSTAB code.

A measure of load amplification for the concrete and MOD-0 blades can also be obtained from ratios of the displacements $\delta$ given by the simple vibrating spring-mass model described in the preceeding section. A complete tabulation for both models is then:

| Harmonic | Load ratio, $L_{concrete}/L_{MOD-0}$ | | Harmonic | Displacement ratio, $\delta_{concrete}/\delta_{MOD-0}$ |
|---|---|---|---|---|
| | Model | MOSTAB | | Model |
| Steady | 1.056 | 0.68 | 1p | 1.03 |
| 2p | 1.575 | 1.59 | 2p | 1.28 |
| 4p | 1.503 | 1.39 | 3p | 1.92 |
| | | | 4p | 1.13 |

It is thus seen that the simple models considered herein are reliable indications of the excessive cyclic moment problem. It now remains to investigate reductions in these load ratios for the concrete blade.

## Blade Flapping Frequency

According to the simple blade models presented in the previous section, the vibratory loads are dependent on the blade flapping inertia $I$ and the flapping natural frequency $\omega$. For the prestressed concrete blade design considered herein, there is a greater degree of control over the variation of flapping natural frequency than there is over the flapping inertia, which is proportional to the blade weight. Thus, for practical purposes, the effects of flapping frequency on hub loads for the concrete-bladed system will be explored for fixed flapping inertia. Accordingly, from equation (H5), the damping ratio is

$$\xi = \frac{k}{\omega} \tag{H8}$$

where $k$ is a constant. Thus, a decrease in blade flapping frequency also results in an increase in damping ratio. For the concrete blade, with $\xi = 0.101$ and $\omega = 2.70$, $\xi = 0.2727$.

The computer program for the damped oscillator model did not isolate the effect of flapping frequency, but presented its effect on Fourier coefficient in a parametric variation with damping ratio. However, the variation of Fourier coefficient at constant flapping inertia for the concrete blade can be readily superimposed on the resultant plots. Calculated results are shown in figure 49 for the 0p, 2p, and 4p harmonics. Also shown on the figure are the points of the concrete and MOD-0 blade designs and the faired constant $I$ lines. (Although no calculations were run for $\omega$ between 2.2 and 2.7, it is unlikely that a resonance would occur in this region.)

Figure 49(a) shows that the steady hub yawing moment will increase substantially with any decrease in the flapping frequency of the concrete blade. The 2p values, however, as shown in figure 49(b), decrease as flapping frequency is reduced to 2.2 and then rise again for further reductions in frequency. For constant concrete flapping inertia, a minimum value of moment is obtained around $\omega = 2.2$. This minimum value is somewhat greater than the MOD-0 value. Moment values below the MOD-0 value can readily be obtained for the 4p harmonic, as seen in figure 49(c). On balance, considering all three harmonics, a modest reduction in concrete blade flapping frequency from 15 to 18 percent ($\omega \simeq 2.3p$ to 2.2p) might seem sufficient to significantly reduce the differences between the cyclic hub yawing moments of the concrete and MOD-0 blades. Minimum cyclic reduction occurs for $\omega = 2.2p$, but with an approximately 60 percent increase in steady loads.

In terms of the ratio of concrete-system moment to MOD-0 system moment (as was done previously with the use of the Fourier coefficient ratio), the following results are obtained from the one-degree-of-freedom damped oscillator model:

LOAD RATIO, $L_{concrete}/L_{MOD-0}$

| Harmonic | Concrete flapping frequency, $\omega$ | | | |
|---|---|---|---|---|
| | 2.70p | | 2.4p | 2.2p |
| | MOSTAB | 1-deg model | 1-deg model | 1-deg model |
| Steady | 0.68 | 1.056 | [a]1.393 | 1.717 |
| 2p | 1.58 | 1.525 | [a]1.251 | [b]1.116 |
| 4p | 1.39 | 1.503 | [a].897 | .576 |

[a]From interpolation of faired values.
[b]Minimum value of flapping frequency variation.

With regard to the indicated increase in steady moment ratio with reduced values of $\omega$, it is noted that the comprehensive MOSTAB code produced a ratio value about 64 percent less than that shown by the simpler damped oscillator model at 2.70p. If this same reduction percentage were applied to the 2.2p value of the steady moment, a ratio value around 1.1 would result. It may be, then, that the decrease in concrete-blade first flapping frequency to 2.2p produces real values of hub yawing moment not much greater than those for MOD-0 for the major harmonics.

It is also of interest to determine the loads relief obtained from reduction in concrete blade flapping frequency as given by the simple vibrating mass model of equation (H7). Substitution of equation (H8) into equation (H7) then yields for fixed flapping inertia,

$$\delta = \frac{1}{\sqrt{\left[1 - \left(\frac{p}{\omega}\right)^2\right]^2 + \left[\frac{0.5454}{\omega}\left(\frac{p}{\omega}\right)\right]^2}} \qquad \text{(H9)}$$

According to equation (H9), maximum values (resonances) are produced at $\omega = p$ for each harmonic. Thus, values of $\omega$ approximately half way between the integers are suggested (i.e., 1.5p, 2.5p).

It was indicated previously that the offending harmonic with this model was the 3p value (this is the harmonic that contributes to the 2p and 4p harmonics in the fixed coordinate system). The variation of $\delta$ with flapping frequency $\omega$ for the 3p harmonic for the concrete blade at fixed flapping inertia was calculated from equation (H9). The resultant plot is shown in figure 50, together with the design points for the MOD-0 and concrete blades. As in the case of the damped oscillator model, the results of figure 50 show a pronounced reduction in vibratory effects for small reductions in flapping frequency below the design value of 2.70p. A reduction to only 2.4p is required to attain MOD-0 levels according to this simple model.

In conclusion, the above exercise with simple vibration models points to the value of a modest reduction in blade flapping frequency in reducing the hub yawing moment. However, these are relatively simple one-degree-of-freedom models, so that the results can only indicate the possible outcome of a reduction in blade flapping frequency. A more comprehensive analysis, such as the MOSTAS code, with a further refined blade would be indicated to verify the result.

## REFERENCES


1. Anon: Summary Report, Federal Wind Energy Program. U.S. Department of Energy. Report DOE/ET-0023/1, Jan. 1978.

2. Sullivan, T. L.; Cahill, T. P.; Griffee, D. G., Jr.; and Gewehr, H. W.: Wind Turbine Generator Rotor Blade Concepts with Low Cost Potential. DOE/NASA/1028-77/13. NASA TM 73835, May 1978.

3. Lieblein, S.; Ross, R. S.; and Fertis, D. G.: Evaluation of Feasibility of Urethane as a Structural Material for Low-Cost Wind Turbine Blades. NASA CR-159530, April 1979.

4. Puthoff, Richard L.: Fabrication and Assembly of the ERDA/NASA 100-Kilowatt Experimental Wind Turbine. NASA TM X-3390, April 1976.

5. Spera, D. A.; Janetzke, D. C.; and Richards, T. R.: Dynamic Blade Loading in the ERDA-NASA 100-kW and 200-kW Wind Turbines. NASA TM X-73711, 1977.

6. Abbott, I. H.; von Doenhoff, A. E.; and Stivers, L. S., Jr.: Summary of Airfoil Data. NACA Report No. 824, 1945.

7. Hoerner, Sighard F.: Fluid-Dynamic Drag. Published by the author, 1965.

8. Fatigue of Concrete. Publication SP-41, American Concrete Institute

9. Nordby, G. M.: "Fatigue of Concrete - A Review of Research." American Concrete Institute Jour., vol. 55, no. 2, Aug. 1958, pp. 191-220.

10. Brockenbrough, ., and Johnson, .: USS Steel Design Manual. May 1974.

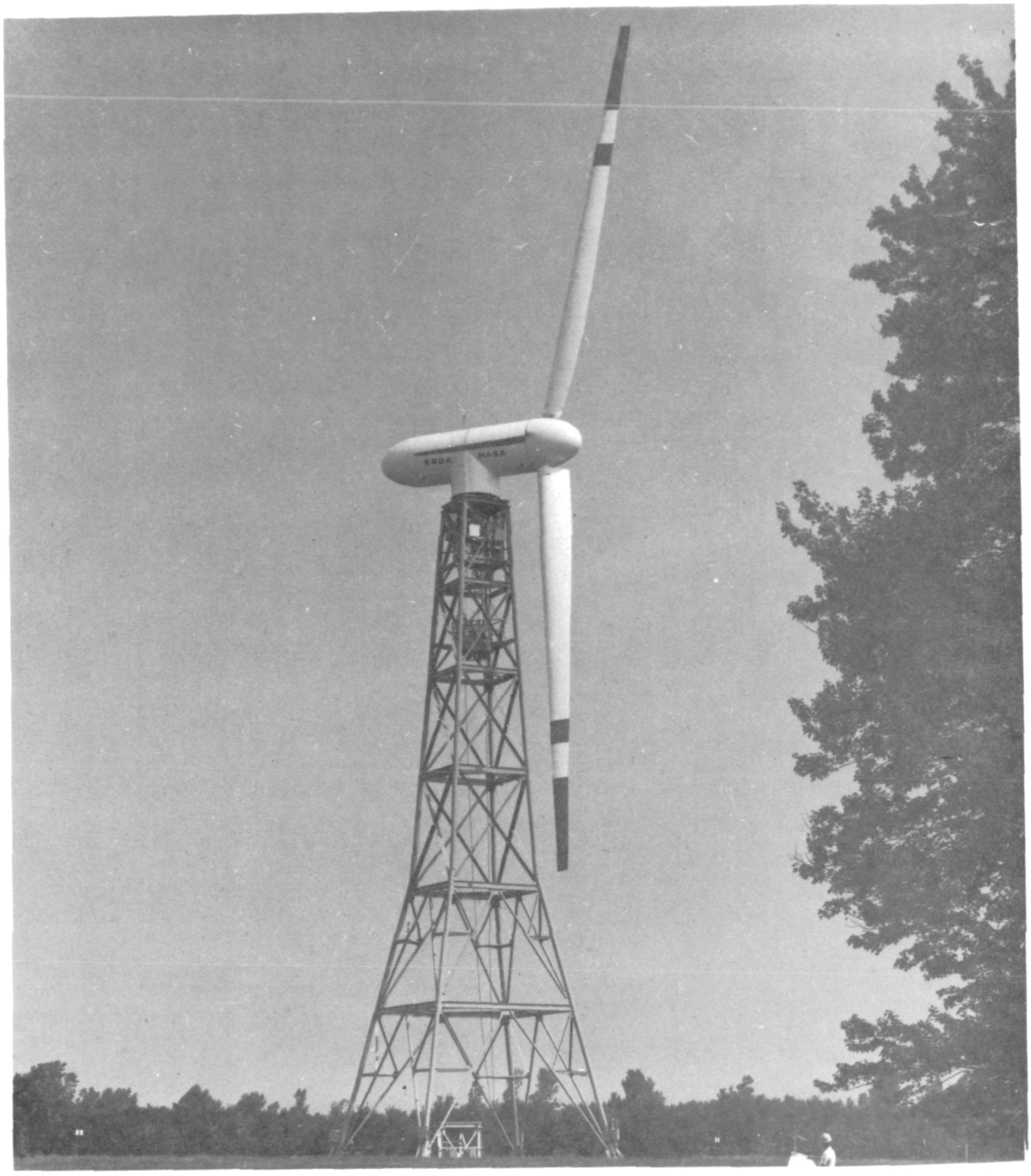

Figure 1. - DOE/NASA 100-kW experimental wind turbine. Designation MOD-0; rotor diameter, 125 foot; aluminum blades.

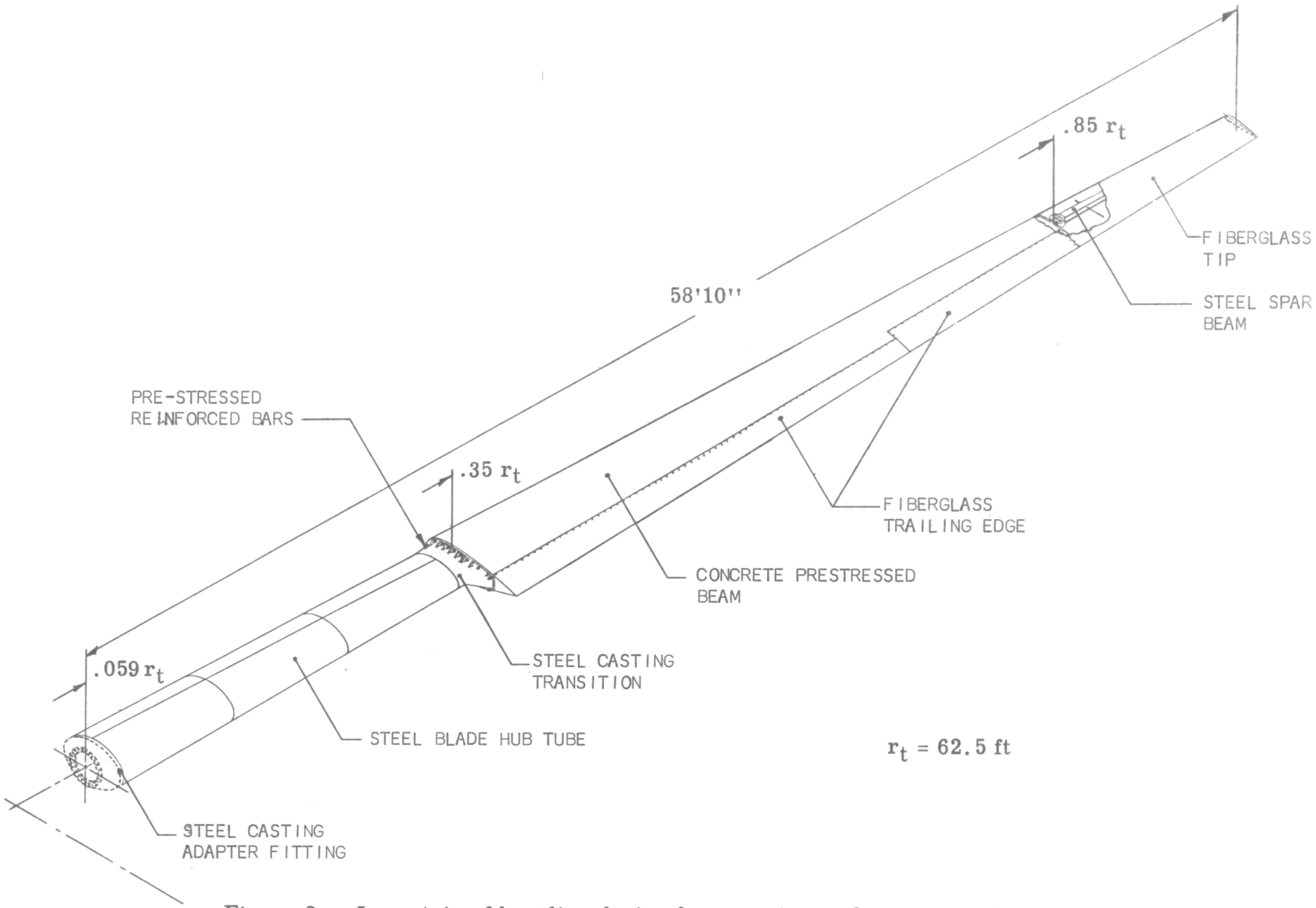


Figure 2. - Isometric of baseline design for pre-stressed concrete rotor blade.

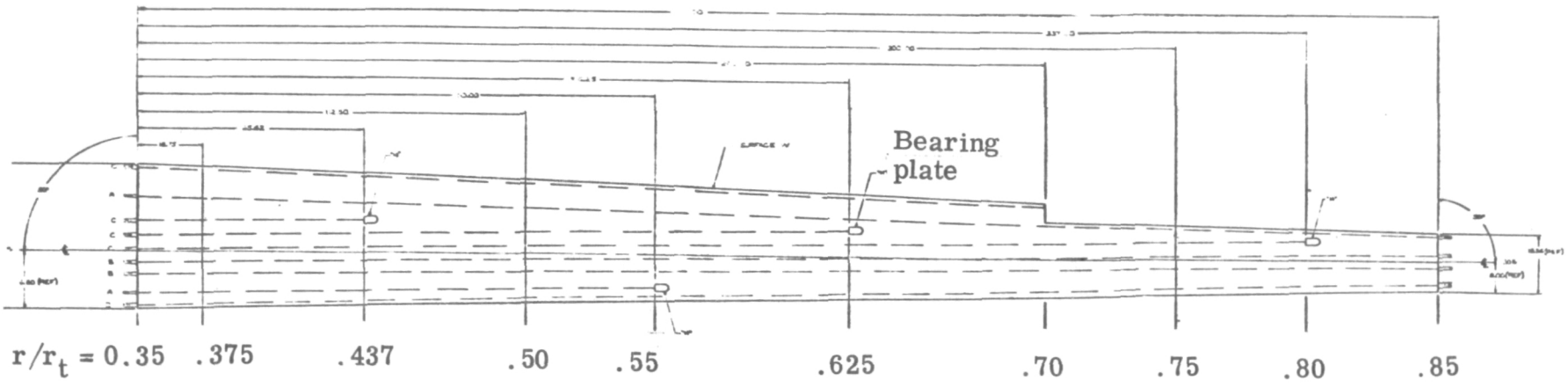


(a) Blade planform.

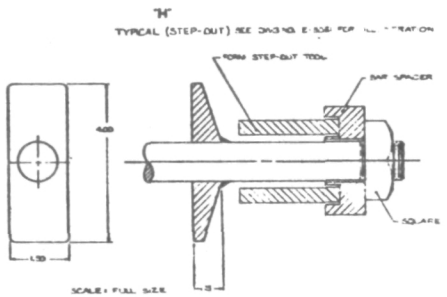


(b) Bearing plate.

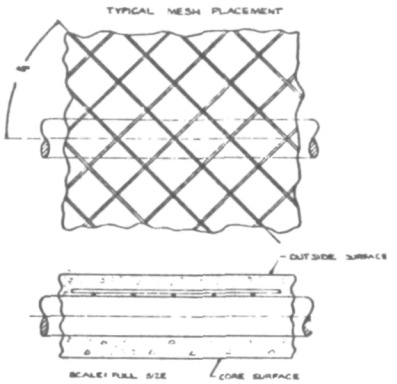


(c) Reinforcing mesh.

Figure 3. - Concrete blade design details.

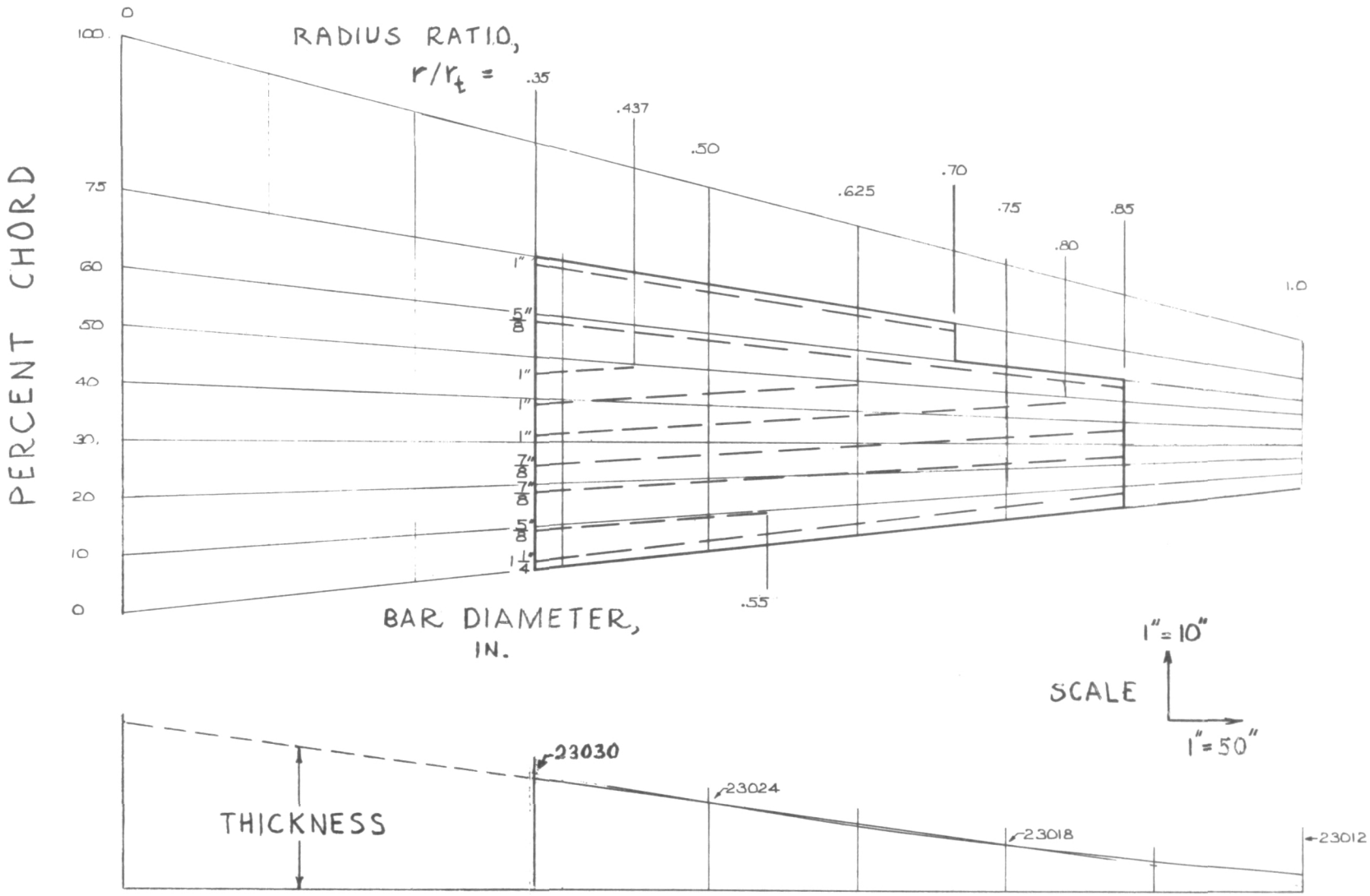


**Figure 4. - Schematic of prestressing bar installation.**

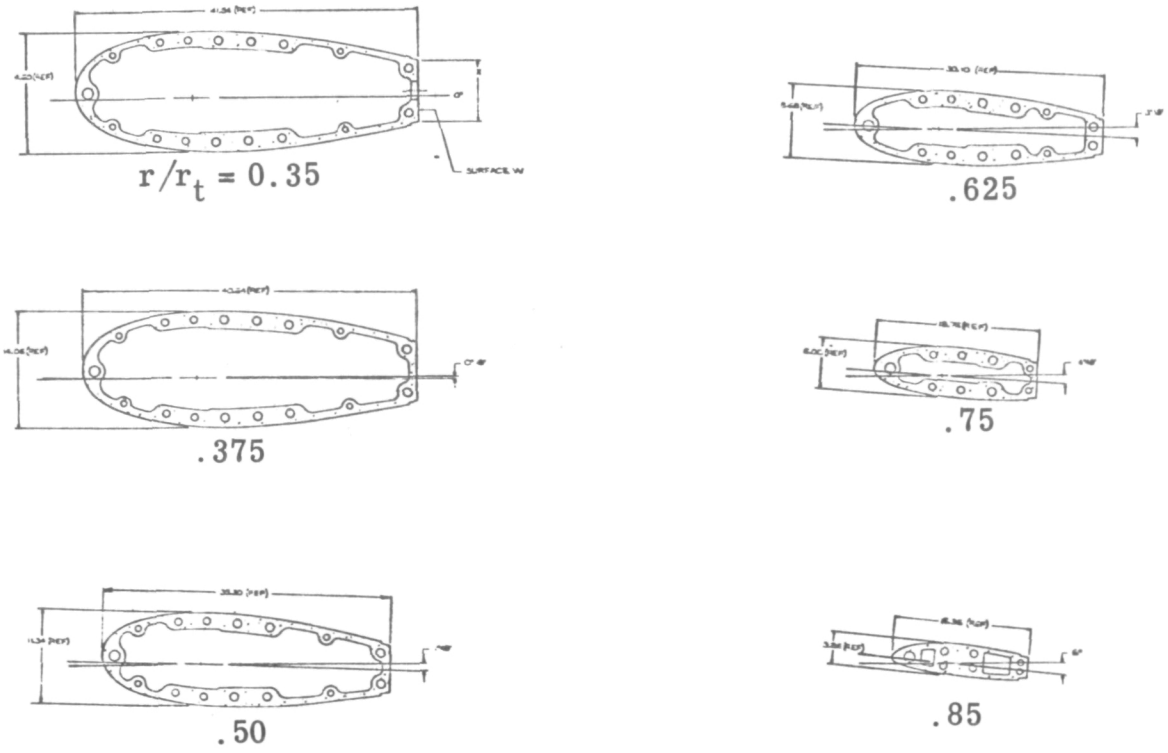


Figure 5. - Concrete blade cross sections.

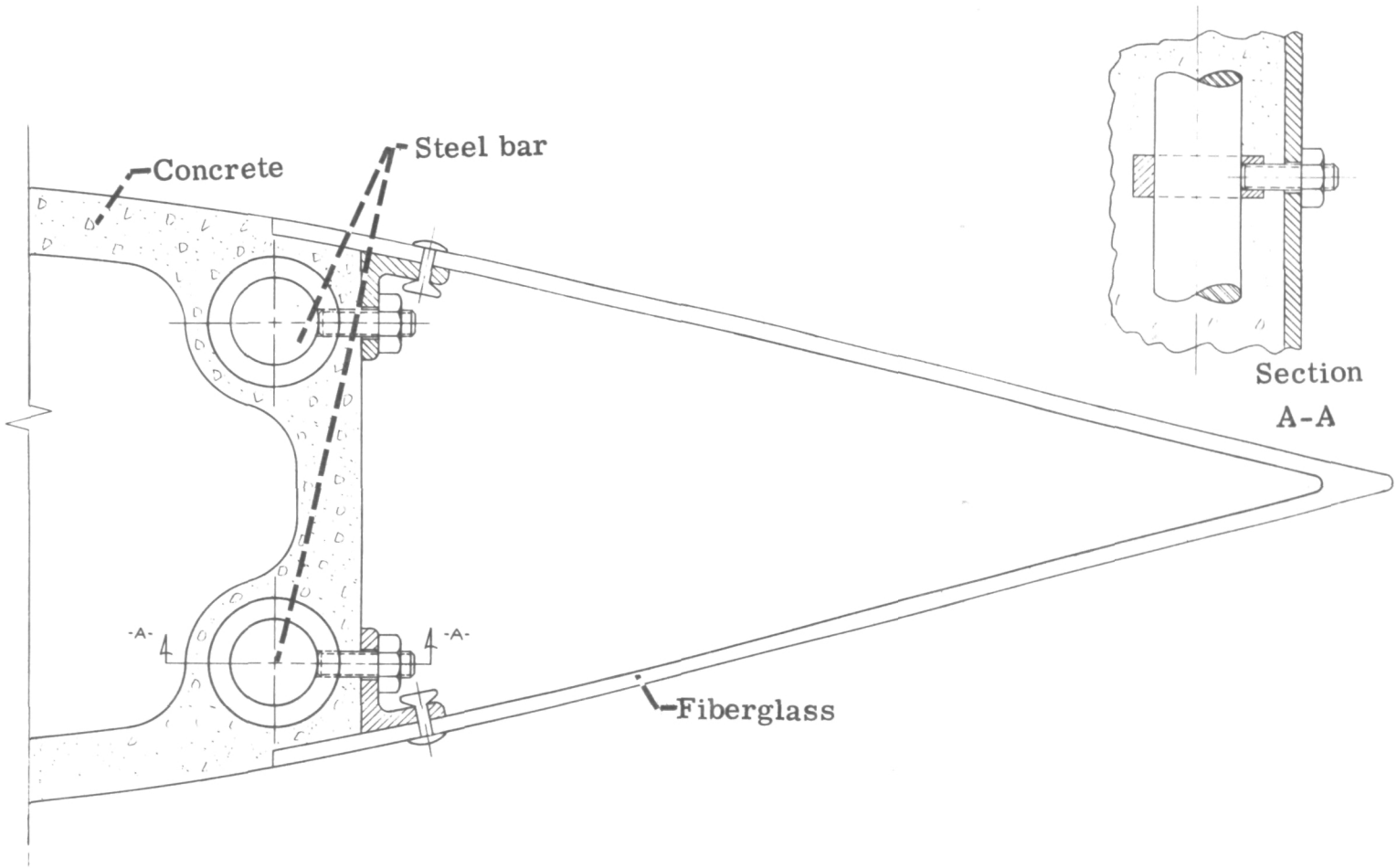


Figure 6. - Fiberglass trailing edge attachment.

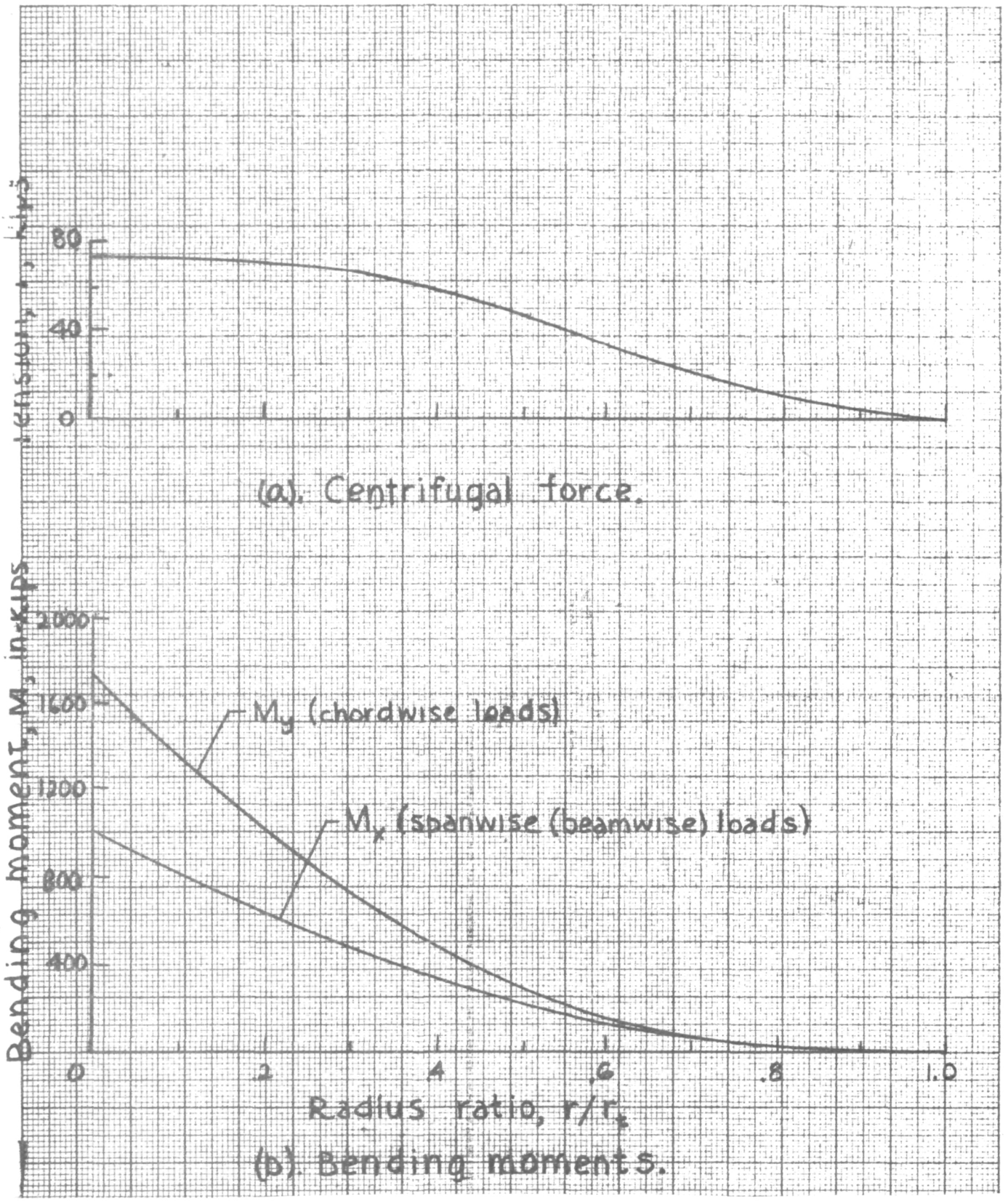


Figure 7. - Cyclic loading of wind turbine blades at design conditions. Rotational speed, 40 rpm; wind speed, 18 mph; $C_\ell = 0.8$.

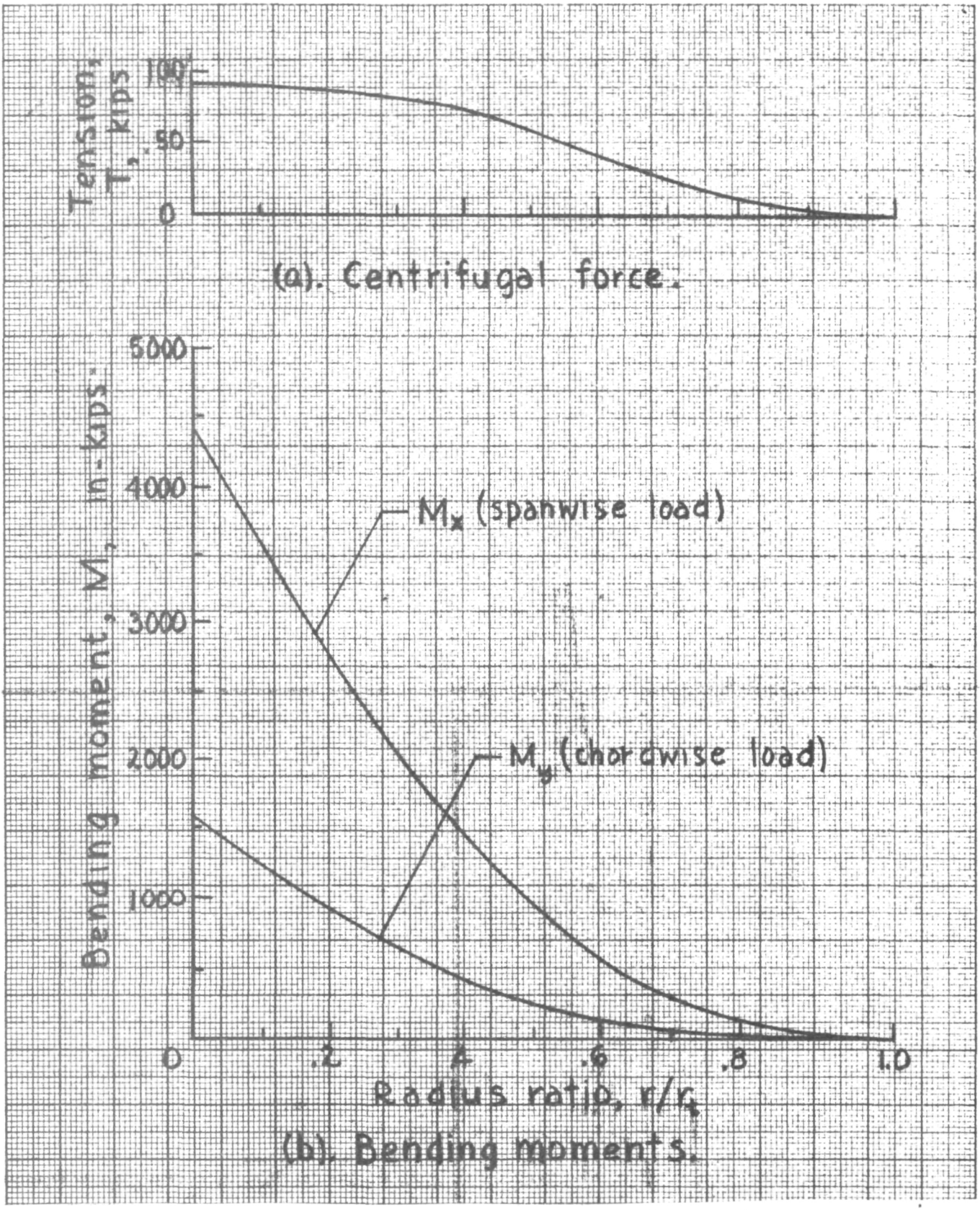


Figure 8. - Static loading of wind turbine blades for emergency shutdown condition. Rotational speed, 45 rpm; $C_\ell = -1$.

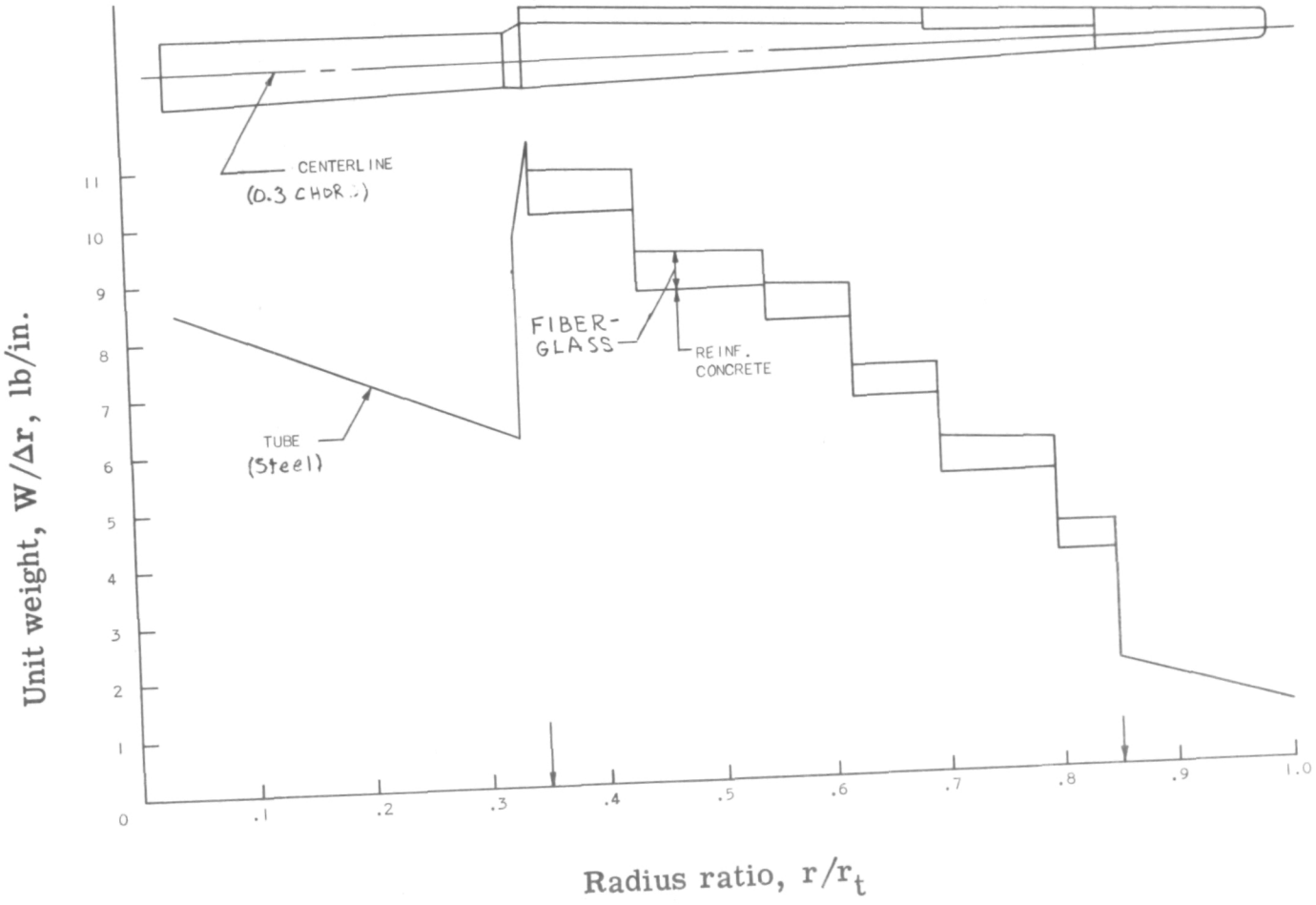


Figure 9. - Spanwise distribution of blade weight.

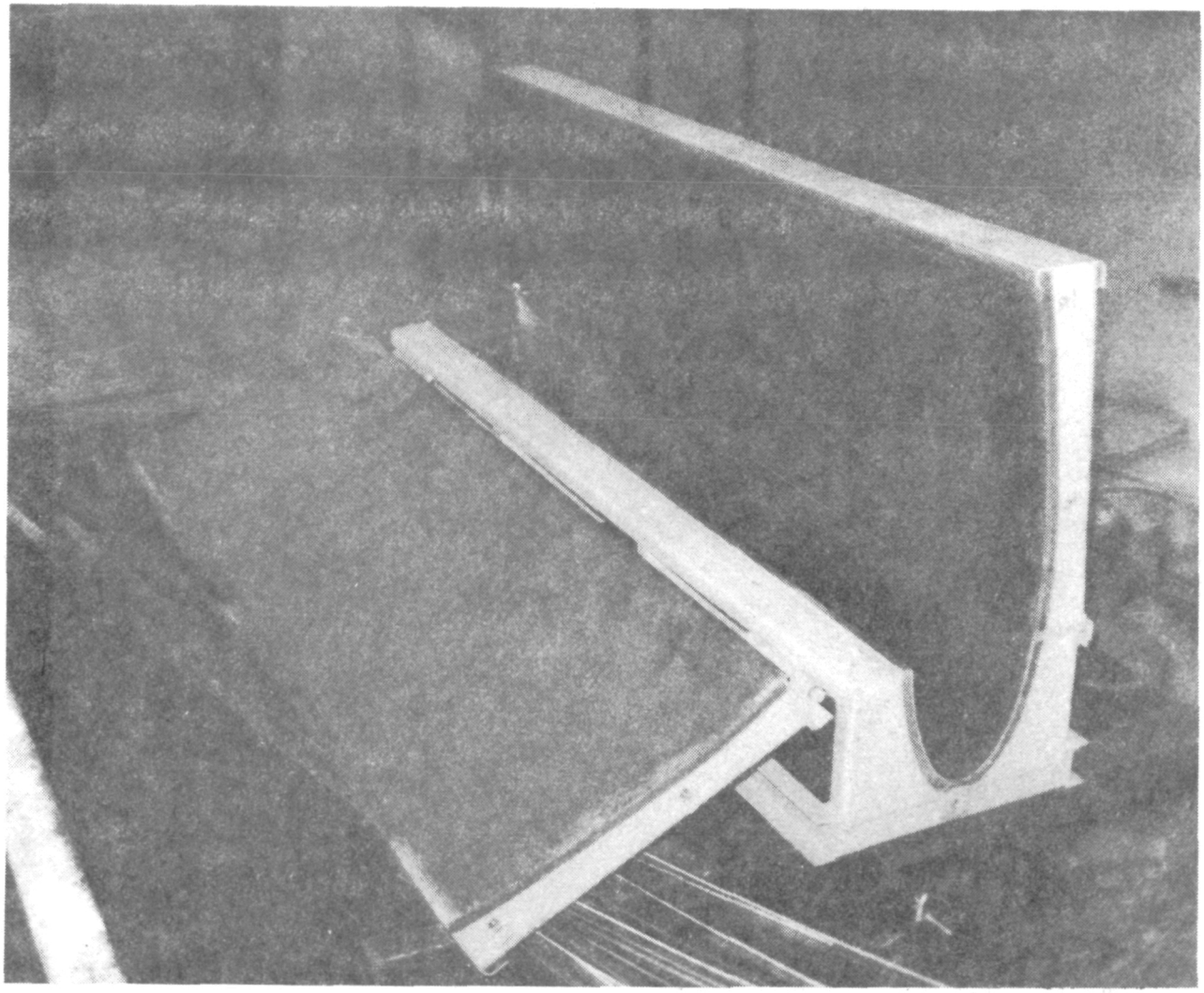

Figure 10. - Concrete form with side hinged open.

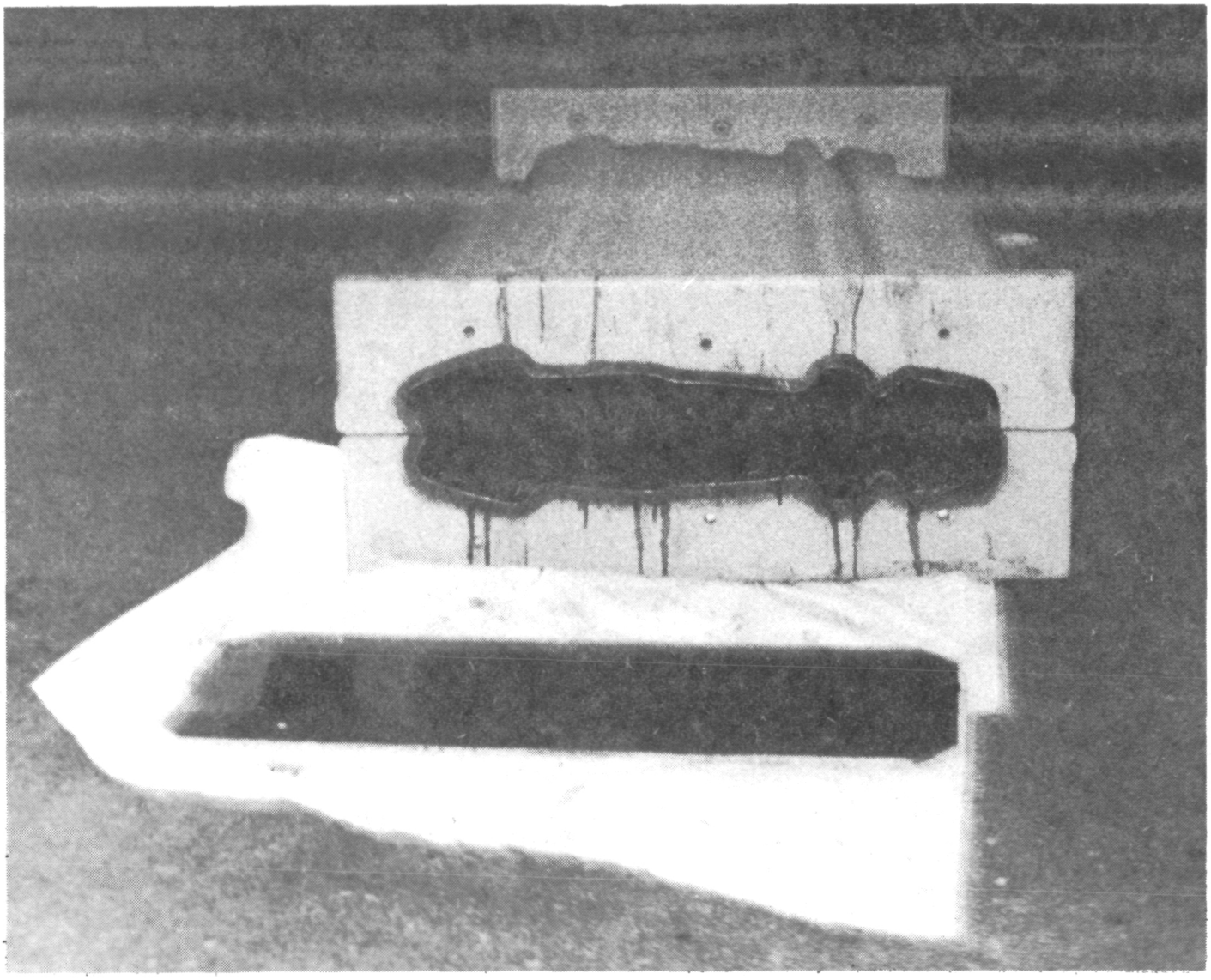

Figure 11. - Foam casting form with end removed.

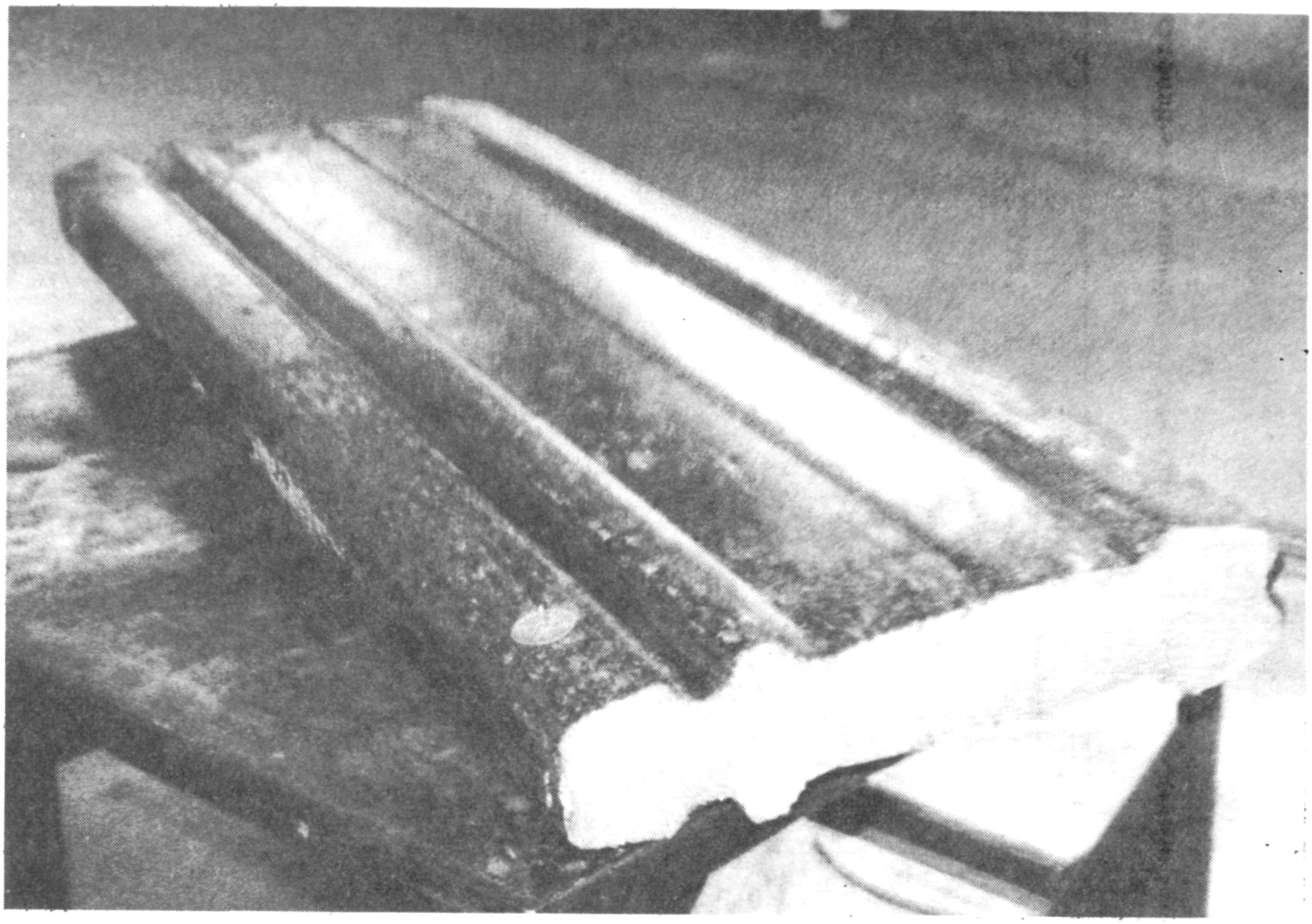

Figure 12. - Foam core ready to install.

Figure 13. - Placing foam core into concrete form.

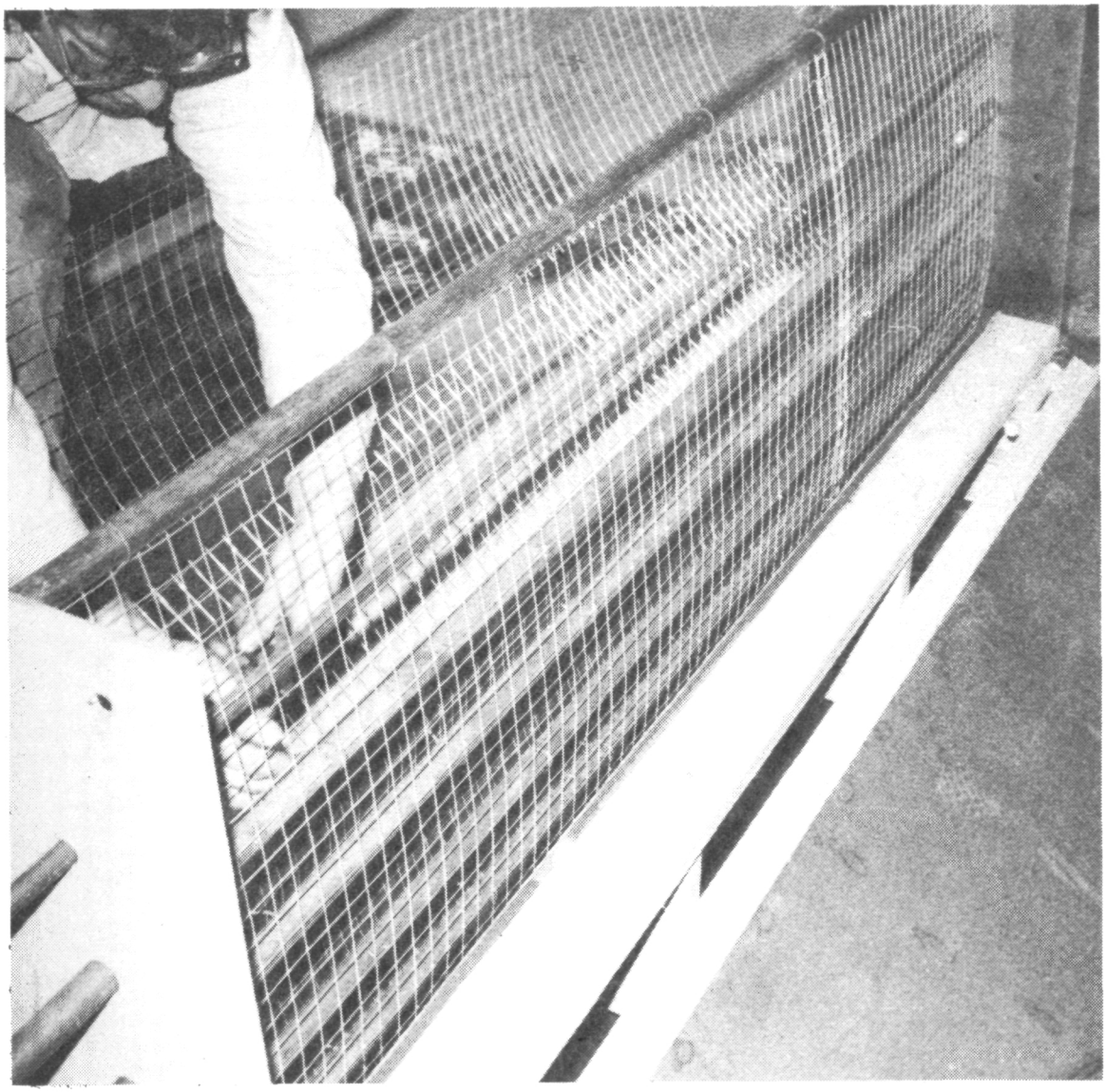

Figure 14. - Installing reinforcing steel in form.

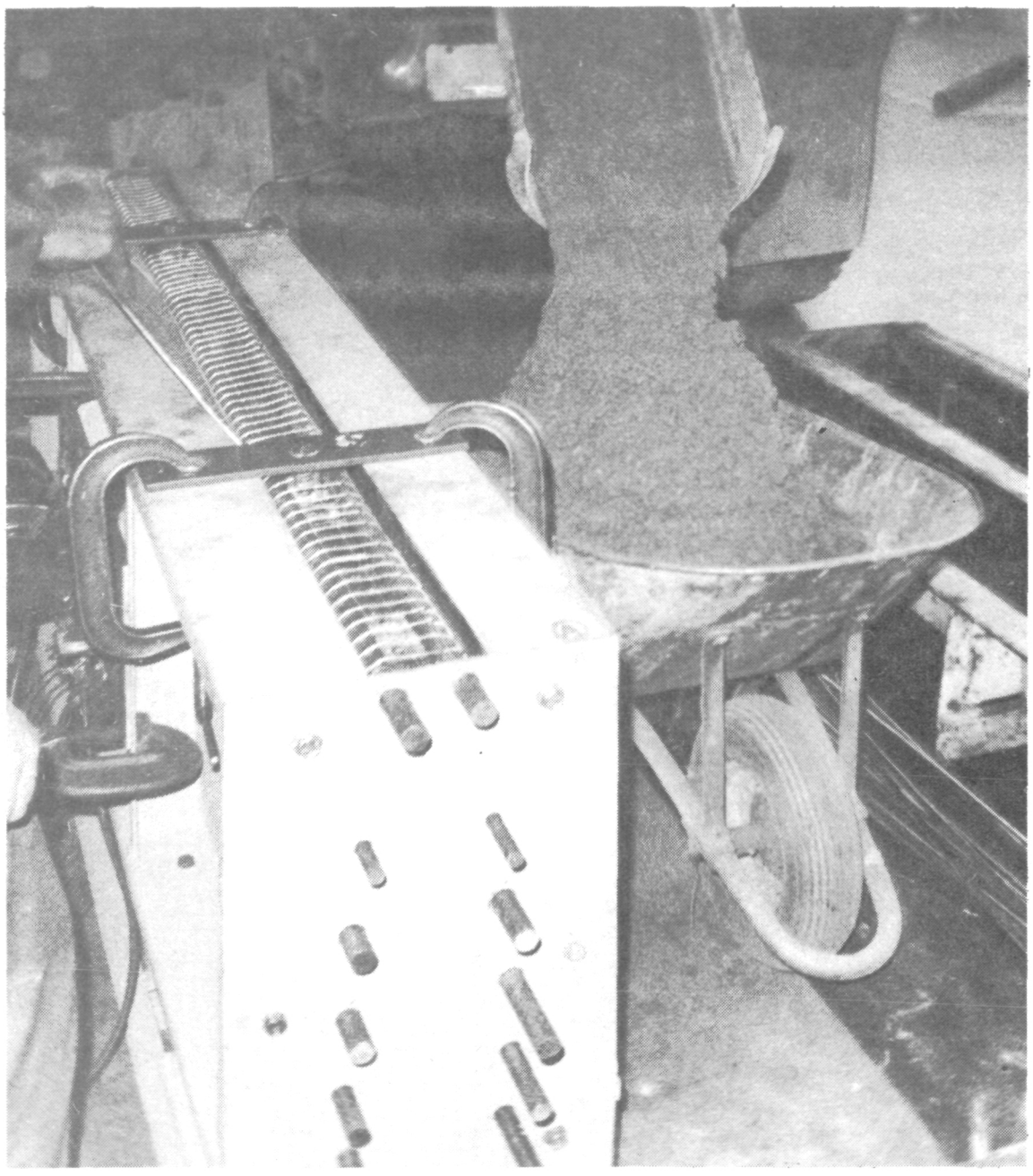

Figure 15. - Readying concrete to pour into form.

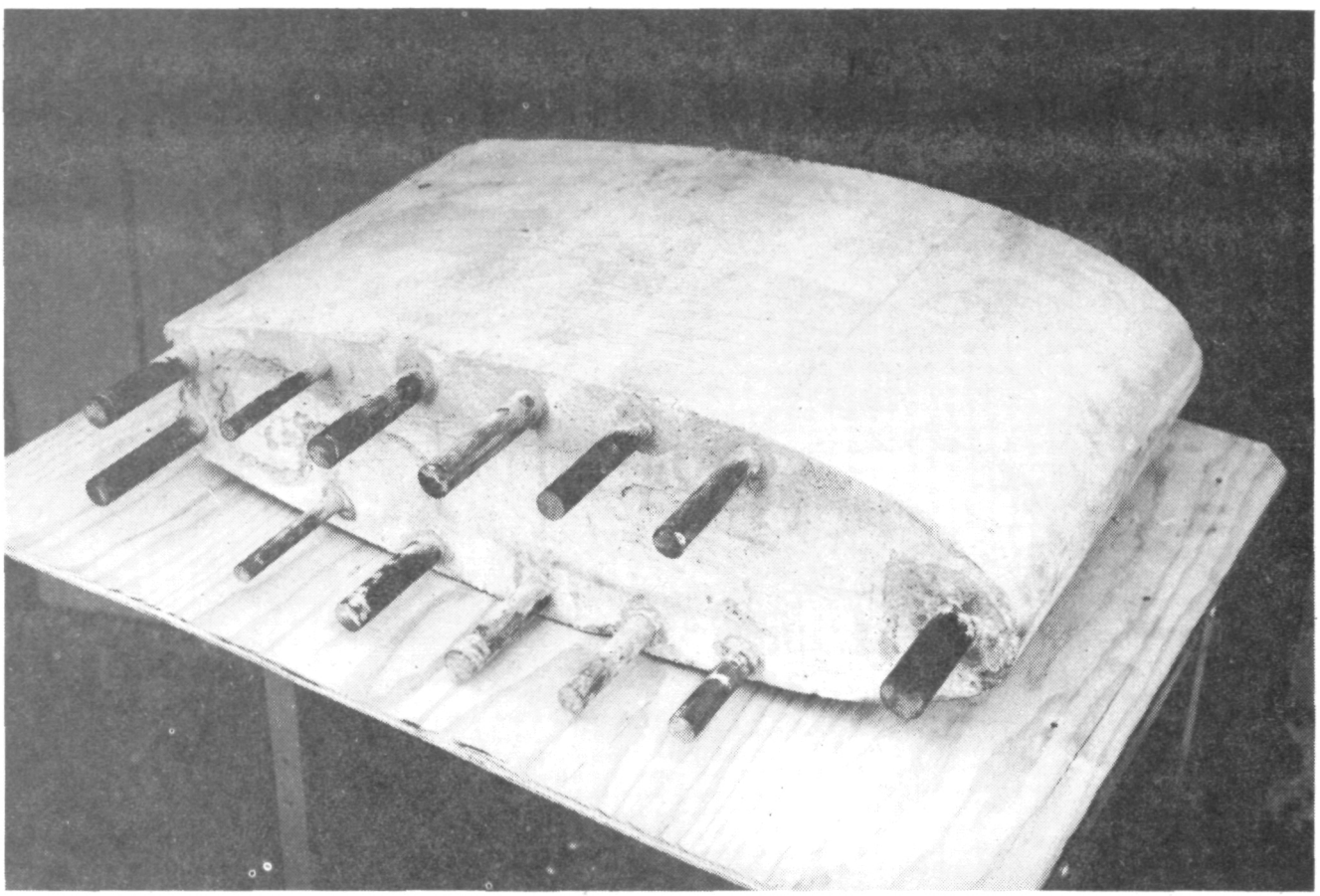

Figure 16. - Section of concrete casting showing longitudinal bars.

Figure 17. - Concrete cross section with fiberglass trailing edge.

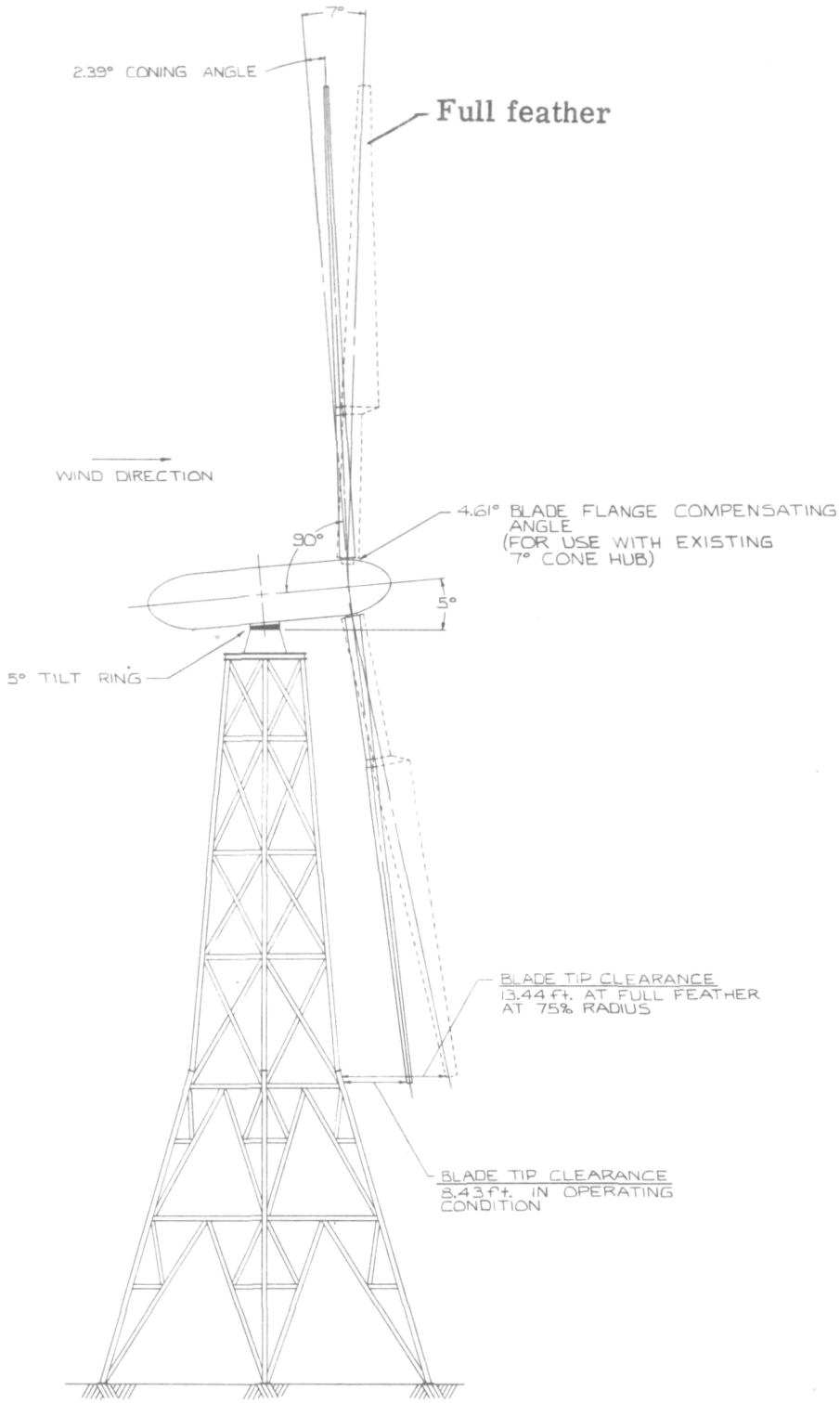


Figure 18. - Scheme I. Rotor downwind of tower. Blades coned downwind.

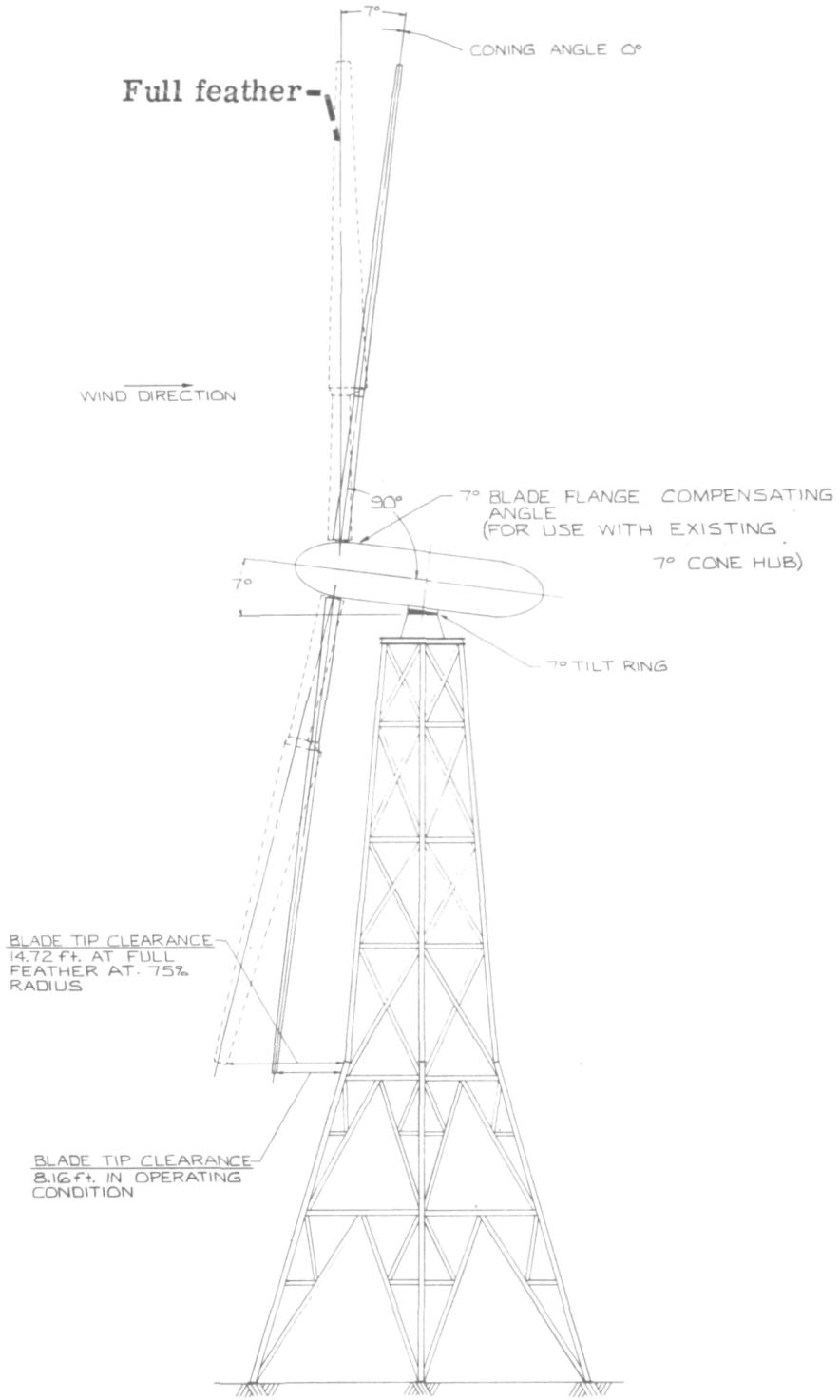


Figure 19. - Scheme II. Rotor upwind of tower. Zero blade coning angle.

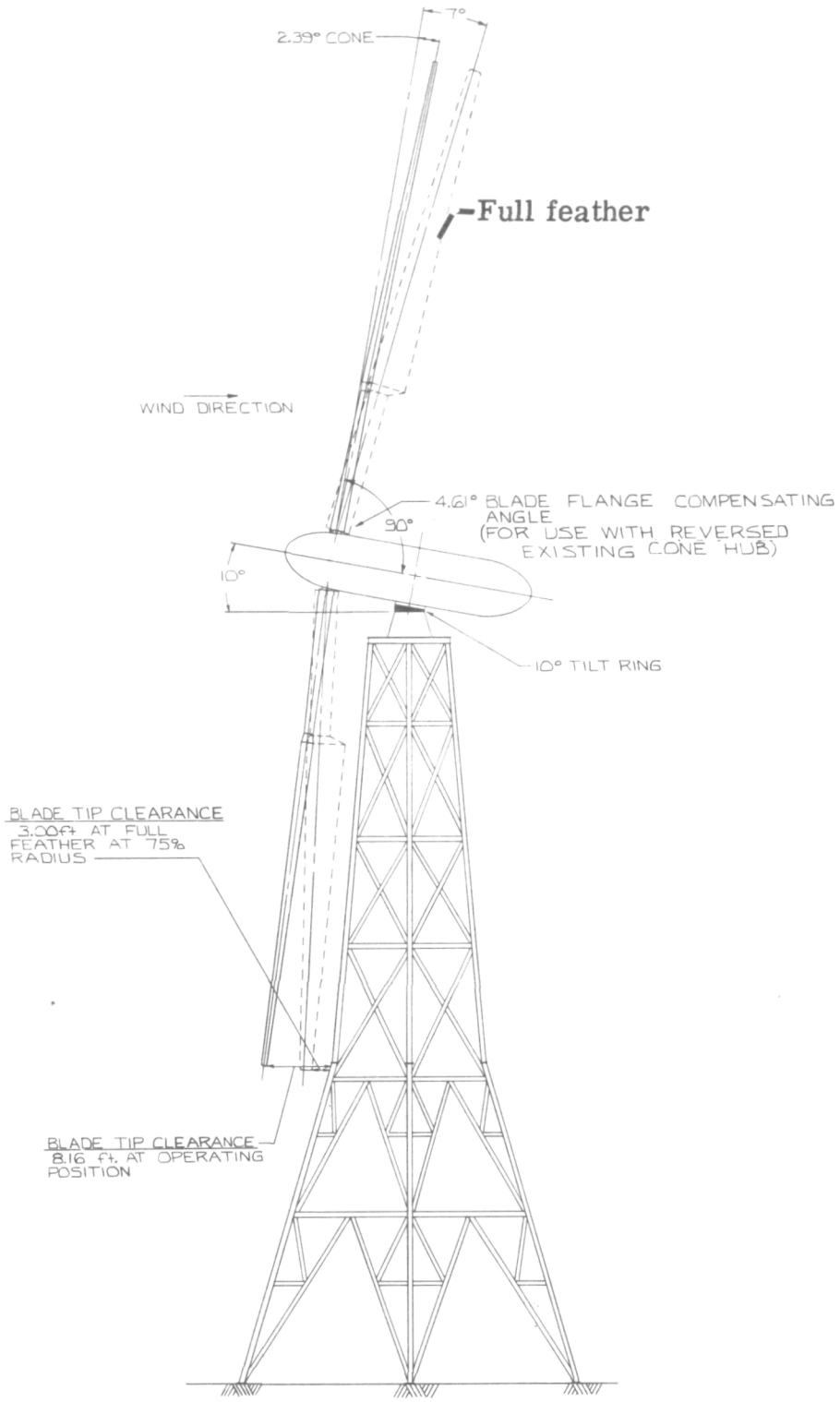


Figure 20. - Scheme III. Rotor upwind of tower. Blades coned downwind.

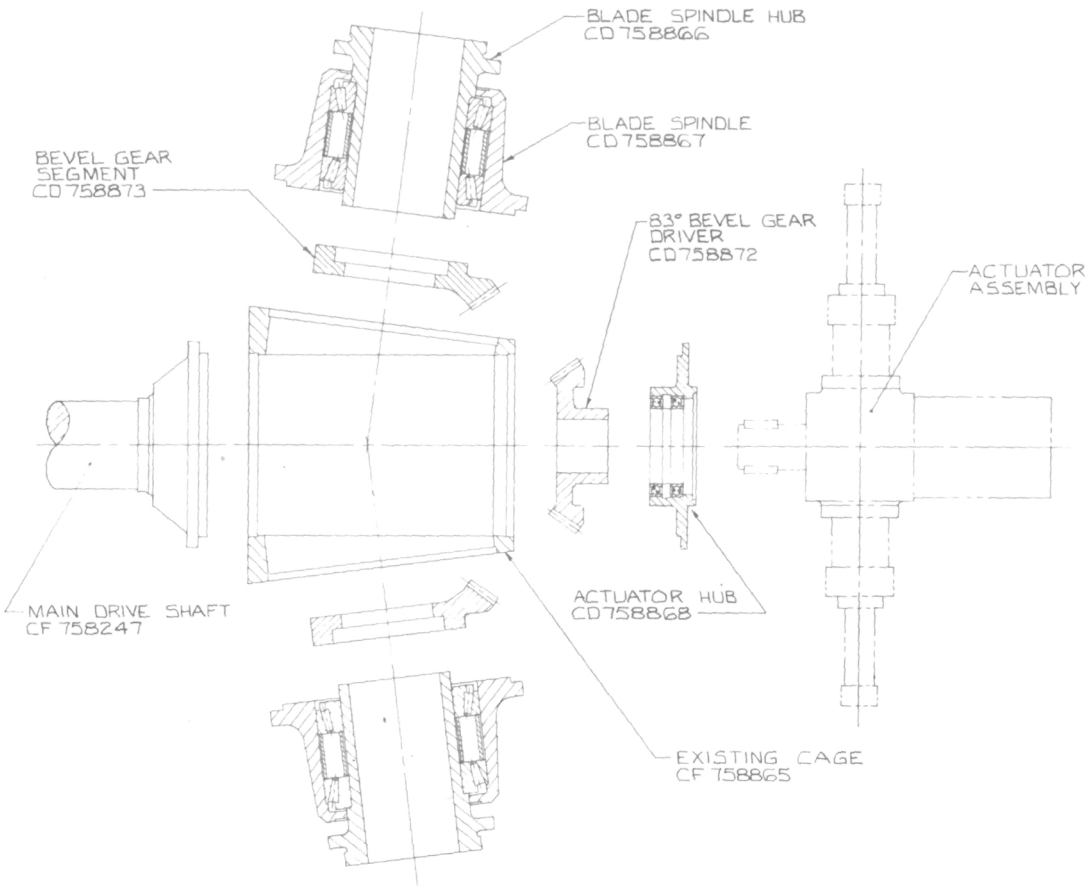


(a) Present hub arrangement for MOD-0 tower.

Figure 21. - Details of hub mechanisms.

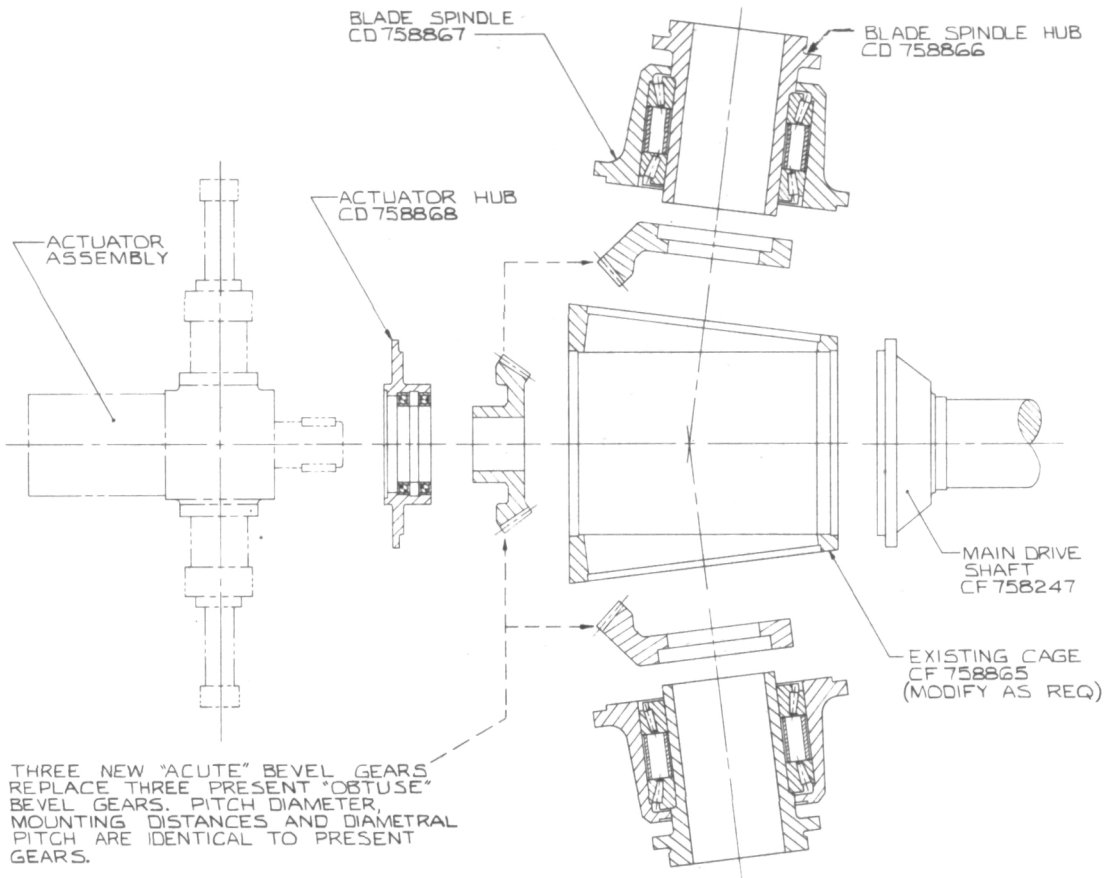


(b) Proposed hub arrangement for scheme III (fig. 20).

Figure 21. - Concluded.

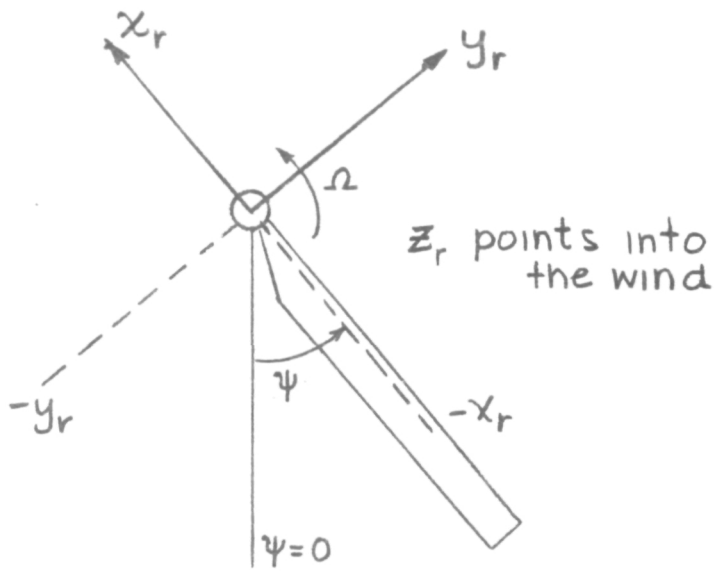


(a). Rotor axes.

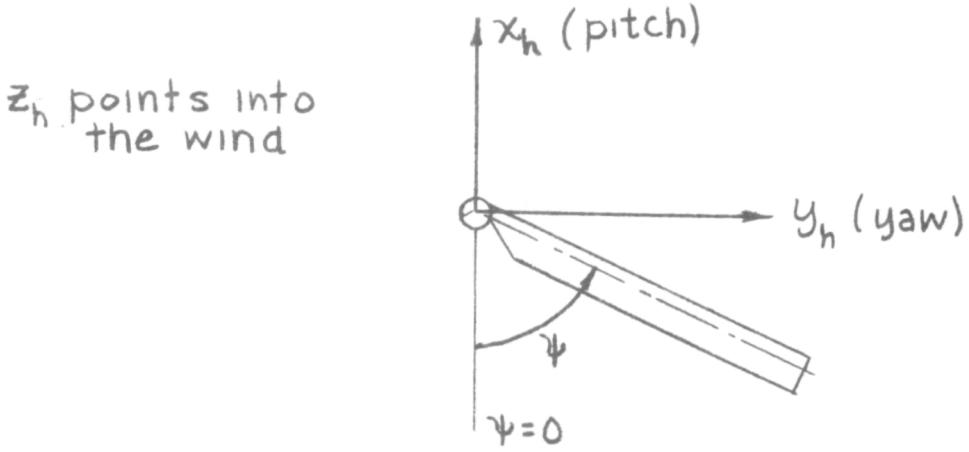


(b). Hub axes.

Figure 22. - Coordinate axes for coupled dynamic analysis. View looking upstream.

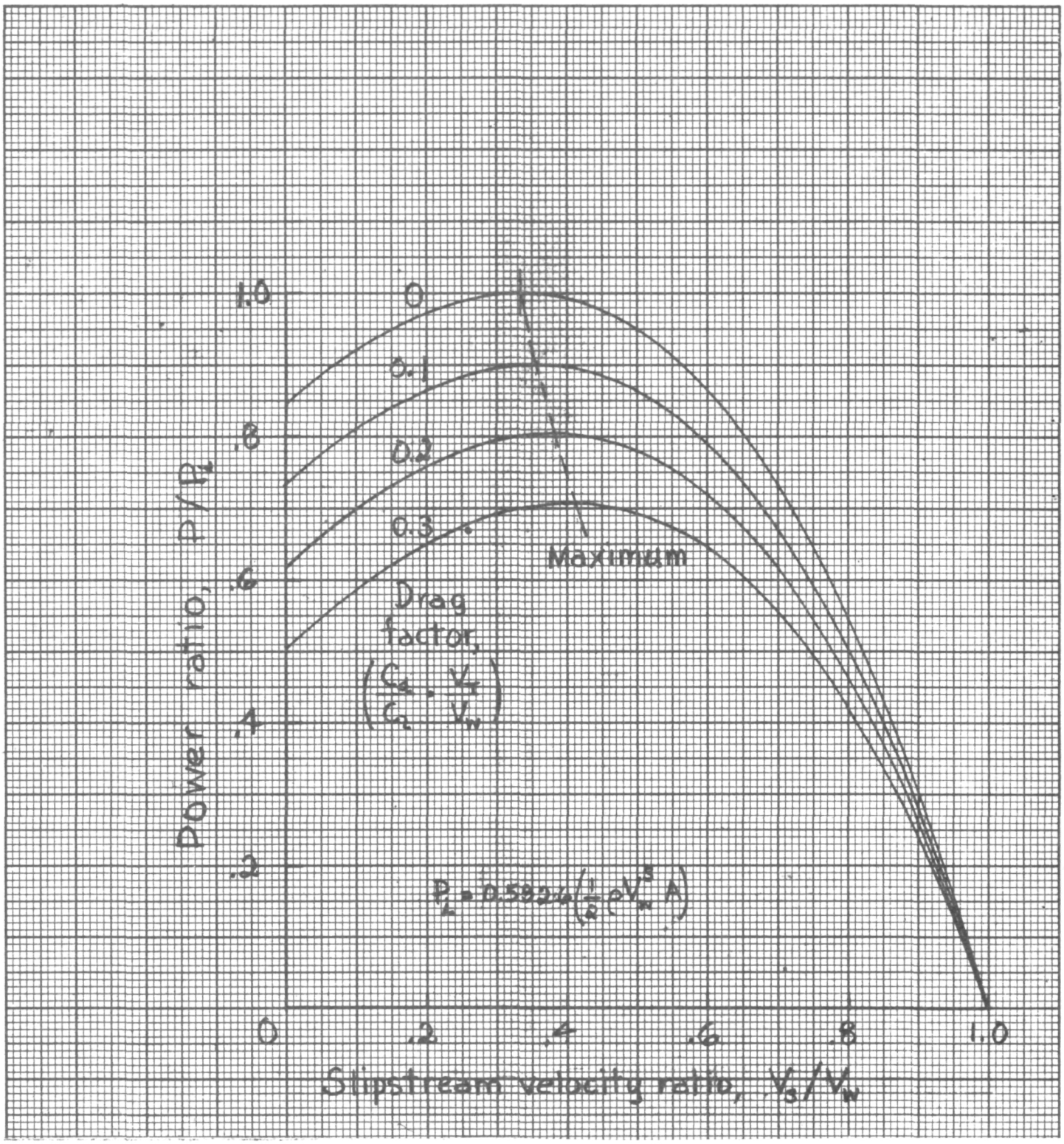


Figure 23. - Aerodynamic power generation for wind turbine rotors. Zero slipstream rotation.

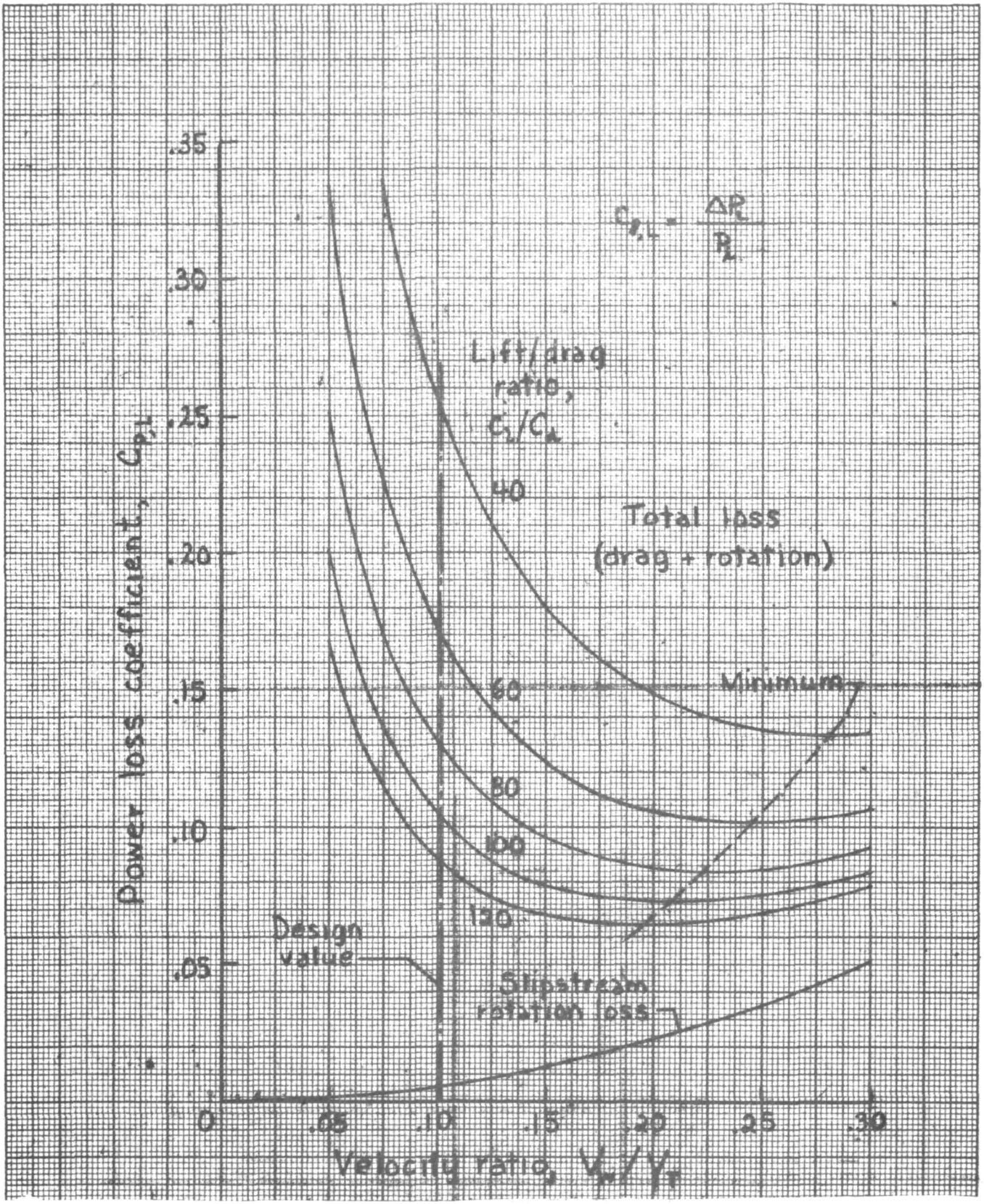


Figure 24. - Aerodynamic power losses in wind turbine rotors. Slipstream, $V_e/V_w = 1/3$.

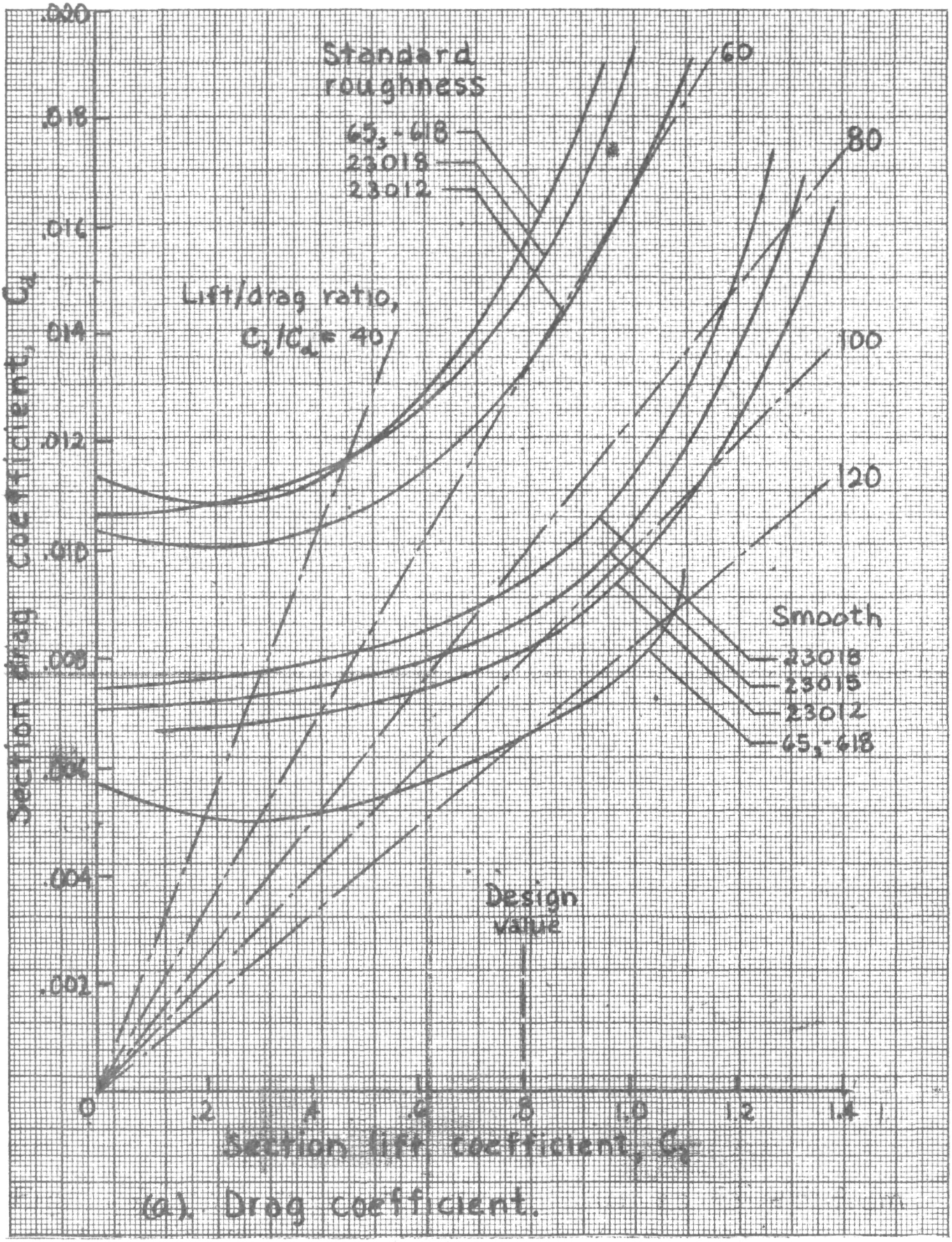


Figure 25. - Airfoil characteristics. Curves faired from data in reference 6 for $R_e = 3 \times 10^6$.

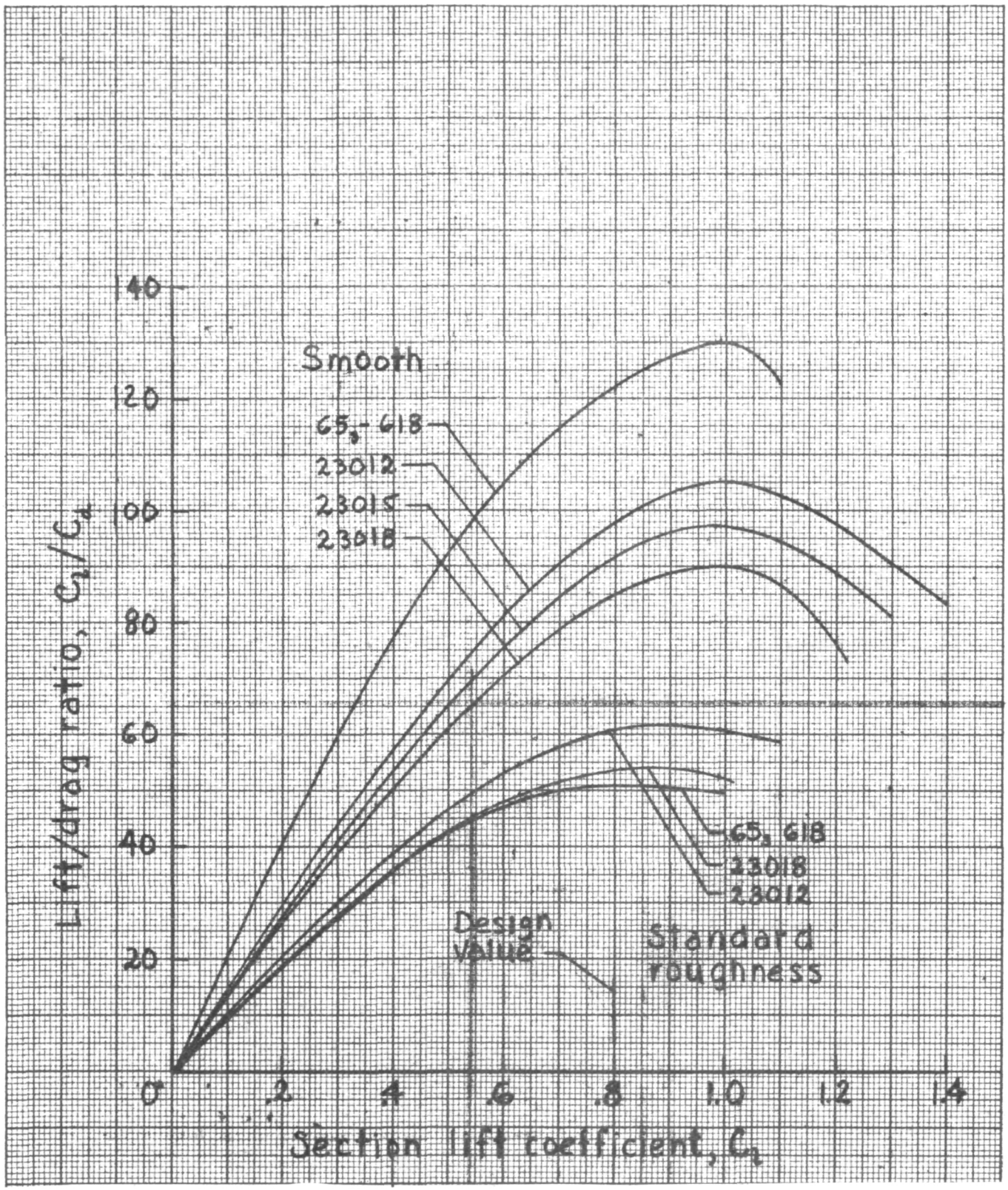


(b) Lift/drag ratio.

Figure 25. - Concluded.

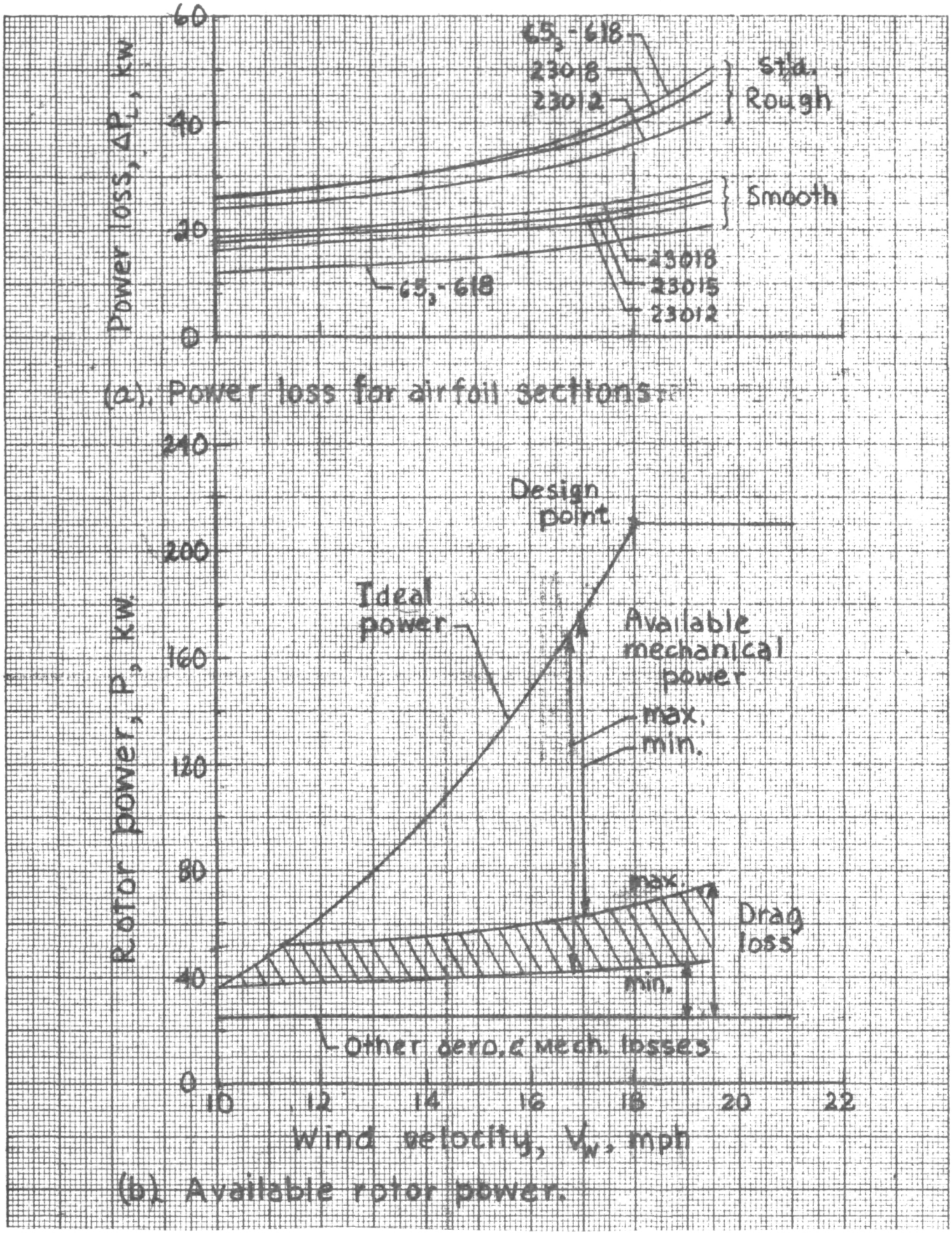


Figure 26. - Effect of airfoil drag on available power for wind turbine blades. Rotor diameter, 125 ft.

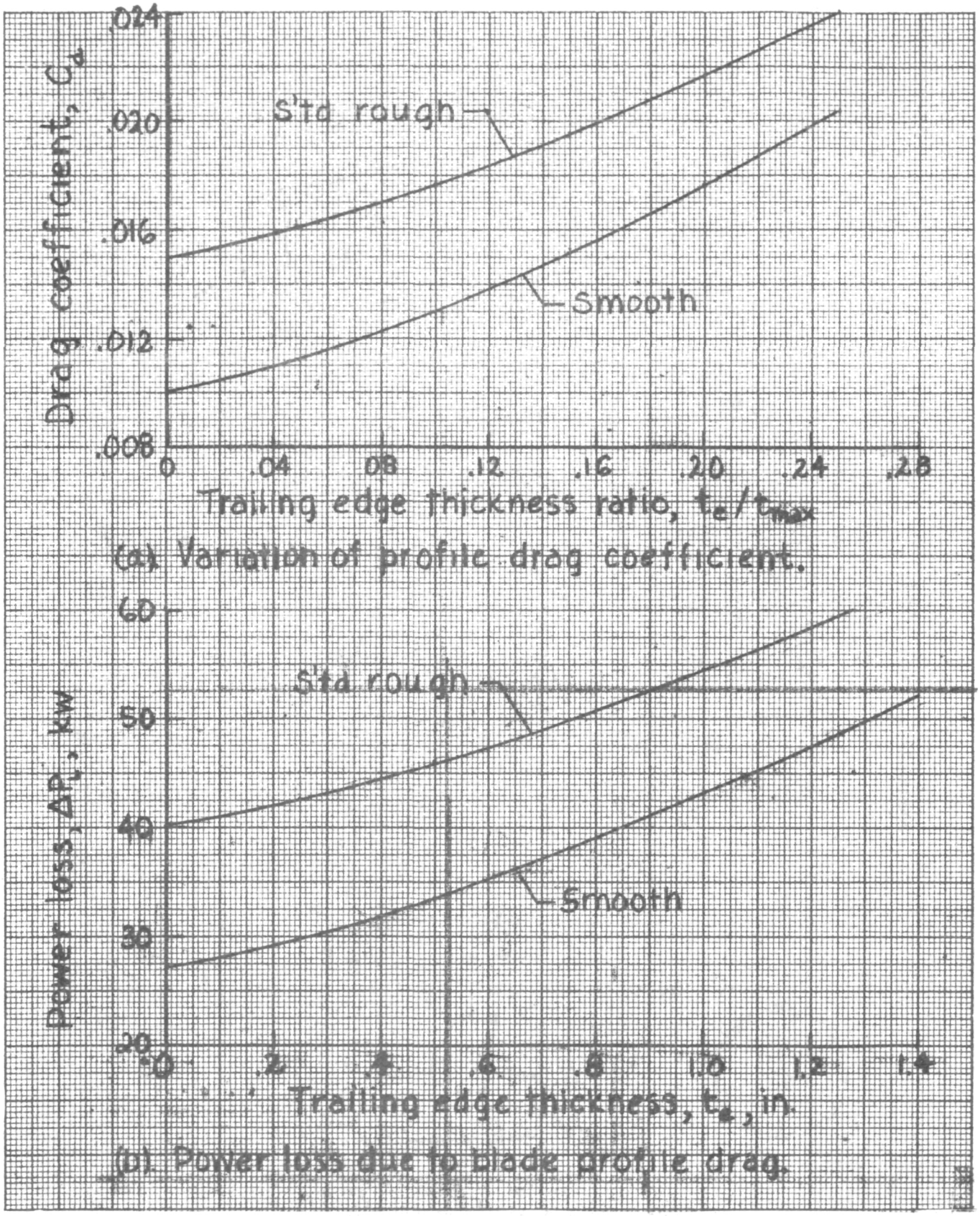


Figure 27. - Effect of blade trailing edge thickness on blade power loss in wind turbine. Design conditions: $V_w$ = 18 mph; diameter = 125 ft; C = 32.5 in.; $C_\ell$ = 0.8; $P_i$ = 210 kW.

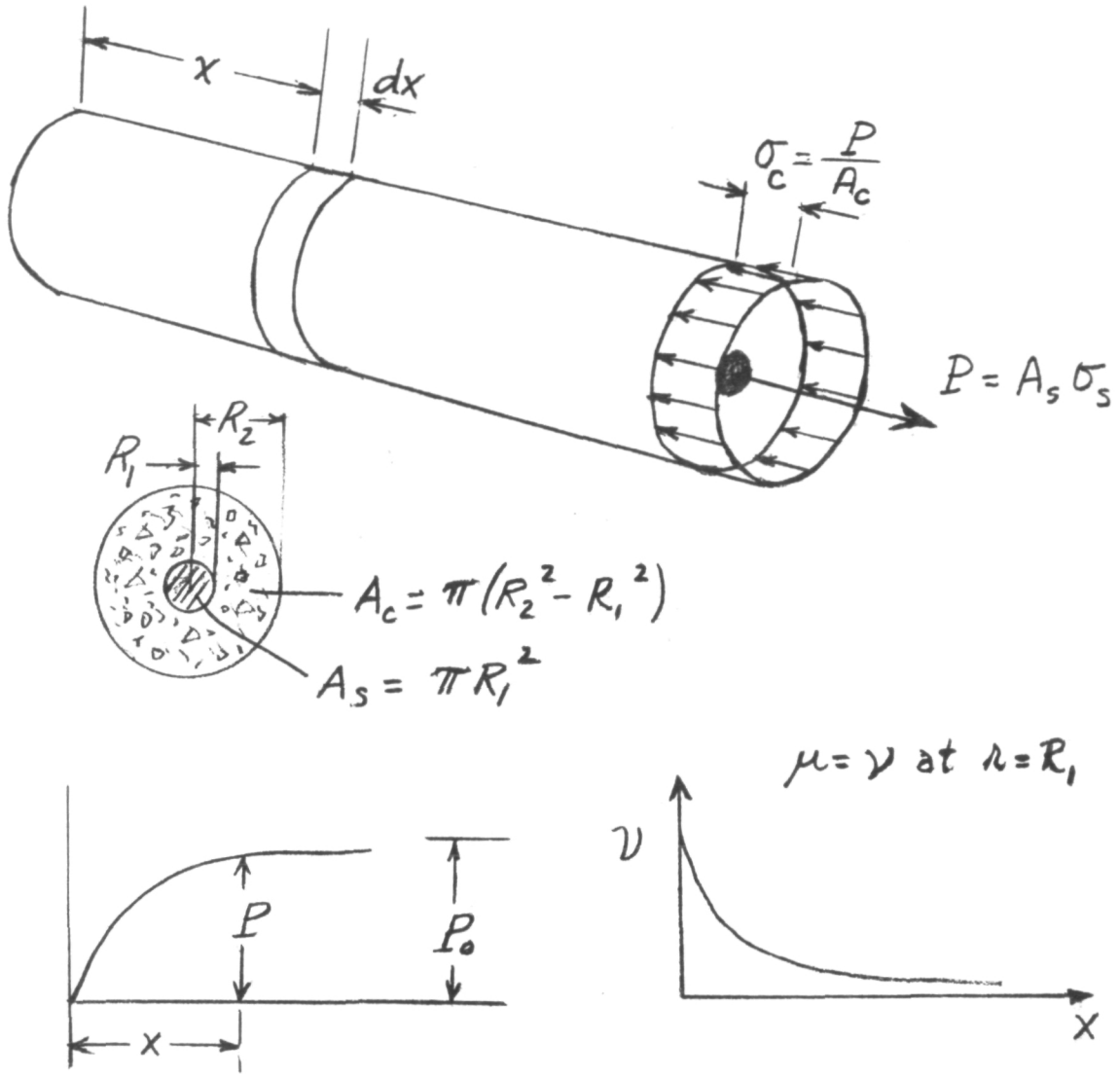


(a). Stress conditions.

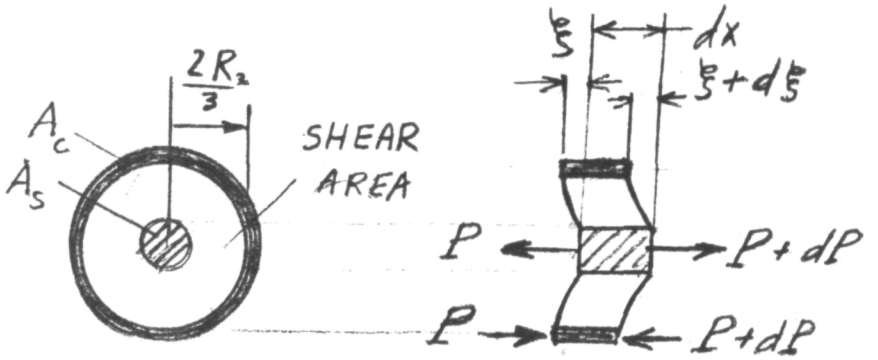


(b) Strain conditions.

**Figure 28. - Simplified model for prestressed concrete.**

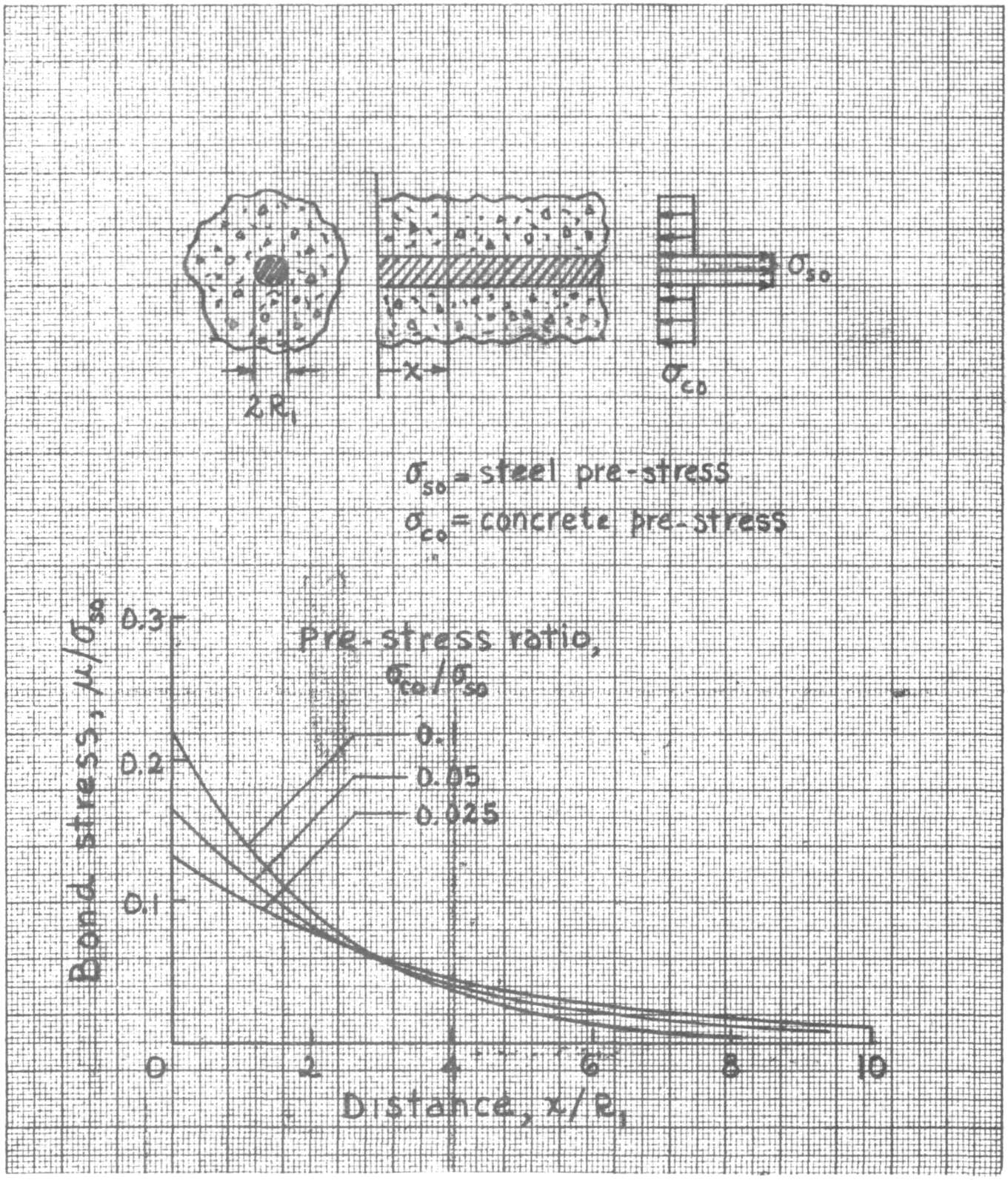


Figure 29. - Bond stresses near end of prestressed bar. Modulus ratios: $E_c/E_s = 0.1$; $G_c/E_c = 0.38$.

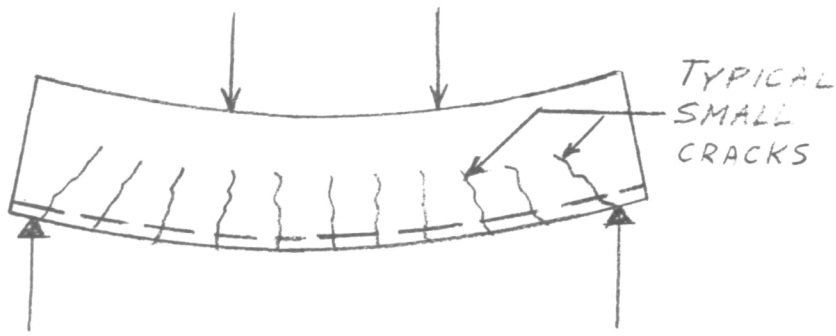


Figure 30. - Concrete beam without prestress.

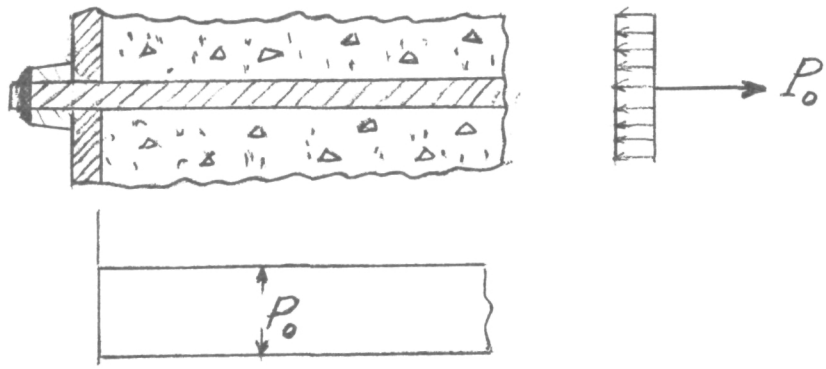


(a) Bar with metal bearing plate.

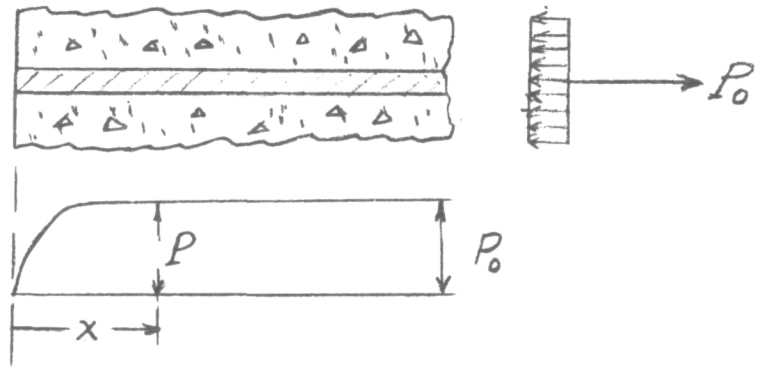


(b) Bonded bar.

Figure 31. - Prestressed bar ends.

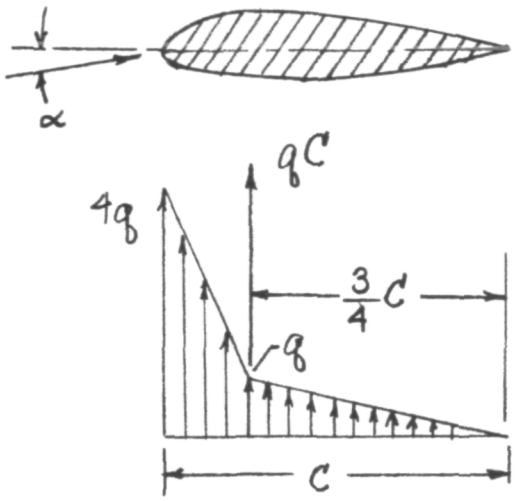


(a). Normal operation.

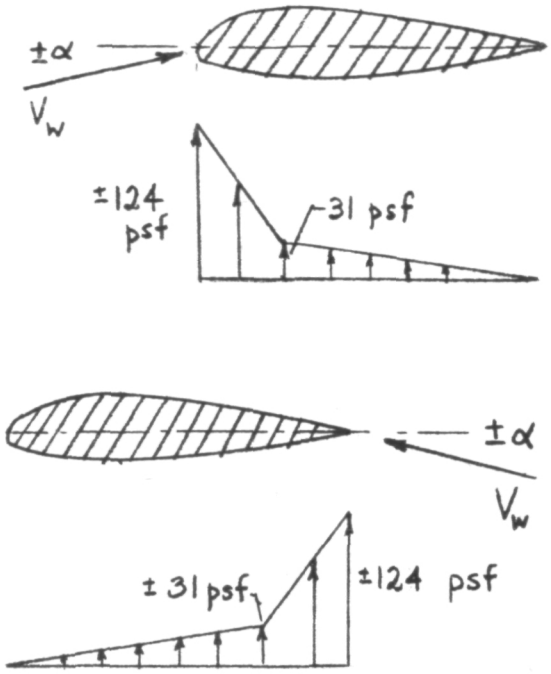


(b). Hurricane wind. Blades feathered; max $C_l = \pm 1$.

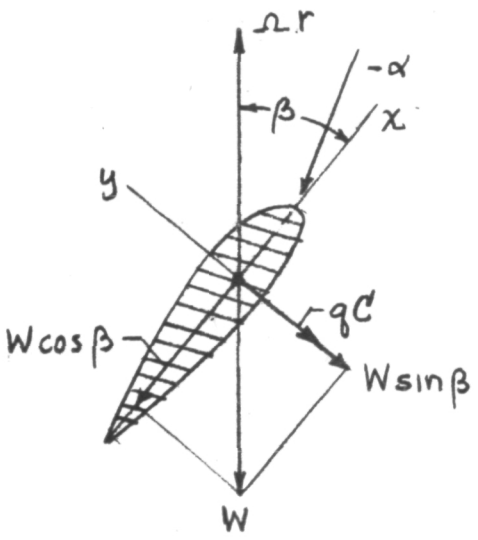


ascending blade

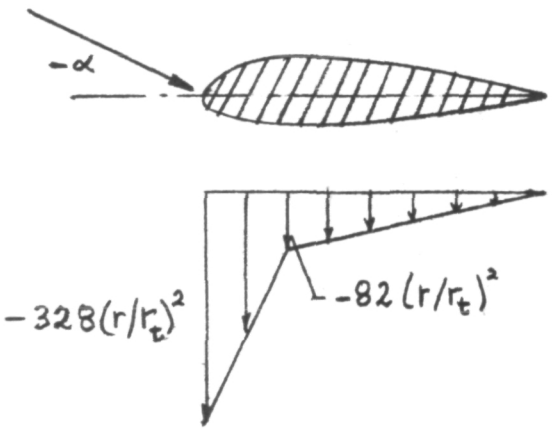


(c). Emergency shutdown; 45 rpm; $C_l = -1$.

Figure 32. - Assumed blade air loading conditions.

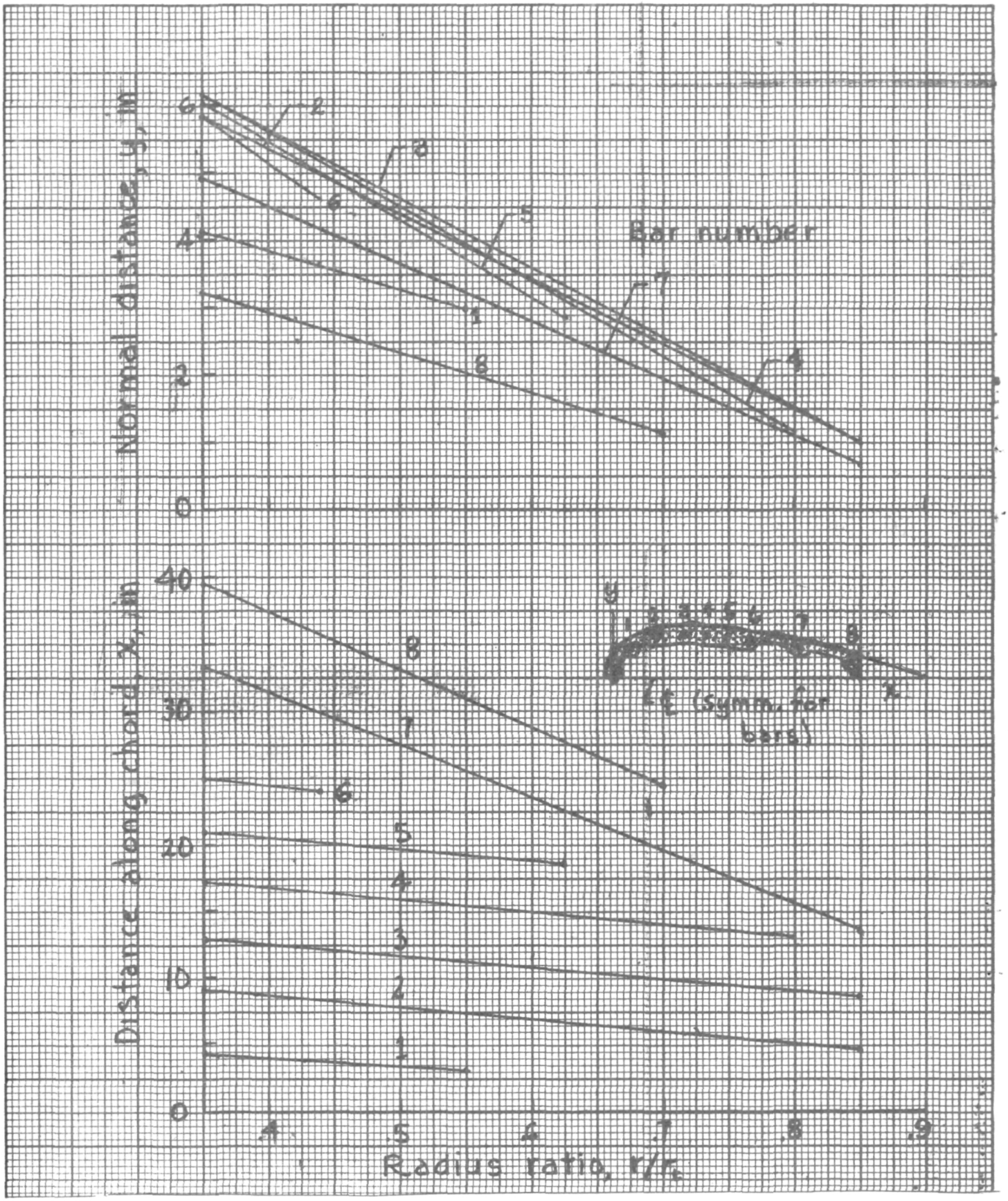


Figure 33. - Reinforcing bar locations.

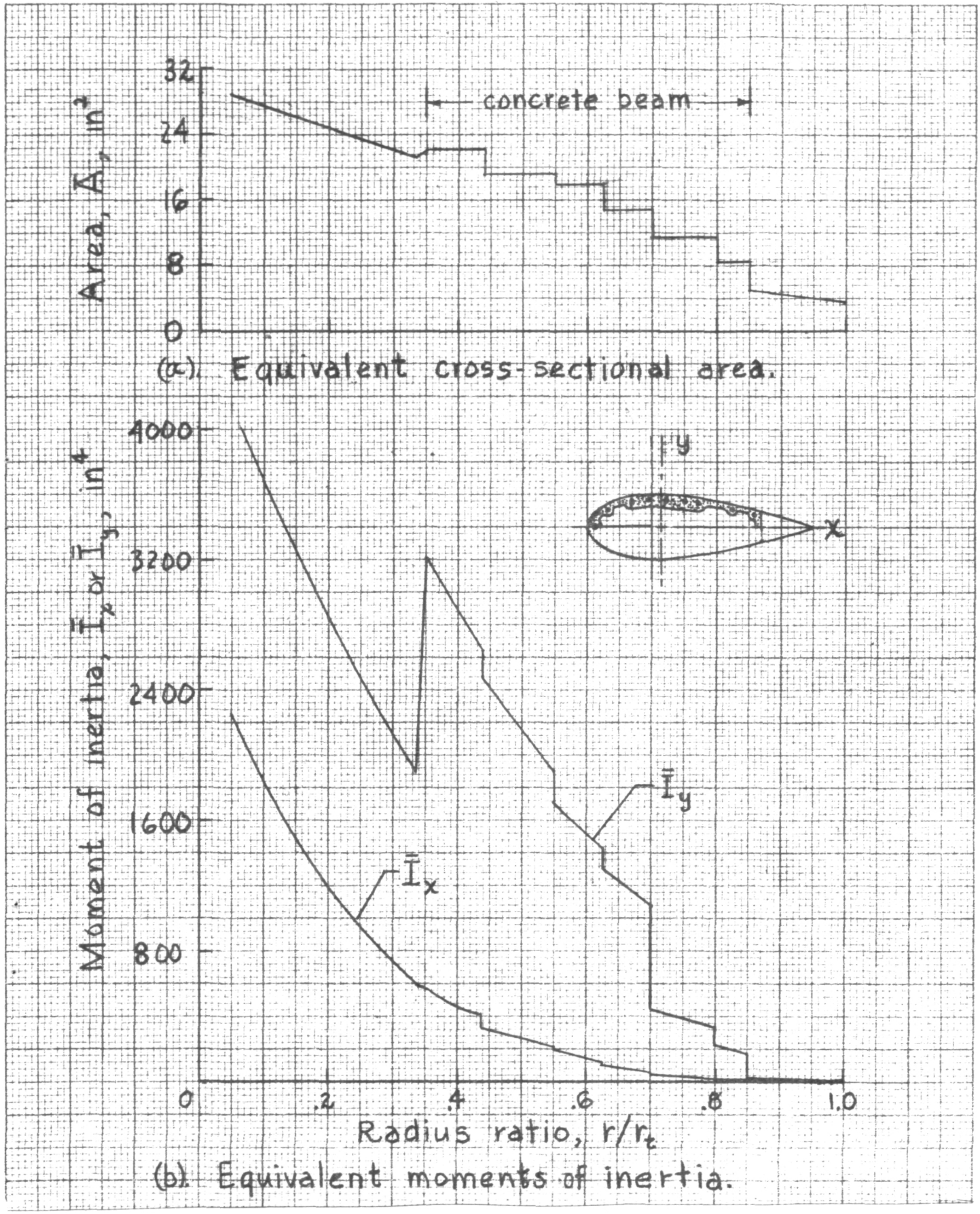


Figure 34. - Steel-equivalent section properties for baseline blade design.

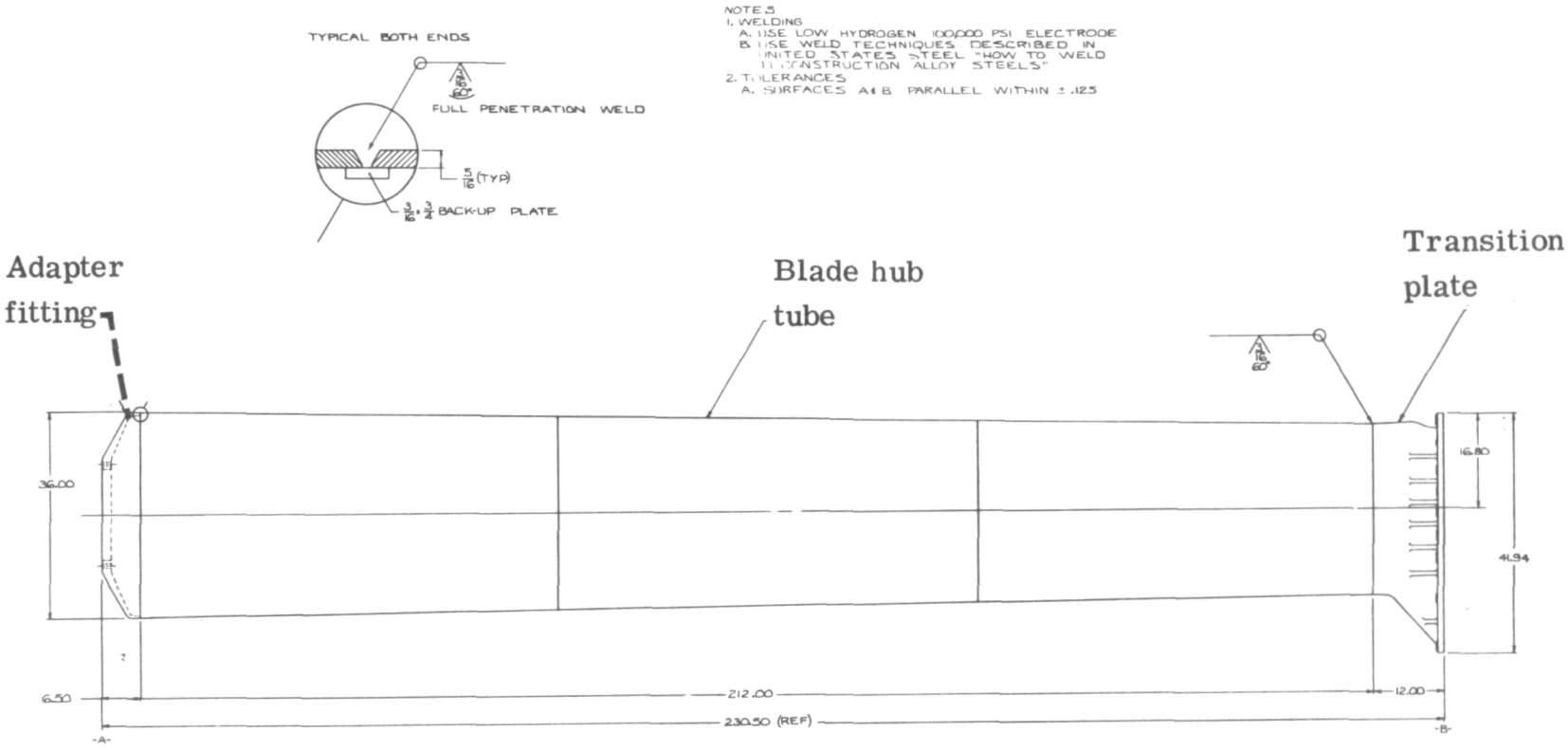


Figure 35. - Blade hub assembly.

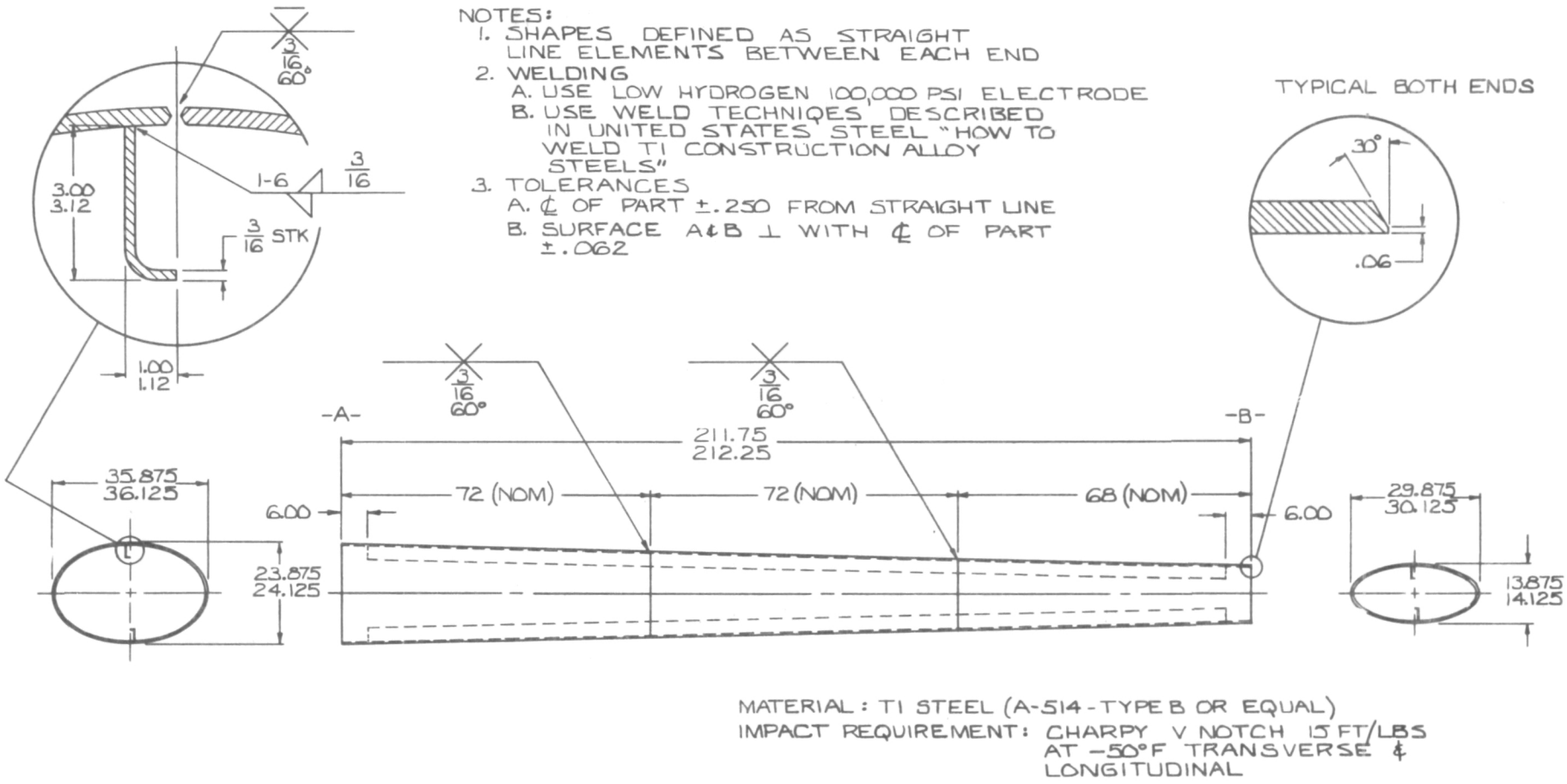


Figure 36. - Blade hub tube.

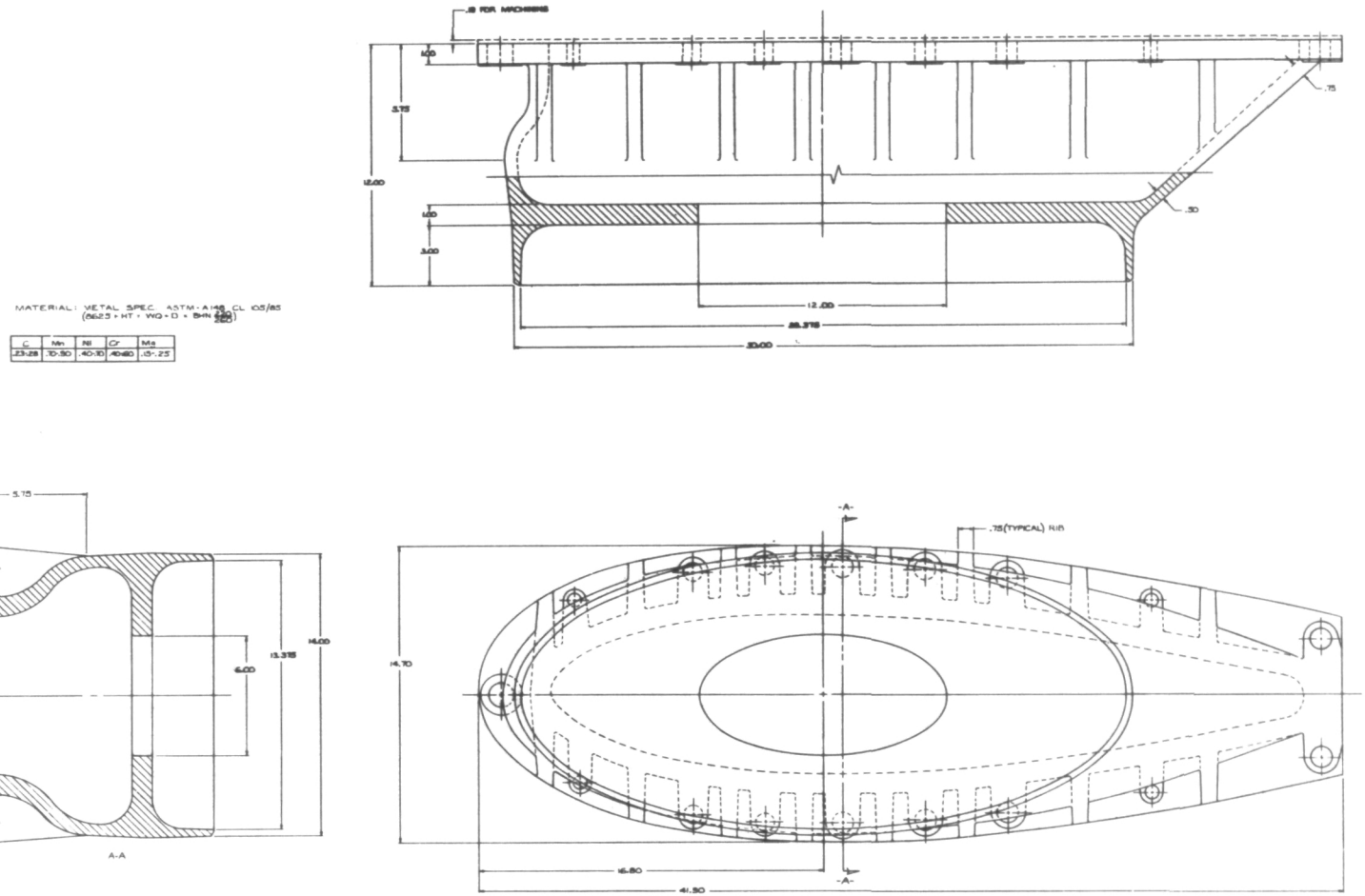


**Figure 37. - Transition plate casting.**

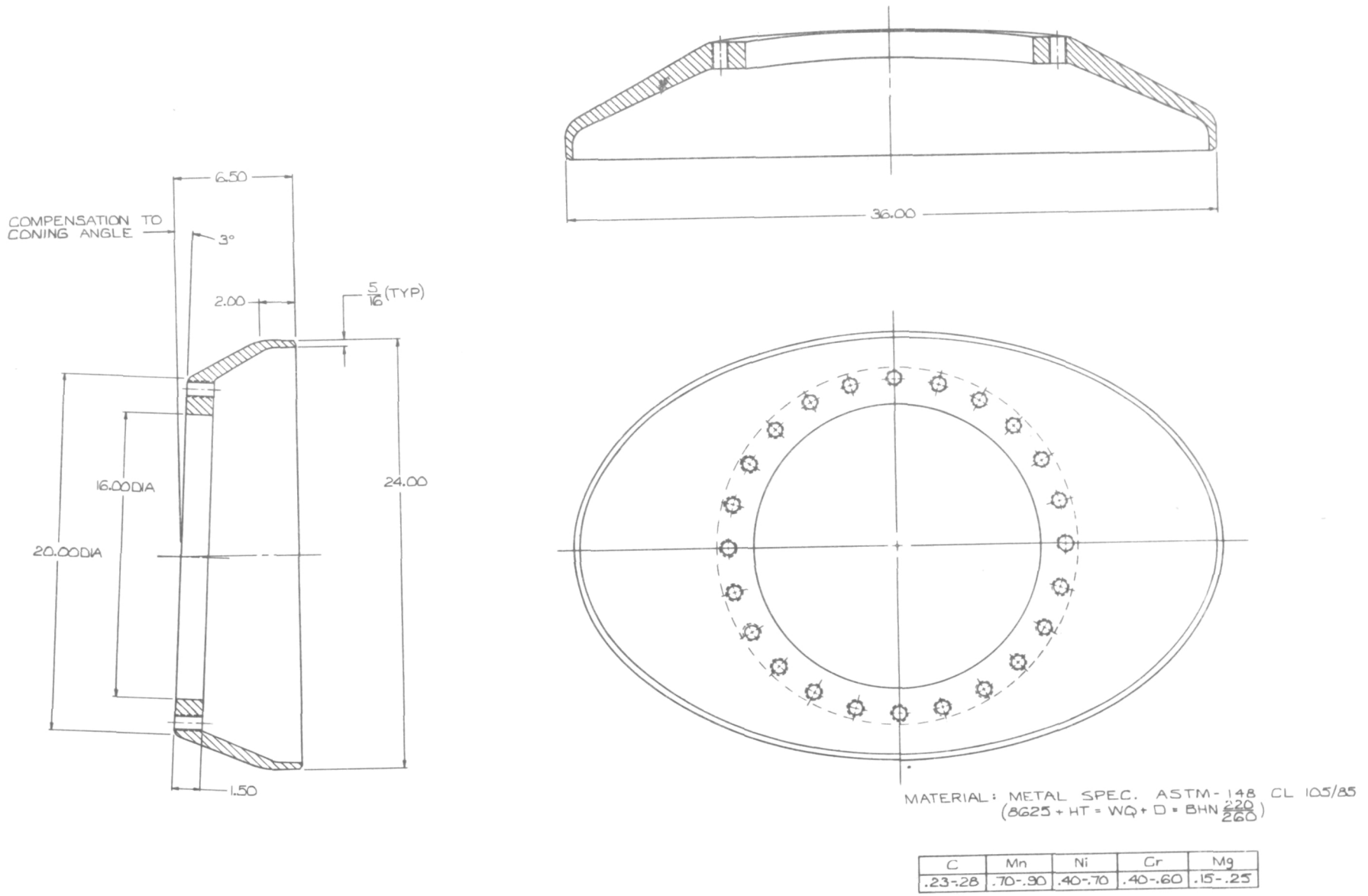


Figure 38. - Adapter fitting.

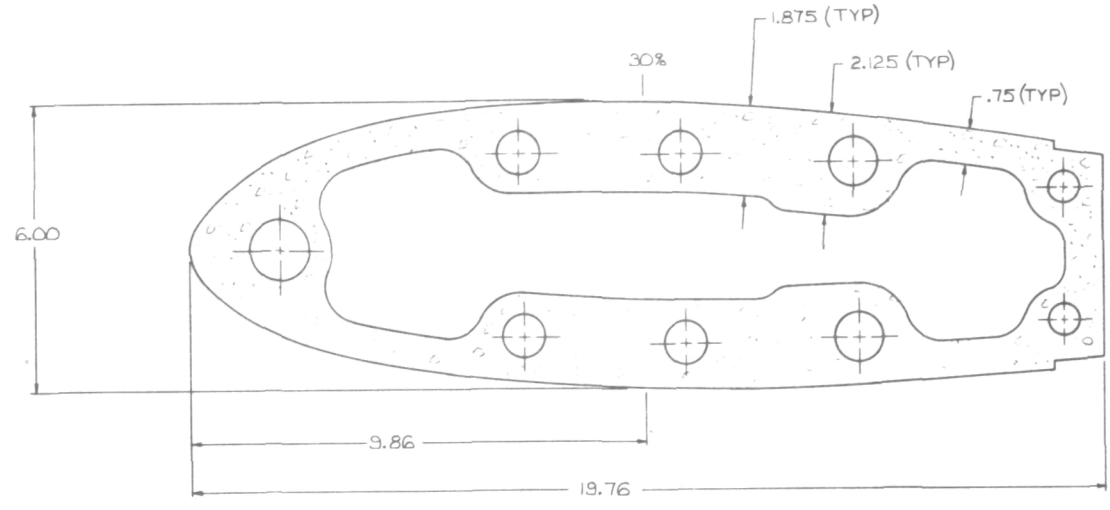


(d) Radius ratio, $r/r_t = 0.75$

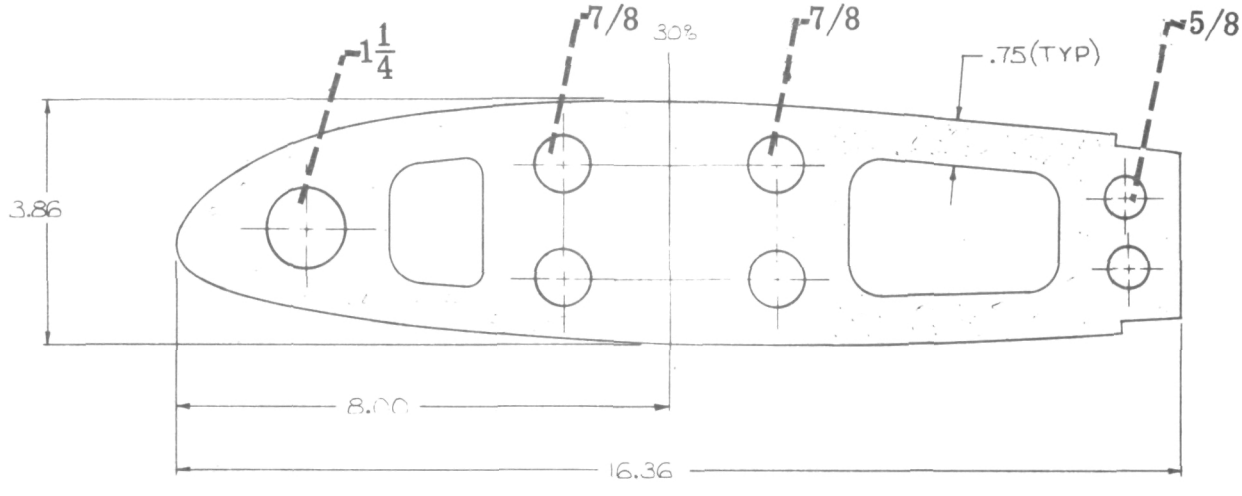


(e) Radius ratio, $r/r_t = 0.85$

Figure 38. - Concluded.

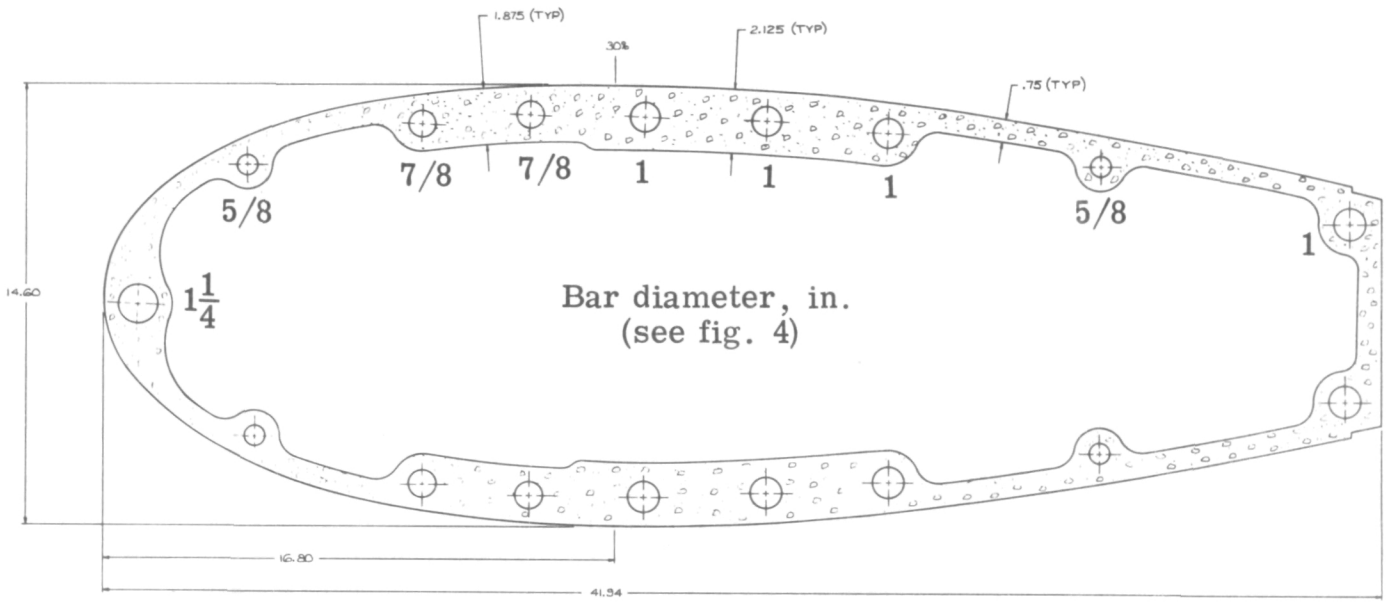


(a) Radius ratio, $r/r_t = 0.35$

Figure 39. - Blade cross section details. (Sections approximately to scale.)

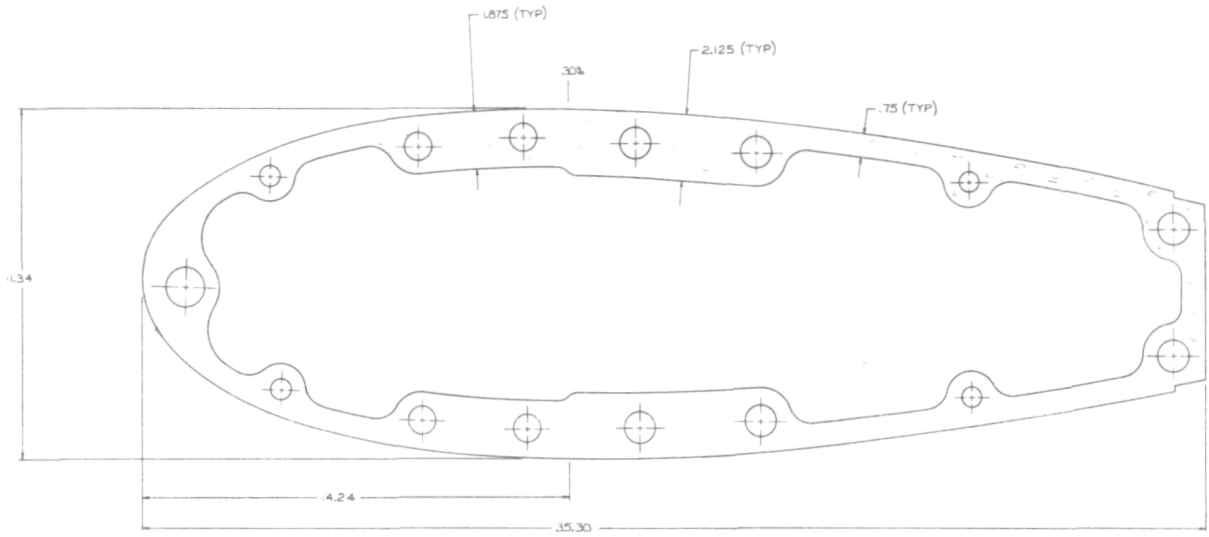


(b) Radius ratio, $r/r_t = 0.5$.

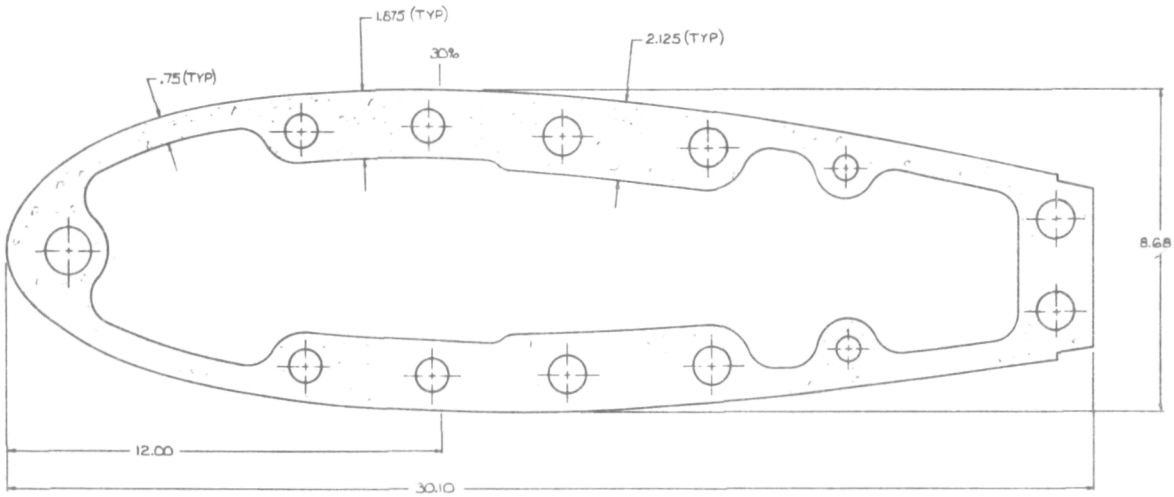


(c) Radius ratio, $r/r_t = 0.625$.

Figure 39. - Continued.

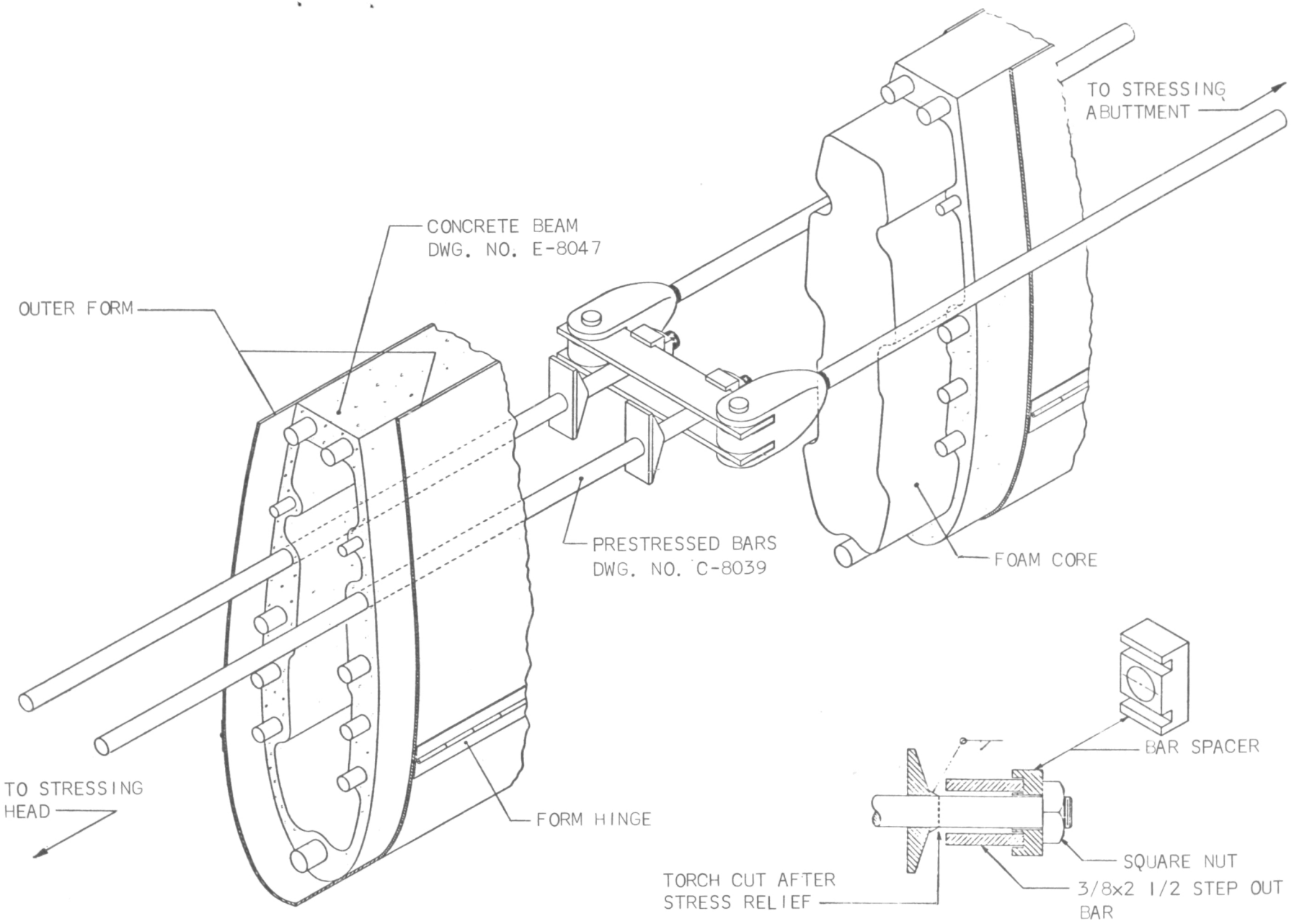


**Figure 40. - Step-out concept.**

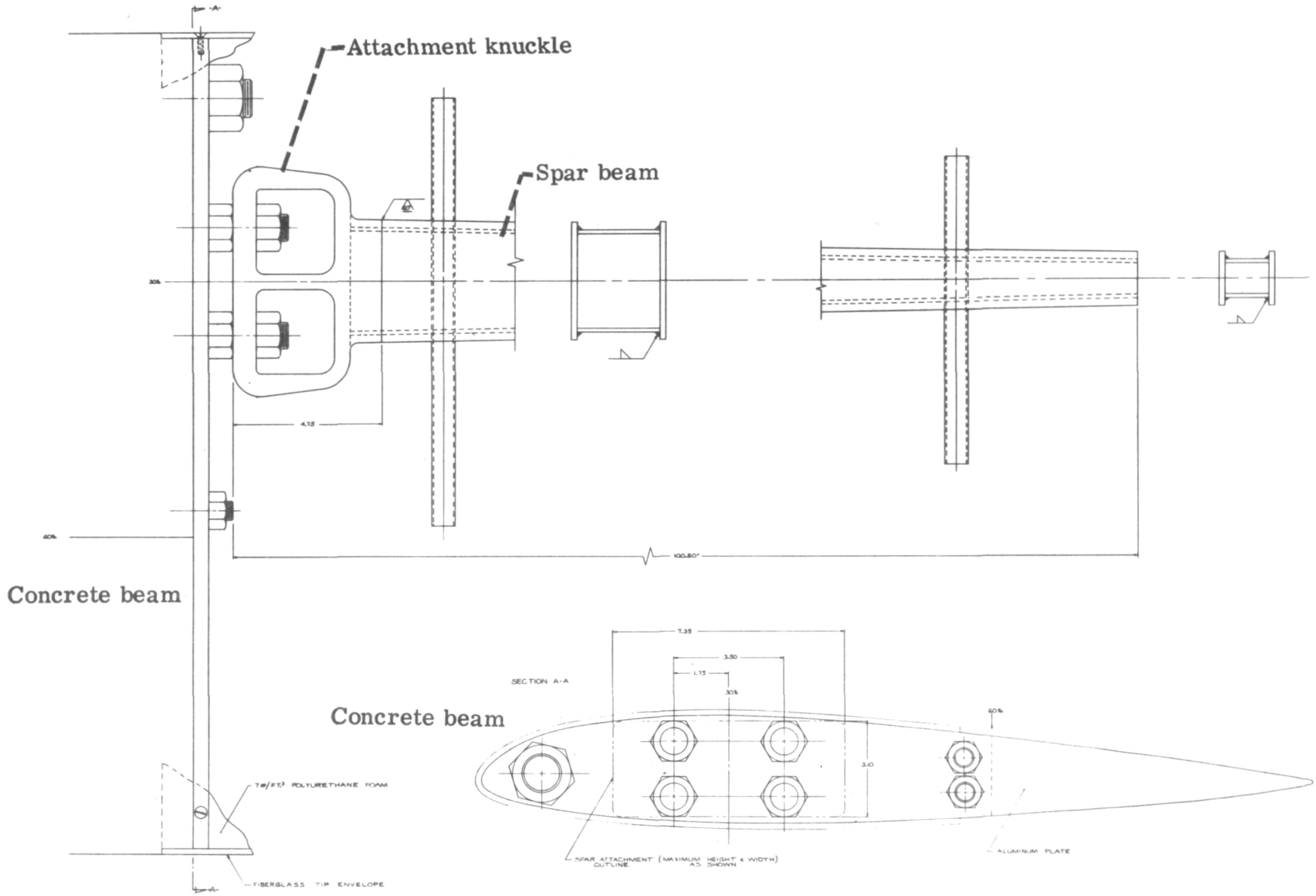


Figure 41. - Blade tip spar and attachment.

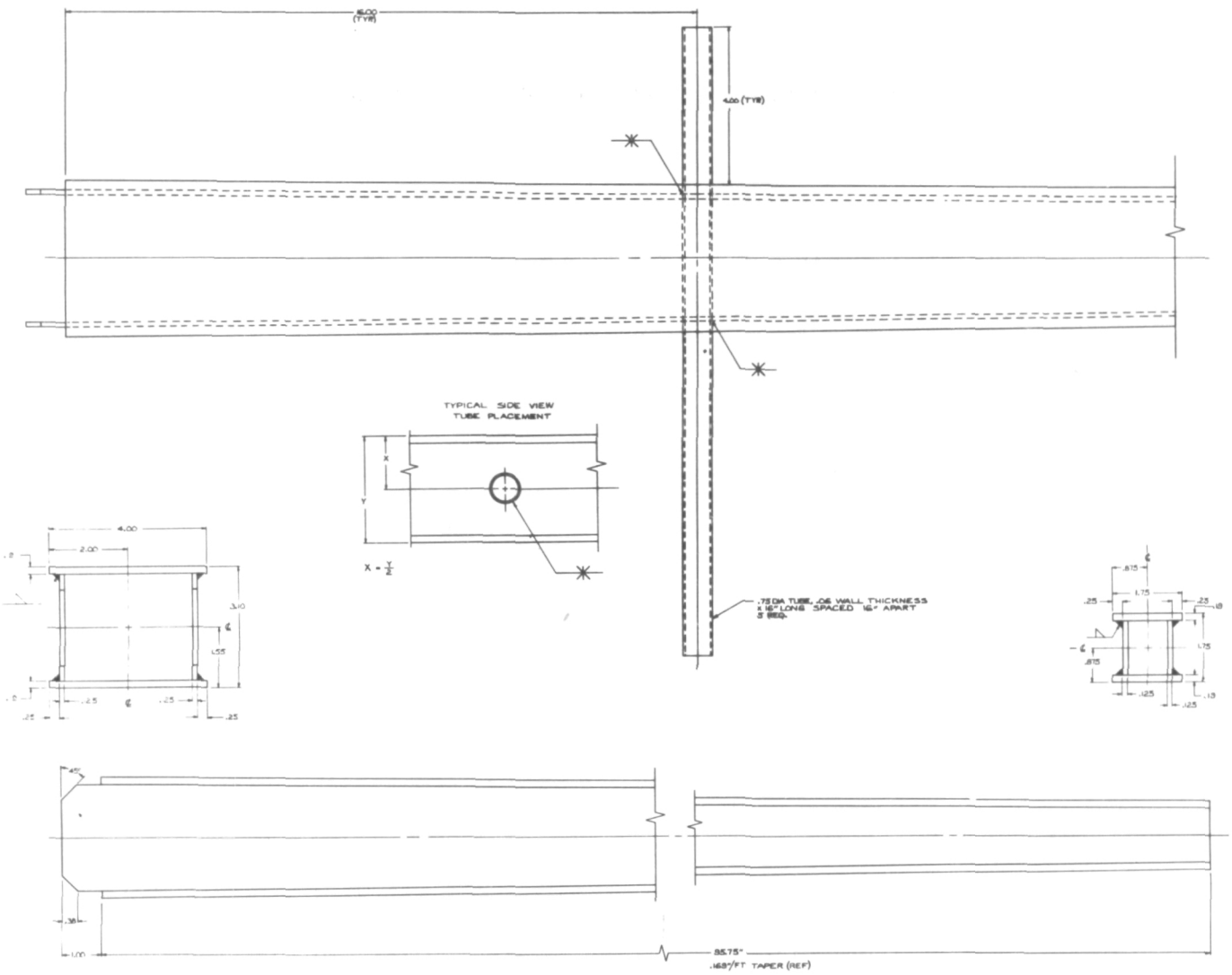


Figure 42. - Detail of spar beam.

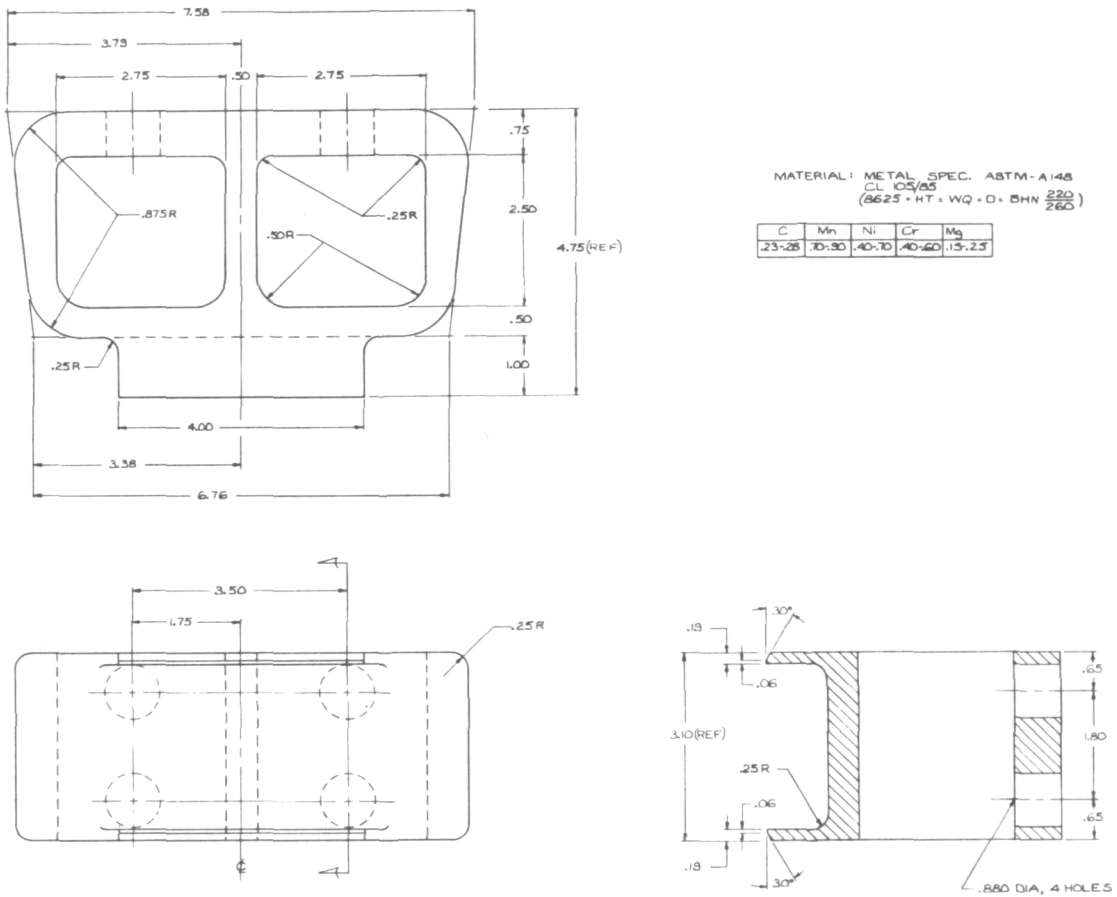


**Figure 43. - Detail of spar attachment knuckle.**

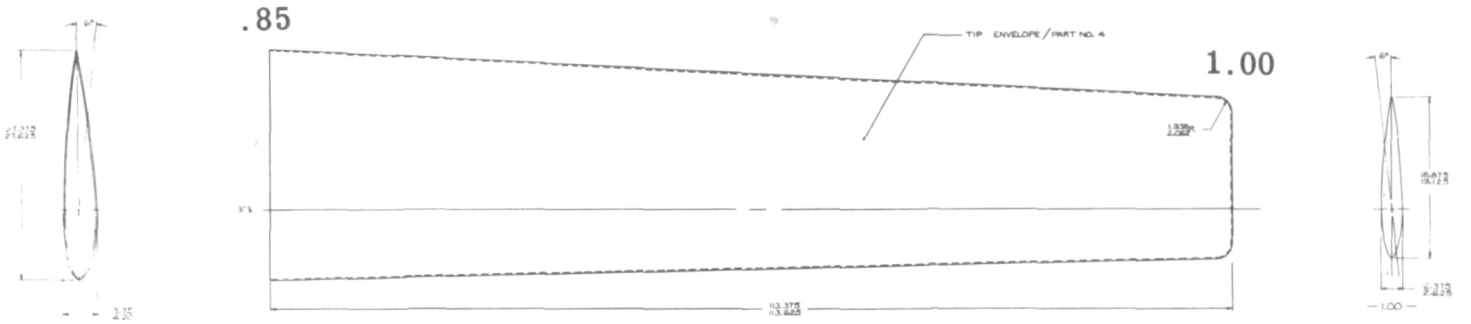


(a) Tip section.

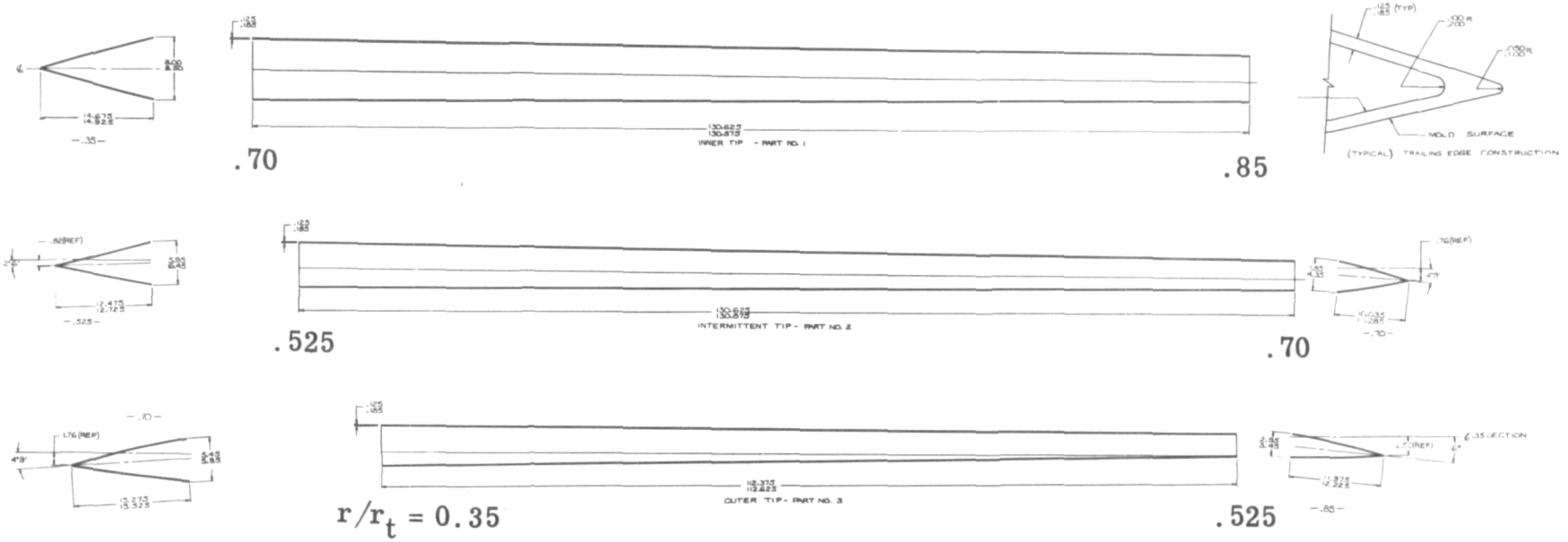


(b) Trailing edge sections.

Figure 44. - Fiberglass envelopes.

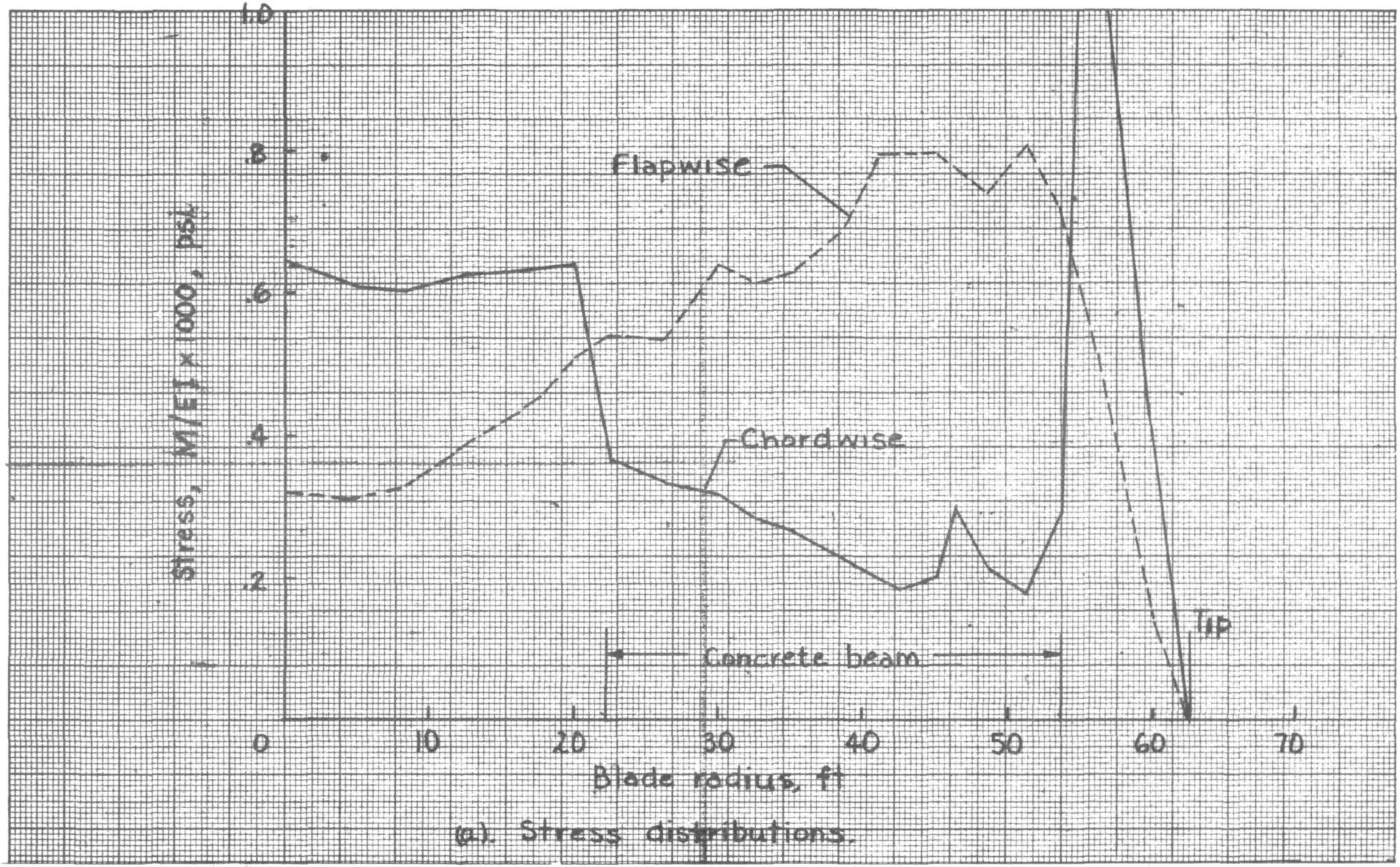


Figure 45. - Example of output from MYRAC computer code for concrete blade.

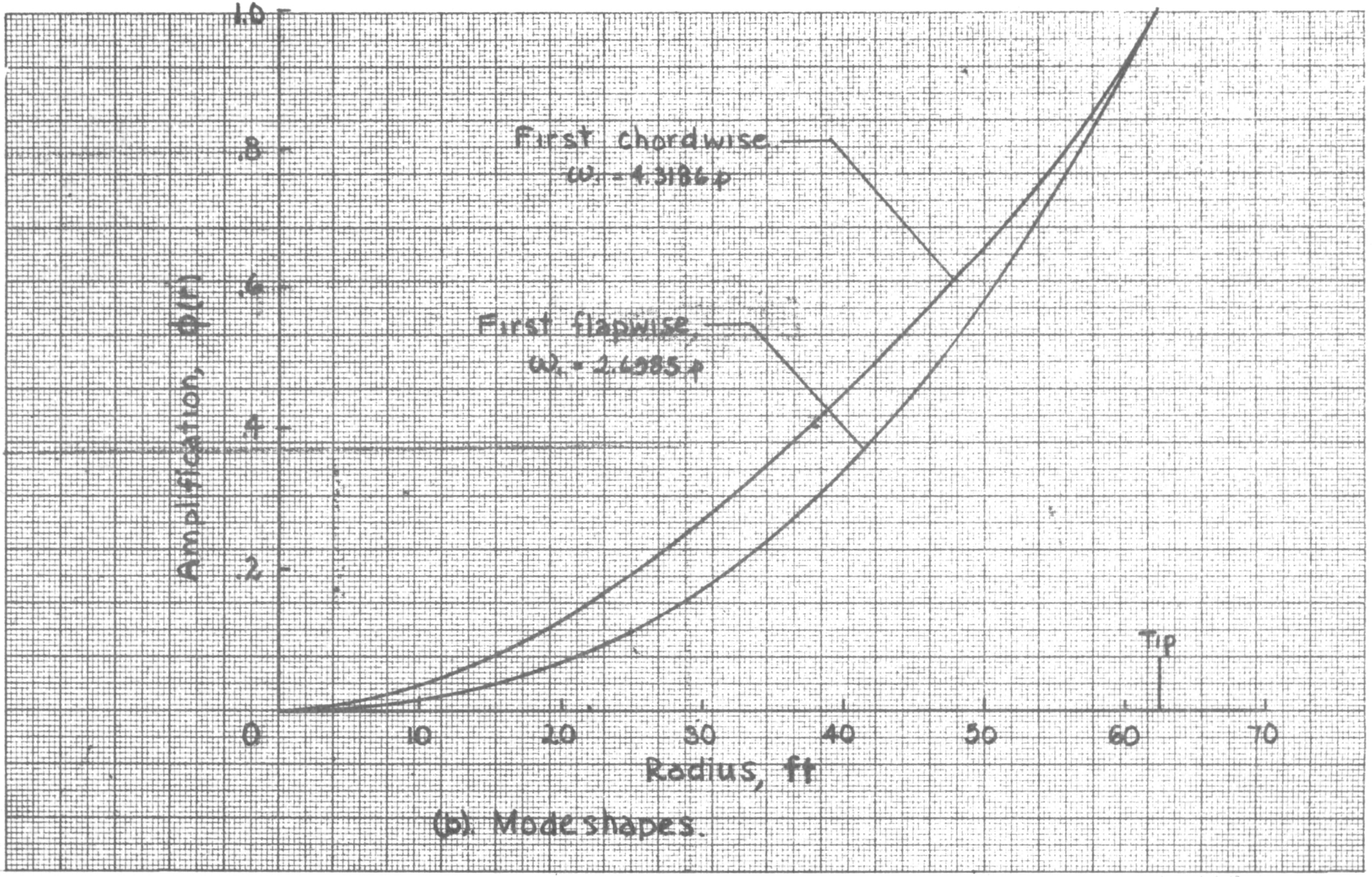


Figure 45. - Concluded.

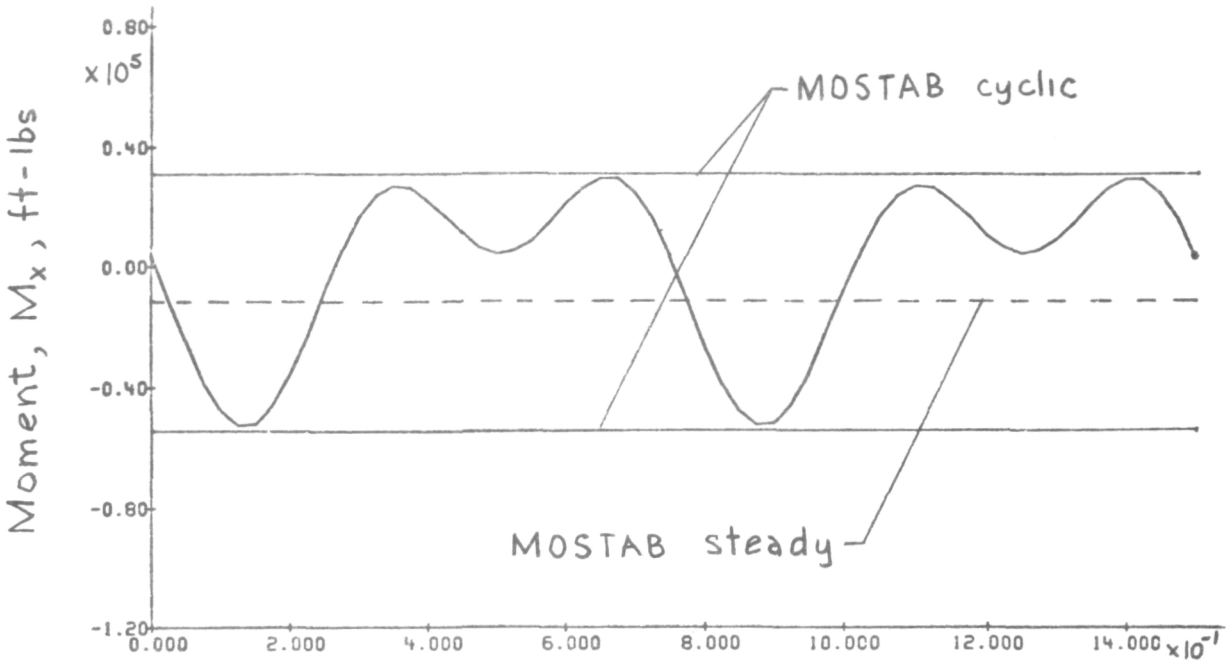


(a). Pitching moment.

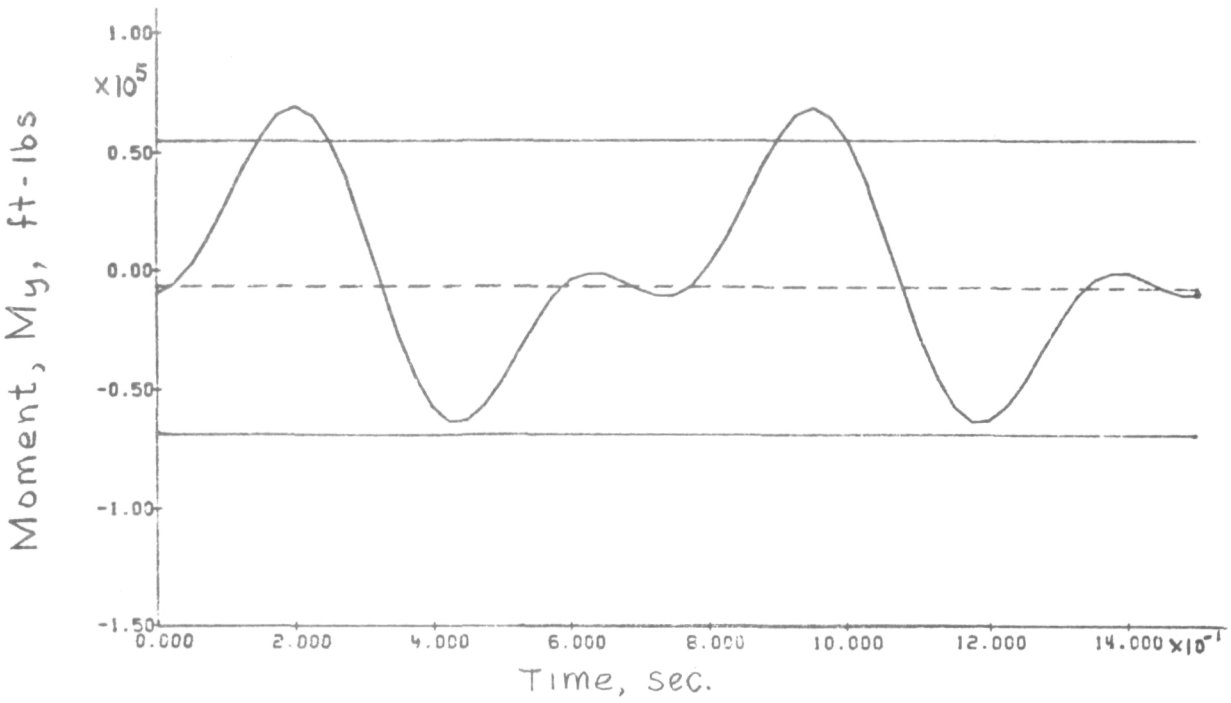


(b). Yawing moment.

Figure 46. - Computer output from WINDLASS code for nacelle moments. Concrete blade, $V_w$ = 26 mph, "soft" yaw drive.

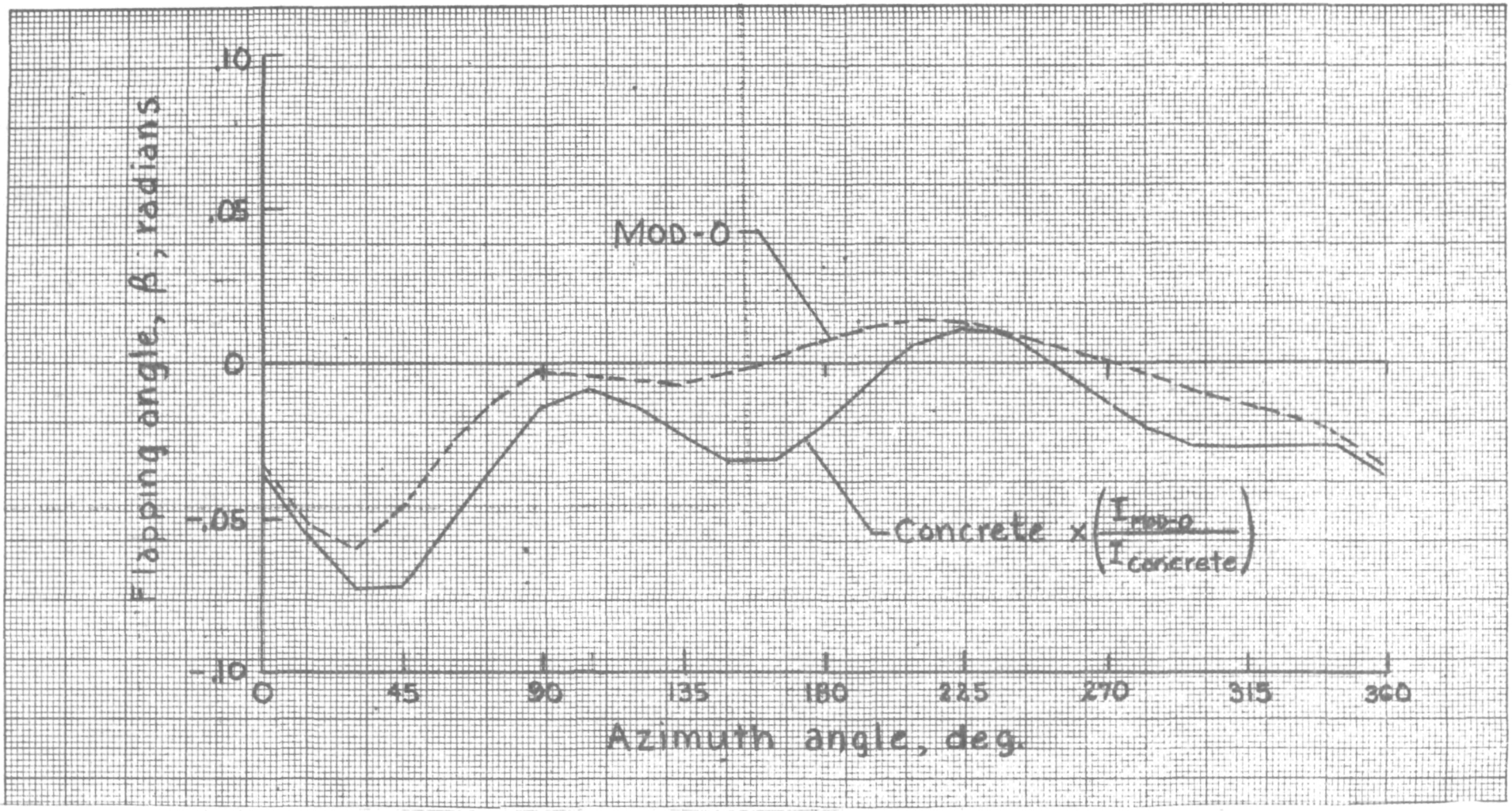


Figure 47. - Variation of blade flapping angle for one rotation.

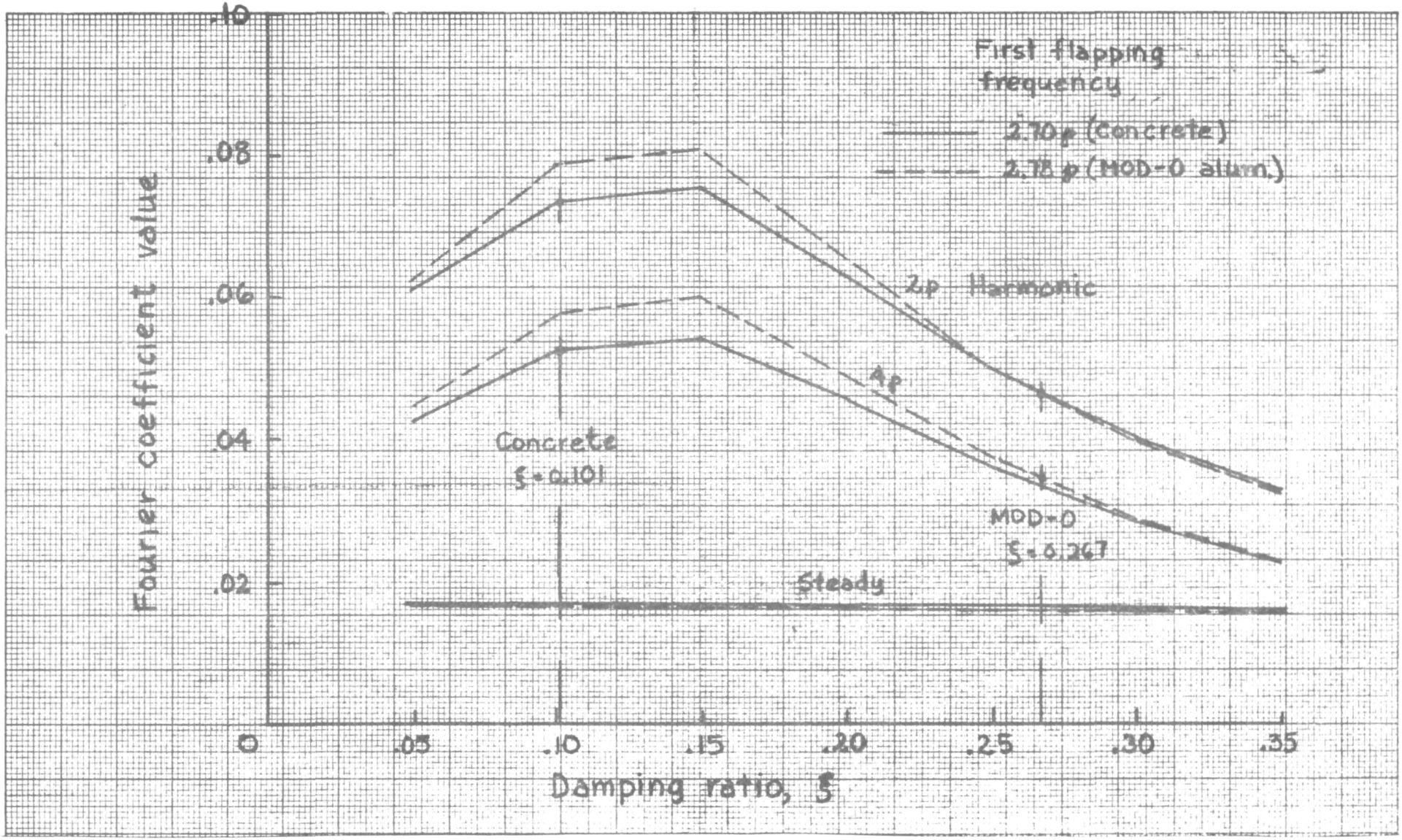


Figure 48. - Effect of damping ratio on hub moment harmonic data. Damped oscillator model (eq. (H6)).

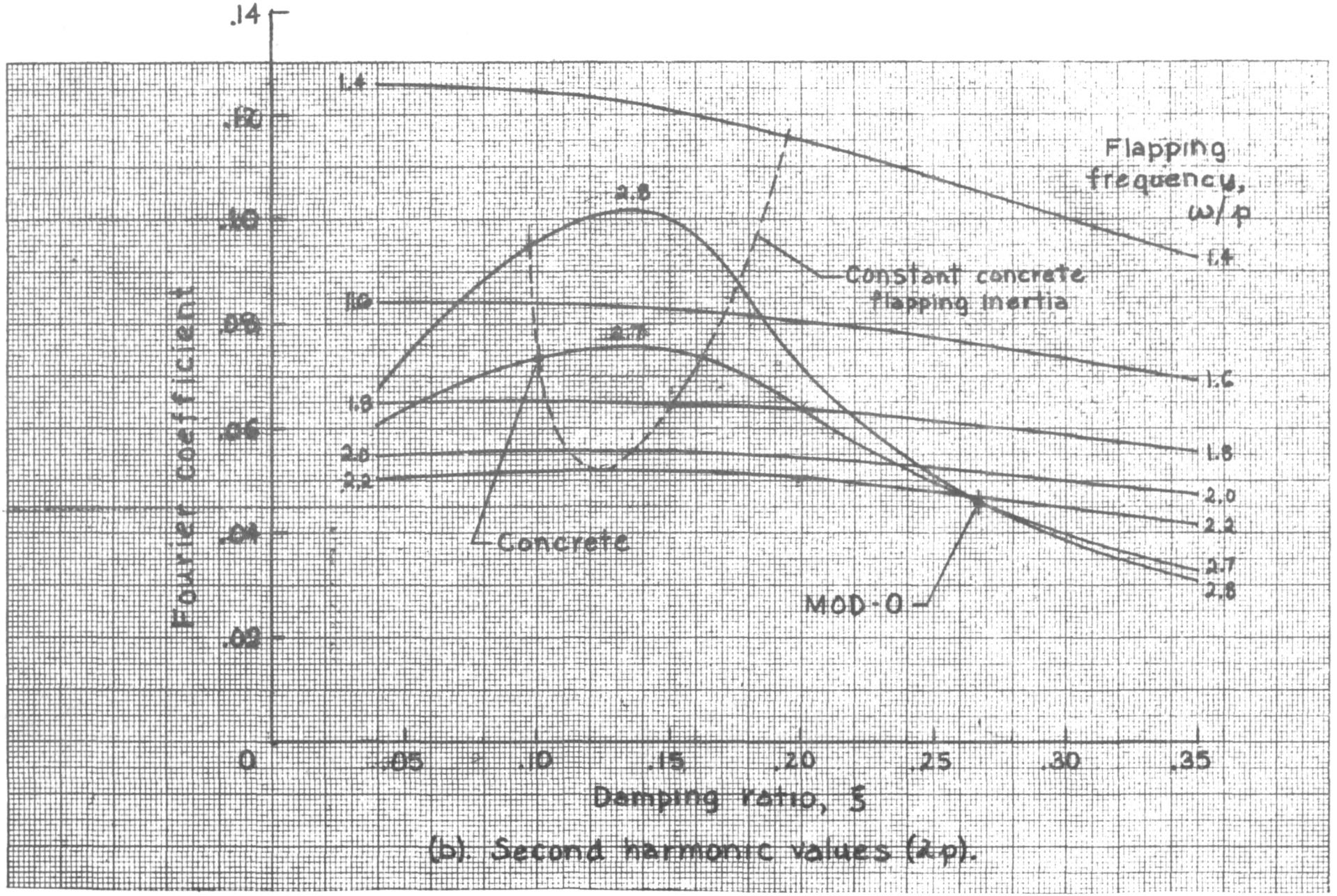


Figure 49. - Continued.

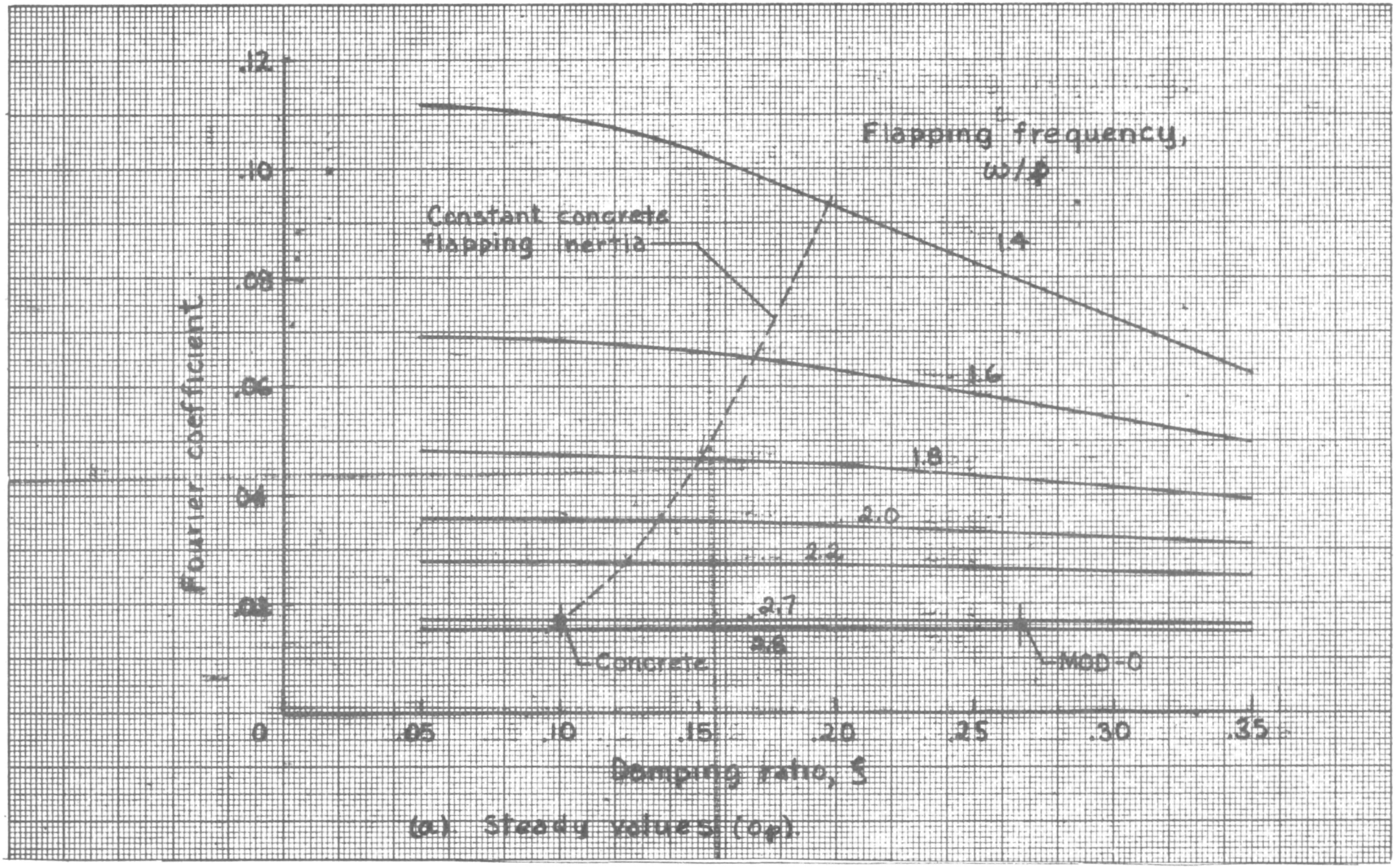


Figure 49. - Variation of hub yawing moment with blade damping ratio and flapping frequency. Damped oscillator model (eq. (H6)).

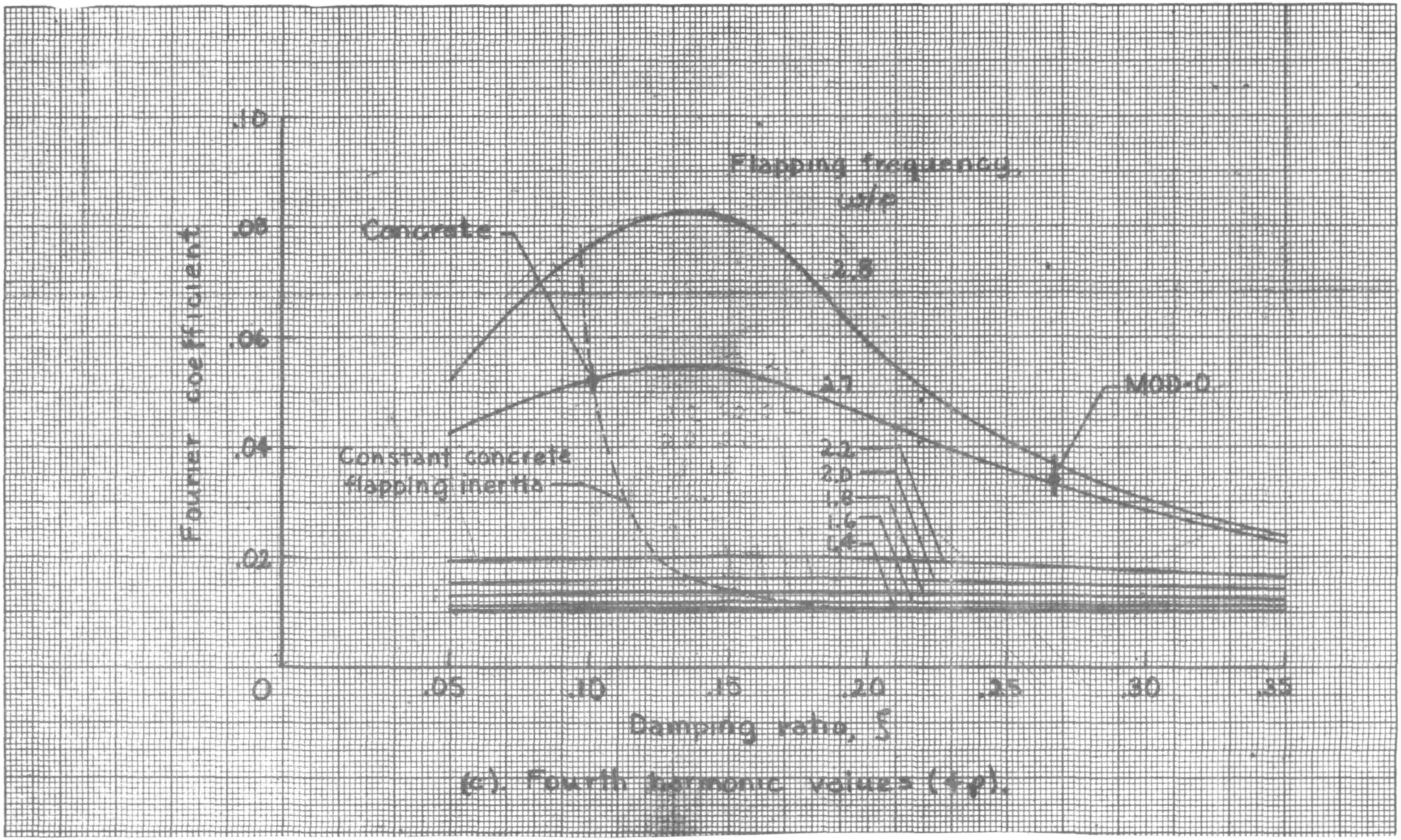


Figure 49. - Concluded.

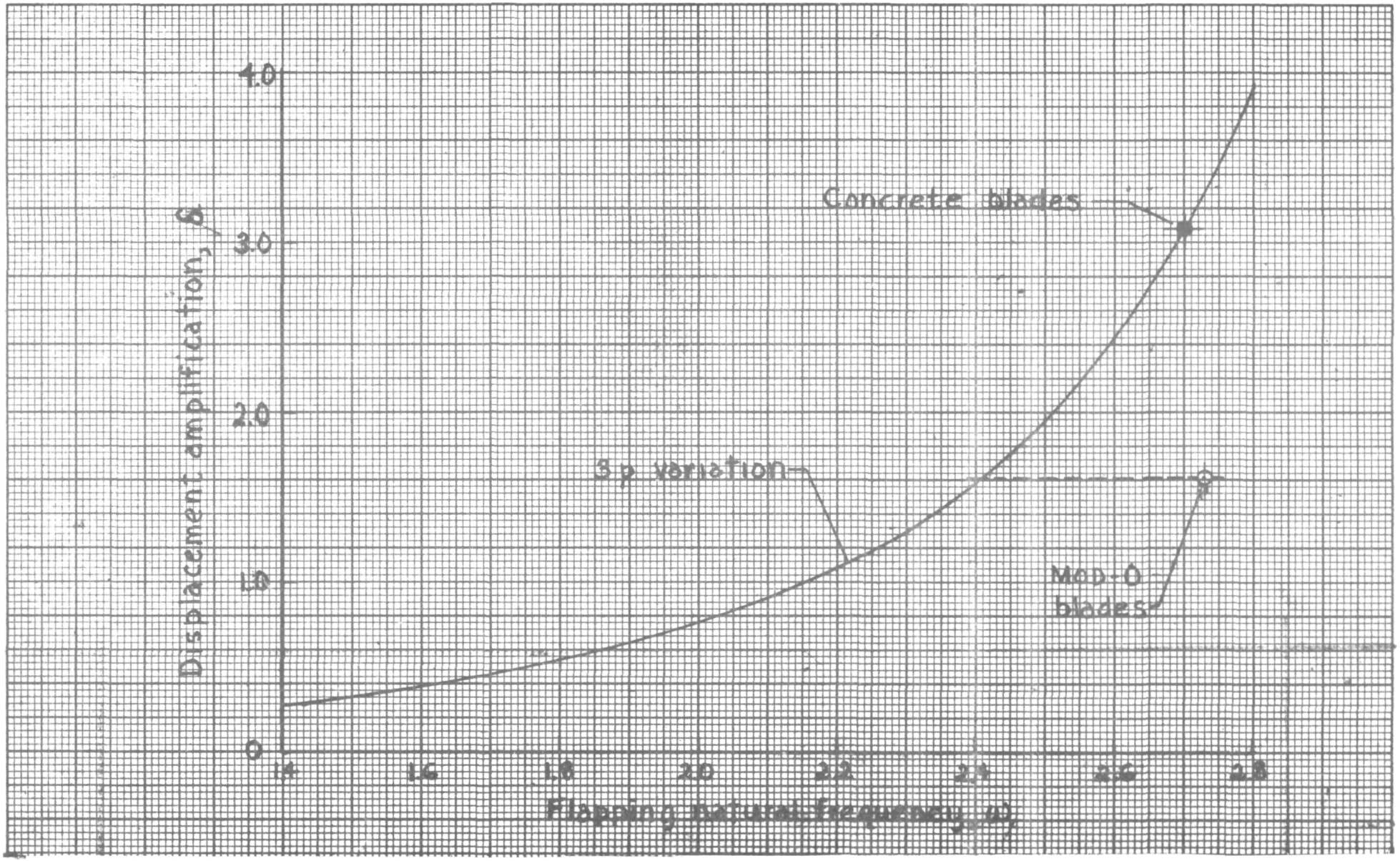


Figure 50. - Variation of displacement with flapping natural frequency with fixed flapping inertia. Vibrating mass model; third harmonic.

| 1. Report No. | 2. Government Accession No. | 3. Recipient's Catalog No. |
|---|---|---|
| NASA CR-159725 | | |

| 4. Title and Subtitle | 5. Report Date |
|---|---|
| EVALUATION OF FEASIBILITY OF PRESTRESSED CONCRETE FOR USE IN WIND TURBINE BLADES | 6. Performing Organization Code |

| 7. Author(s) | 8. Performing Organization Report No. |
|---|---|
| Seymour Lieblein, Technical Report Services; D. S. Londahl, Donn B. Furlong, and David P. Peery, Tuthill Pump Co.; and Mark E. Dreier, Paragon Pacific, Inc. | TRS 104 |

| 9. Performing Organization Name and Address | 10. Work Unit No. |
|---|---|
| National Aeronautics and Space Administration<br>Lewis Research Center<br>Cleveland, Ohio 44135 | 11. Contract or Grant No.<br>NAS3-20596, NAS3-20813, and Purchase Order C-25906 |

| 12. Sponsoring Agency Name and Address | 13. Type of Report and Period Covered |
|---|---|
| U.S. Department of Energy<br>Distributed Solar Technology Division<br>Washington, D.C. 20545 | Contractor Report |
| | 14. Sponsoring Agency ~~Code~~ Report No.<br>DOE/NASA/5906-79-1 |

15. Supplementary Notes

Final report. Prepared under Interagency Agreement EX-76-I-01-1028. Project Manager, Thomas P. Cahill, Wind Energy Project Office, NASA Lewis Research Center, Cleveland, 44135.

16. Abstract

As part of the DOE/NASA research program on wind energy, a preliminary evaluation was conducted of the feasibility of the use of prestressed concrete as a material for low-cost blades for wind turbines. A baseline blade design was achieved for the DOE/NASA MOD-O 100 kW experimental wind turbine that met aerodynamic and structural requirements. Calculated blade weight and cost were 4900 lb and around $18 000, compared to 2000 lb and around $200 000 for a MOD-O aluminum blade. Significant cost reductions were indicated for volume production. Casting of a model blade section showed no fabrication problems. Coupled dynamic analysis revealed that adverse rotor-tower interactions can be significant with heavy rotor blades. Design options are discussed. Areas of further investigation are identified to verify the design approach and to provide the property data base required for concrete blade design.

| 17. Key Words (Suggested by Author(s)) | 18. Distribution Statement |
|---|---|
| Wind turbine<br>Rotor blades<br>Concrete | Unclassified - unlimited<br>STAR Category 44<br>DOE Category UC-60 |

| 19. Security Classif. (of this report) | 20. Security Classif. (of this page) | 21. No. of Pages | 22. Price* |
|---|---|---|---|
| Unclassified | Unclassified | | |

* For sale by the National Technical Information Service, Springfield, Virginia 22161

☆ U.S. GOVERNMENT PRINTING OFFICE: 1980-657-145/5211